Ministero dell'Istruzione,
dell'Università e della Ricerca

Università degli studi
di Palermo

Dipartimento di Chimica e Fisica della Terra ed
Applicazioni alle Georisorse ed ai Rischi Naturali (CFTA)

The Monticchio crater lakes: fluid geochemistry and circulation dynamics

PhD coordinator:
Prof. Francesco Parello

PhD thesis by:
Dr. Marco Nicolosi

Tutor:
Prof. Pasquale Mario Nuccio

Co-tutor:
Dr. Antonio Caracausi

Dottorato di ricerca in geochimica (GEO-08)
XXII CICLO (2008 – 2010)

CONTENTS

1.0 - Introduction

Crater lakes are strongly influenced by volcanic or post-volcanic activities and, thanks to their position, act as chemical traps for magmatic volatiles. If high gas fluxes of magmatic origin find conditions favourable to the gas accumulation into lake waters, gaseous eruption can happen.

Lake Nyos and lake Monoun (Cameroon) and Lake Kivu (Rwanda) are the three crater lakes in the world known to be rich in dissolved CO_2. Catastrophic CO_2 outgassing occurred on 15th August 1984 at Lake Monoun and on 21st August 1986 at Lake Nyos, killing 37 and people 1700 people, respectively (e.g., Kerr, 1986; Kling, 1987; Kusakabe et al., 1989, Sano et al., 1990). From these two dramatic events the attention on crater lakes has grown up.

For a long time, the geochemical monitoring of crater lakes has been considered a powerful tool not only for the study of magmatic activity (in active area) but also for the mitigation of the Nyos-type gas disasters (Kusakabe, 1994). Nevertheless, until now, only a few crater lakes have been well investigated (Delmelle and Bernard, 2000; Gunkel et al., 2008).

The Mediterranean geodynamic setting makes Italy a land rich in volcanic activity, both in the past and the present, and many crater lakes were formed (e.g. Bolsena, Vico, Bracciano, Monticchio, Mezzano, Martignano, Albano, Nemi, Averno). Most of them were investigated mainly focusing on the following aspects: dendrogeomorphology, palynostratigraphy, water chemistry and biology (e.g. Follieri M. et al.,1997; Allen et al., 1999; Calace et al. 1999; Fantucci R., 2007; Schettler and Albéric, 2008).

The capability of crater lakes to accumulate gases makes them ideal places to investigate origins and fluxes of gases released from deep seated gases. In that view, lake water circulation coupled with isotope geochemistry of dissolved volatiles in lakes can help us to distinguish among different origin of gases from the Earth interiors. Noble gases exchange with atmosphere at lake surface and, in meteoric water, they are equilibrium concentrations with atmosphere at given T-P conditions.

Here, a geochemical study of Monticchio lakes (Lago Piccolo and Lago Grande, fig. 1.1), placed in two maar craters of Mt. Vulture Volcano (Southern Italy), is presented. In Lago Piccolo high concentrations of dissolved mantle derived gases was founded (e.g. Fornai, 1992; Chiodini et al., 2000; Cioni et al., 2006; Caracausi et al. 2009). According to Cioni et al. (2006), it is a meromictic lake, therefore gas accumulation in deep waters is favoured by its water circulation features. Preliminary data suggest that dissolved gases of Lago Grange have a similar origin to those of LPM (Caracausi et al. 2009). Previous studies on Lago Grande

mainly focused on paleoclimatic aspects (e.g., Robinson, 1994; Allen et al., 1999), genesis of sediments and water chemistry (Schettler & Albéric, 2008), water quality and biological aspects (Mancino et al., 2009).

The high gas amounts (mainly CO_2 and CH_4) of dissolved gases in deep waters of Monticchio lakes suggest the necessity of investigations on these lakes not only focused on the genesis of the gases, but also to understand their hazardous nature. Carbon dioxide is generally coupled with mantle derived helium (e.g., Sano et al. 1990; Kipfer et al., 1994; Aeschbach-Hertig et al., 1996) and , taking into account that CO_2 is the most abundant volatile in Monticchio lakes, our investigations could contribute to improve the knowledge about mantle derived helium fluxes in continental areas (Oxburgh et al., 1986; Griesshaber et al. 1992).

In Monticchio lakes the water is the main carrier of gases (in solution), no significant free gas emissions are present, therefore a geochemical study of gases must take into account several processes such as thermal or chemical stratification of water body, chemical cycle of species and water dynamics. That so being, by means of physical-chemical parameters and water and gas chemistry, we investigate the water circulation within the lakes.

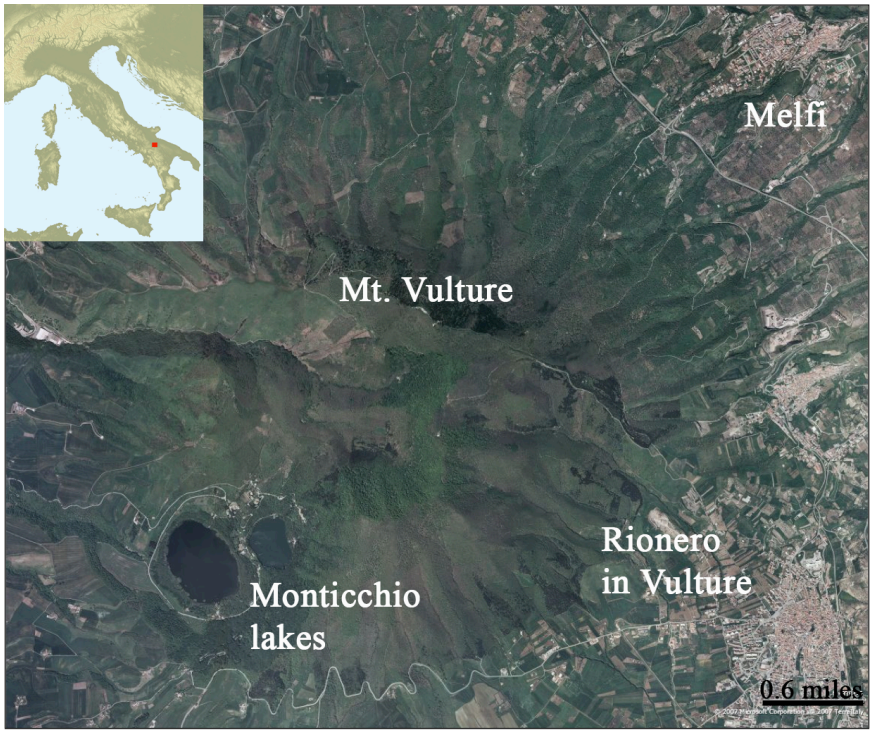

Figure 1.1 - Satellite image of Mt. Vulture (Google maps). The Monticchio crater lakes are located in two maars of southwest portion of Mt. Vulture volcano.

The aims of this study on Monticchio lakes mainly are: i) the assessment of volatiles and heat transfer processes within the lake by means of lake water dynamics; ii) to estimate the lake stability conditions in relation to the budget of dissolved volatiles ; iii) to identify the origin of

volatiles; iv) tentatively to assess the significant geochemical features of gases (i.e., pristine isotope compositions and abundance ratios) coming from Mt. Vulture depth and finally dissolved into water of the two lakes.

2.0 Geological setting

The Monticchio lakes are located on Monte Vulture, a Quaternary volcano, in southern Italy, that lies within the Apennine accretionary prism (fig. 2.1), the evolution of which was governed by the westward subduction of the Adriatic plate. This subduction system is also responsible of Tyrrhenian Sea formation that is the associated back-arc basin (e.g., Beccaluva et al., 1989; Mantovani et al., 1993; Doglioni et al., 1999).

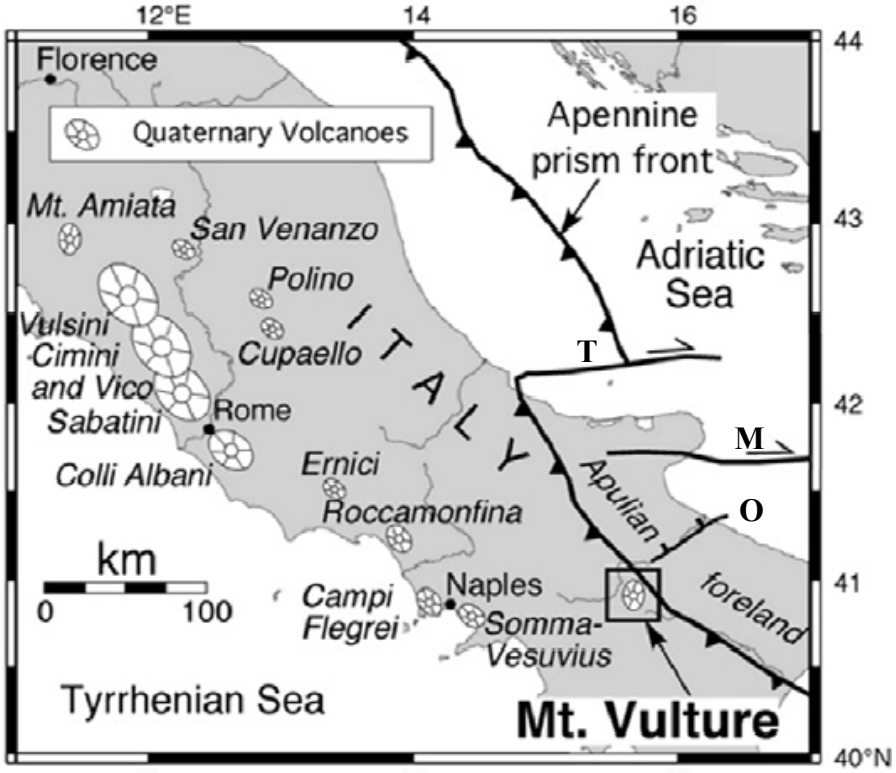

Figure 2.1 – Sketch map of central-southern Italy with the main Quaternary volcanism and front of the Apennine prism; T, Tremiti line (E–W); M, Mattinata line (E–W); O, Ofanto graben (ENE–WSW) (modified by D'Orazio et al. 2007).

The whole subduction front shows an eastward rollback motion, of about 1-7 cm yr^{-1}, as a consequence of the eastward asthenospheric flow that pushes the subducting Adriatic slab (Doglioni et al., 1994). Furthermore, the slop of the slab is increased both by the weight of the slab itself and by the asthenospheric horizontal thrust (Doglioni et al., 1994).

During the Pleistocene, the different thickness of Apulo-Adriatic plate (110 Km thick in Puglia and 70 Km in central Adriatic plate) and the interference of the Apulian continental crust with the belt, slowed down the roll-back of the southern Apennines front (Doglioni et al., 1994). As a result of Pleistocene evolution, the Apennine chain is split into two parts with different features: the northern and the southern Apennine. The margin of these two areas

corresponds to Ortona-Roccamonfina line, which has been interpreted as a lithospheric discontinuity (Mantovani et al., 1993; Patacca et al. 1993). Since the middle Pleistocene, the central Adriatic plate underwent high subsidence rates, while the Apulian foreland and the Bradanic foredeep underwent uplift (Doglioni et al., 1994).

Mongelli (1975) and Console et al. (1993) interpreted the Tremiti alignment as a right-lateral lithospheric rupture separating the Adriatic plate into two blocks, generating a trans-tensional window between two different segments of the Apennine slab (Doglioni et al., 1994). Other active faults, parallel to the Tremiti line, are the Mattinata Line (Funicello et al., 1991) and its offshore prolongation (Finetti et al., 1987), localized in the southern part of the Gargano promontory. Another evidence of the differential slab retreat is the trans-tensional opening of the northern border of the Ofanto graben in the Tertiary (Funicello et al., 1991) (fig. 2.1, 2.2).

As inferred for Mt. Etna volcano (Doglioni et al. 2001), Mt. Vulture is located along a vertical slub window, which is a rupture of the slab related to the Tremiti, Mattinata and Ofanto transfer zones. The faults system associated with the vertical window allowed the ascent of the Vulture magmas (e.g., Paternoster 2005; Schiattarella 2005; D'Orazio et al., 2007) (Fig. 2.2).

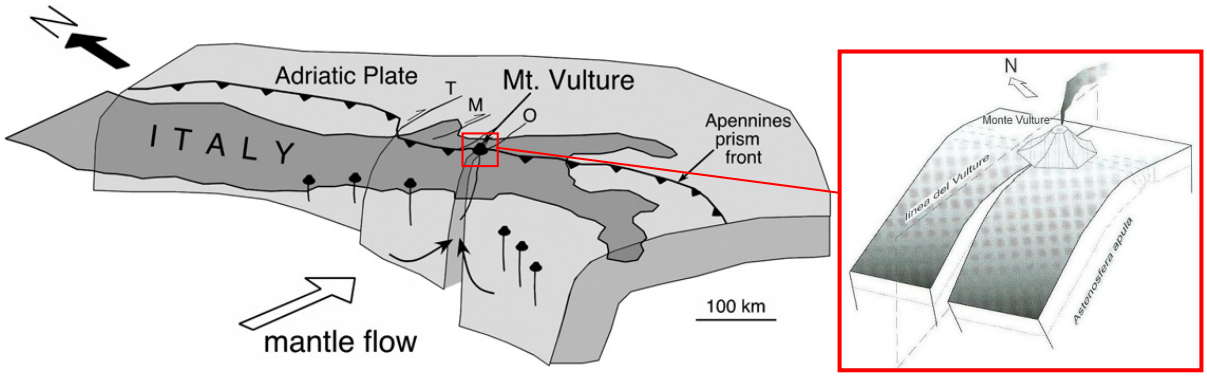

Figure 2.2 - Cartoon showing the vertical slab window inferred beneath the Southern Apennines. The relative eastward mantle flow enriched with fluids/melts from the Adria Plate subduction could have converged and flowed into the slab tear, which allowed the formation of Mt. Vulture volcano. T, Tremiti line (E–W); M, Mattinata line (E–W); O, Ofanto graben (ENE–WSW) (modified from D'Orazio et al., 2007). The detail of Mt. Vulture area is from Schiattarella & Beneduce (2006).

Mt. Vulture is strongly different from the other major quaternary volcanoes of Italy, which are aligned along the west side of the Apennine chain. Like Mt. Etna, it is located in the external part of the subduction hinge; therefore, it cannot be sourced directly by the slab, but by the asthenospheric upwelling along slab tear faults (e.g., Doglioni et al., 2001; Trua et al., 2003; De Astis et al., 2006).

Mt. Vulture volcano formed at the intersection between the NW-SE (Apennine) and the NE-SW (Ofanto-Sele) fault system (Ciaranfi et al., 1983). The sedimentary basement is represented by pre-Pliocene flysches at the structural highs and by lower-Middle Pliocene sediments which filled the structural lows (Cello and Mazzoli, 1999 and reference therein).

The Mt. Vulture activity started about 750 Ka up to 140 Ka, with long quiescent periods; the last volcanic phase produced two maar craters, in which Lago Piccolo (from now on LPM) and Lago Grande (from now on LGM) of Monticchio are located. The volcanic complex is formed by many eruptive centres composed of pyroclastic products and subordinate lava flows and domes with strong silica undersaturated character and alkaline potassic to ultrapotassic affinities (De Fino et al., 1982, 1986). The erupted products range from foidites (nephelinites, haüynites, and leucitites) and melilitites to phonolitic tephrites, tephritic phonolites, phonolites and trachytes (Melluso et al., 1996; Beccaluva et al., 2002; De Astis et al., 2006). In addition to the silicate volcanic rocks, Stoppa and Principe (1998) identified carbonatitic tuffs and lapilli in the pyroclastic succession of the Monticchio Lake maars. Rosatelli et al. (2000) investigated calciocarbonatite ejecta within the pyroclastic surge deposits in the lower portion of the volcanic succession. In the carbonatitic-melilititic tuffs of the Monticchio Lakes formation, ultramafic xenoliths and megacrysts were also found (Jones et al., 2000; Downes et al., 2002).

3.0 Sampling and analyses

3.1 Sampling methods

The waters and dissolved gases samples of Monticchio Lakes were collected between September 2008 and June 2010 in 8 different sampling campaigns (listed in Tables in appendix I) and ever in the same sampling point (fig. 3.1). Also others sampling points was used to verify the lateral continuity of physical-chemical parameters (yellow point in fig.3.1, the continuity was verified; data not reported).

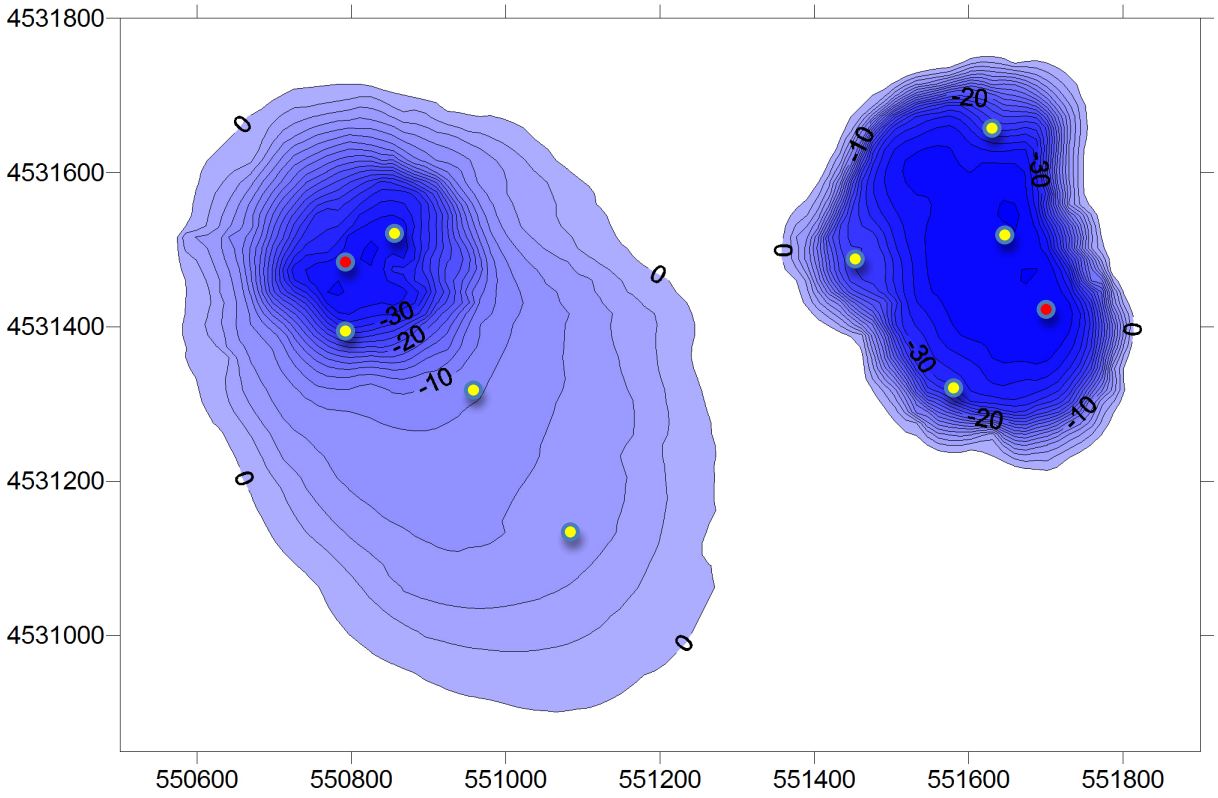

Figure 3.1 - Bathimetric map of Monticchio lakes (from data of Caracausi et al. 2009) with sampling points of this work (red points) and sampling point used to verify the lateral continuity of physical-chemical parameters (yellow points). The Monticchio lakes have a surface of about 1.7×10^5 m^2 and 4.3×10^5 m^2 and a water volume of about 4.0×10^6 m^3 and 3.2×10^6 m^3 for LPM and LGM, respectively (Caracausi et al., 2009).

The sampling device used to collect the deep lake waters is a 2 litre water sampler, specifically designed by Ageotec (Bo – Italy) for trace elements sampling and constructed of clear polycarbonate, polyethylene and silicone.

The water samples were stored in HDPE (High-density polyethylene) bottles, in different aliquots: untreated for δD and $\delta^{18}O$, unacidified for anions, filtered (through a 0.45 μm filter) and acidified (with ultrapure HNO3) for cations. The water samples for trace elements and

NH_4^+ were filtered (through a 0.45 μm filter), acidified (with ultrapure HCl) and stored in polypropylene and dark glass bottles, respectively.

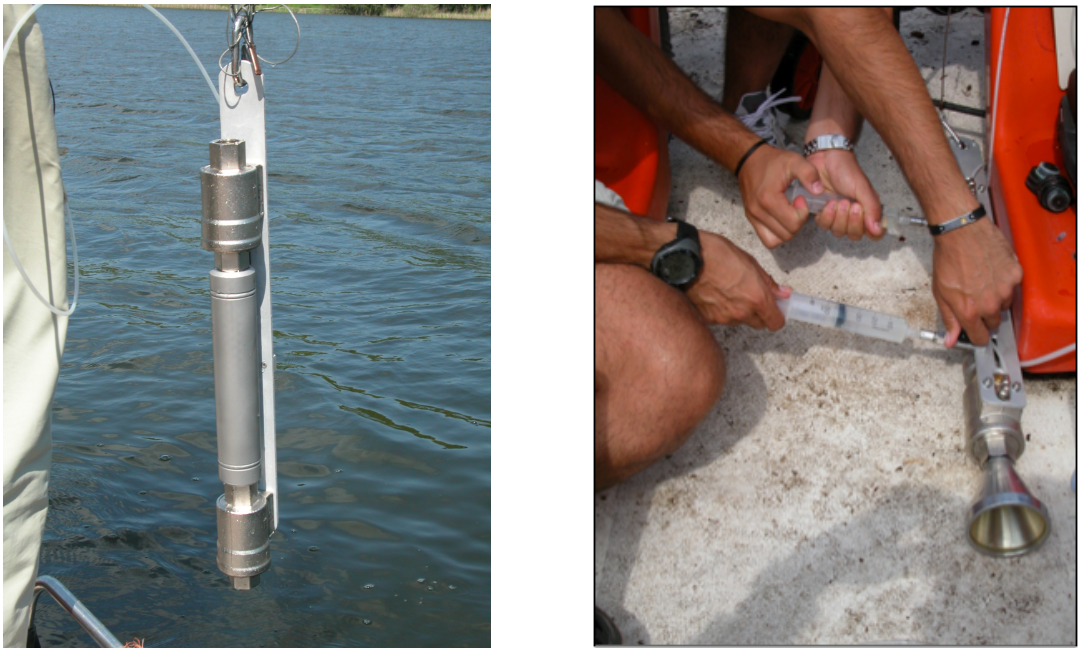

Figure 3.2 - a) Stainless-steel cylindrical sampler for dissolved gases, which is equipped with pneumatic valves at the two endings; b) Stainless-steel cylindrical sampler, similar to that one used for dissolved gases (see text), during the sampling of TDIC.

The waters for the analysis of dissolved gases were sampled by using stainless-steel cylindrical samplers equipped with two pneumatic valves at the two endings (fig. 3.2 a); the valves were controlled from the boat by a small air compressor (Cosenza et al., 2008; Caracausi et al., 2009). The concentrations of the dissolved gases and the isotopic compositions of He, Ar and CH_4 were determined in the laboratory after the gas extraction from waters (Capasso and Inguaggiato, 1998).

The samples of total dissolved inorganic carbon (TDIC) were collected by means of the stainless-steel sampler for dissolved gases, equipped with two additional ball valves (Swagelok type) for the water extraction by means of syringes (fig. 3.2 b). A forced introduction of water from a ball valve permits to fill the syringe at the other valve with lake water (piston effect). This TDIC sampling consists of the precipitation of lake water TDIC using $SrCl_2$ and NaOH solution at pH≈13 (e.g., Kusakabe et al., 1990; Bishop, 1990; Nojiri et al., 1993; Kusakabe et al., 2000; Zhang S. et al., 2009).

3.2 Analytical methods

Temperature, pH and electrical conductivity (EC) were determined using a multiparametric probe (AGEOTEC IM71), with extremely high accuracy, within the values of 0.005°C, 0.05pH units and 0.005 mS/cm^2, respectively.

The determination of major ions was performed in the laboratory by a Dionex DX 120 ion chromatograph (accuracy within 2%) using a Dionex CS-12A Ion Pac column for cations (Na^+, K^+, Mg^{2+}, Ca^{2+}) and a Dionex AS14A ion Pac column for anions (F^-, Cl^-, SO_4^{2-}).

The determination of minor and trace elements was carried out by inductively coupled plasma optical emission spectrophotometer (ICP-OES, Horiba Jobin Yvon equipment, model ULTIMA 2) except for Fe^{2+} and SiO_2 which were determined by molecular spectrophotometry (ICP-MS, Agilent 7500ce). The analytical errors for each element are shown in appendix (tab. A2 in appendix I).

D/H isotopic ratio in water was carried out using the Kendall and Coplen (1985) technique (reaction with zinc at 450°C), while $^{18}O/^{16}O$ analysis measurements were performed by CO_2-water equilibration techniques (Epstein and Mayeda, 1953).

The analytical device for hydrogen is a Thermo Delta XP CF mass spectrometer equipped with a TC-EA peripheral and interfaced with a CONFLO III device. $^{18}O/^{16}O$ ratios were measured with an AP 2003 CF-IRMS. TDIC amounts and carbon isotopic ratio were measured with a Finnigan Delta-S mass spectrometer. The isotopic results are reported in δ per mil units vs. V-SMOW standard and V-PDB standard for hydrogen, oxygen and carbon, respectively. The standard deviation of the measurements is about ±1‰ for D/H and ±0.2 ‰ for $^{18}O/^{16}O$ and $^{13}C/^{12}C$.

The ^3H water content (reported in Tritium Units, TU) was determined using electrolytic enrichment followed by liquid scintillation counting (standard deviation varies between ±0.6 and ±1.0 TU, depending on ^3H activity of the water samples).

The chemical composition of the dissolved gases were performed with a Perkin Elmer 8500 gas chromatograph with Ar carrier gas (He for Ar measurements) on a 4 m Carbosieve SII column and double detector (TCD and FID). The detection limits are 500 ppm vol. for O_2 and 1ppm vol. for CO and CH_4. The analytical error is about ±3% for all species.

The abundances and the isotopic values of dissolved He and Ne were measured in a split-flight-tube mass spectrometer (Helix SFT) equipped with a purification line, for the separation of noble gases from the gaseous mixture. A quadrupole mass spectrometer was used for measurement of $^4He/^{20}Ne$ ratio. Ion beams of $^3He^+$ and $^4He^+$ were simultaneously detected by a double collector system, which keeps the error in isotopic ratios within 0.5 % of

measurement. Purified atmospheric helium was used as a running standard. $^{3}He/^{4}He$ ratios (R) were determined against an air standard and are expressed relative to the atmospheric ratio (1.39×10^{-6}) as R/Ra. The overall uncertainty of R/Ra is ± 2% of the value. ^{36}Ar and ^{40}Ar were measured in a multicollector mass spectrometer (Argus).

The carbon and hydrogen isotope analysis of methane were determined by a Delta Plus XP CF-IRMS instrument (Thermo, Bremen, Germany) coupled with a TRACE 2000 GC equipped with a Poraplot-Q (Superchrom) capillary column (30 m x 0,32 mm i.d.) and using a helium flux as gas carrier. GC III combustion interfaces were used to produce carbon dioxide from methane. High-temperature conversion (GC-TC interface) provides on-line methane conversion into hydrogen gas suitable for isotope analyses.

All sampling and analytical devices were provided by the Istituto Nazionale di Geofisica e Vulcanologia (INGV), section of Palermo. The tritium concentrations was carried out in the laboratories of Instituto Tecnológico e nuclear (ITN) of Sacavém (Portugal).

4.0 Results and discussions

4.1 Physical-chemical parameters

Temperature, pH and electrical conductivity are key parameters, which are able to promptly provide significant features of lake waters. We acquired those parameters along vertical profiles (at the sampling points of figure 3.1) by means of a high resolution multiparametric probe.

The water temperatures of LPM and LGM show a clear influence of seasonality on shallow layers due to the variation of air temperature and solar irradiance. Both lakes show the typical thermal stratification: epilimnion, thermocline and hypolimnion (Wetzel, 2001). Furthermore in LPM, from about 15 m of depth towards the bottom, we observed the same increase of temperature (about 2°C), unchanged between September 2008 and June 2010 (Fig. 3.1 a). This fits well with the results of previous investigations (Chiodini et al.,1997 and references therein), confirming a constant heat flux from the bottom of LPM and the presence of a monimolimnion below 15 m of depth.

The thermal stratification of LGM suggests the possibility of the typical water movement: water mixing in cooler periods and water stratification in summertime (Wetzel, 2001) (for details see section 4.2).

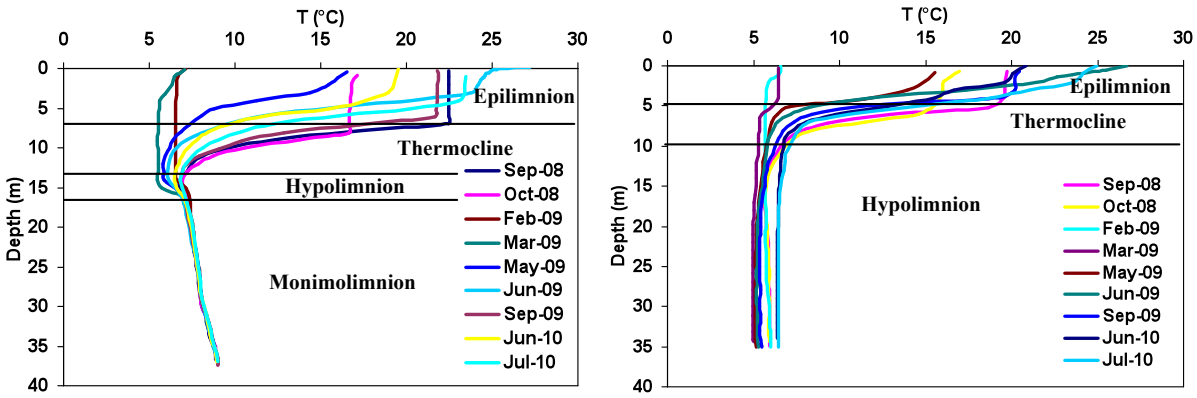

Figure 4.1 - Plots of temperature versus depth for LPM (a) and LGM (b), from September 2008 to July 2010. The thermal stratification is shown; the limits between thermal layers (i.e., epilimnion, thermocline and hypolimnion) change from month to month, so border lines are approximate. The error on the temperature datum is within the profile sign.

The profiles of electrical conductivity (EC), with depth, in LPM are stable during the observation period with values of 0.4 mS/cm^2 from the surface to the depth of 14 m. Between 14 and 16m occurs a sharp increase of EC up to 1 mS/cm^2, below 30 m the EC progressively increase from 1 to 1.6 mS/cm^2 (fig. 3.1 b).

In the LGM the EC is constant with depth for all sampling periods except for September and October of 2008 which showed an EC increase in the deep zone, near the error bar.

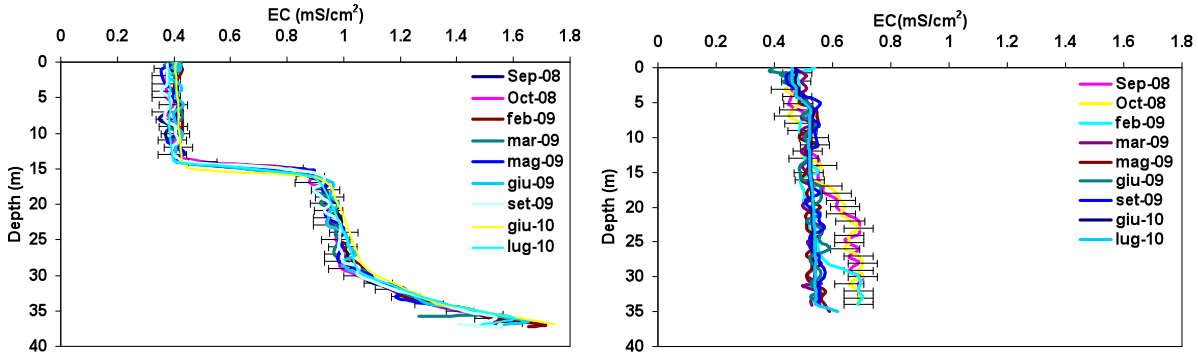

Figure 4.2 - Plots of electrical conductivity (EC) versus depth for LPM (a) and LGM (b), from September 2008 to July 2010. To simplify the graph, the error bar is inserted only in one profile for each plot (from now on). All values are referred to 25°C.

The pH values measured in the shallow waters of LPM show seasonal variations (fig. 4.3 a). The pH displays a sharp decrease between 5 and 16 m. of depth, then it keeps almost constant with a moderate increase (within 0.2 pH units) near the lake bottom; these pH values range between 5.9 and 6.6, moving towards the lowest values during the summer. The shallow part of LGM (fig. 4.3 b) shows a similar behaviour to the LPM, with pH values varying with seasons; below the shallow waters the pH displays a sharp decrease down to about 5 metres, then a more regular decrease towards the lake bottom is shown. In cold periods the LGM values between deep and shallow layers are more homogeneous than in hot periods (the pH variations are also discussed in carbonate system chapter).

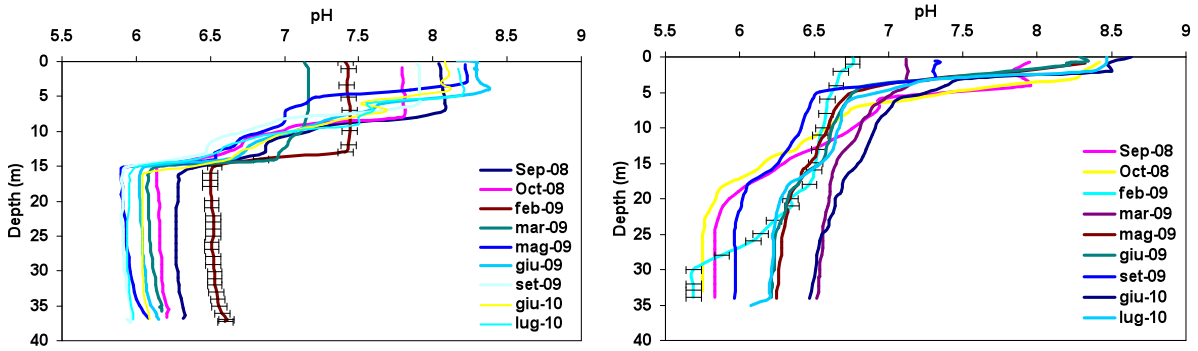

Figure 4.3 - Plots of pH versus depth for LPM (a) and LGM (b), from September 2008 to July 2010.

Despite the surface waters of Monticchio lakes are in contact with atmosphere, the pH values (up to 8.6) are higher than that in air saturated water (pH=5.6). The range of pH variation depends on the amount of carbon dioxide released or consumed, and on the buffering capacity of the water. An important mechanism that controls the pH of surface waters of Monticchio lakes is the photosynthesis (Schettler and Albéric, 2008). This process reduces the amounts of

dissolved carbon dioxide resulting in an increase of water pH and in the shift of dissociation equilibria. Above pH 8.5 the concentration of CO_3^{2-} increases significantly and favourable conditions for carbonates precipitation are established (Wetzel R.G., 2001; O'Sullivan and Reynolds, 2003; see also carbonate system).

pH in deep waters of LPM is controlled by speciation of carbonate species (see section 4.3). Simulations with PHREEQC code show the saturation with siderite below 18 m (high content of Fe was found in the sediments by Schettler and Albéric, 2008). The probable precipitation of siderite would shift the solution pH to lower values (Kusakabe et al. 2000) as follow:

$$Fe^{2+} + HCO_3^- \rightarrow FeCO_3 + H^+$$

4.2 Water chemistry

4.2.1 Major elements

The water chemistry of Mt. Vulture is widely treated in literature (e.g. Barbieri & Morotti, 2003; Gambardella et al. 2006; Paternoster et al., 2009), but only a few data of Monticchio lakes water chemistry were published (Cioni et al. 2006 and references therein; Schettler & Albéric 2008).

In the LPM distribution of cations and anions shows a high variability with depth, but constant amount over time. Calcium has a higher spatial variability compared to Mg, Na and K, in a decreasing order; the highest Ca concentrations can be found in the deepest portions, where water is more acidic. The temporal variability is low, suggesting negligible mixing processes (fig. 4.4 a, b; Fig. 4.5 b).

The LPM waters show high concentrations of bicarbonate, which decrease from bottom to surface in favour of an increasing of chloride and sulphate (fig. 4.5). The deep waters of LPM have concentration unchanged over time. Between the depth of 12 and 18 m, a weak, but quick increase of SO_4 highlights the oxic-anoxic boundary layer.

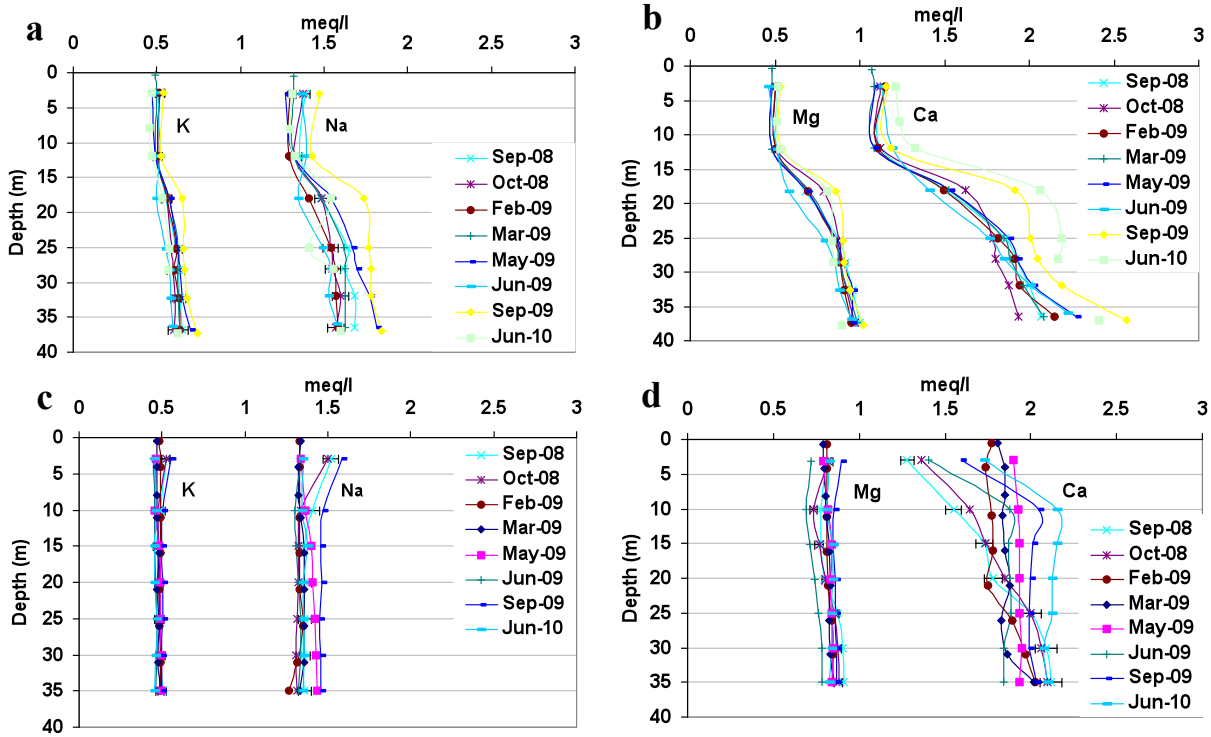

Figure 4.4 - Vertical concentration profiles of major cations in LPM (a, b) and LGM (c, d).

In the LGM the calcium has the greatest spatial variability, due to its unconservative nature, but this happens only in periods of stratification (from June to November). In these months the trend of samples shows a decreasing of Ca, from depth towards surface (fig. 4.4 and fig.

4.5 b). The other cations have a low or null variability both with depth and time (fig. 4.4 c, d). The waters of LGM show a decrease of HCO_3^- towards the bottom, due to the pH decrease and the consequent repartition of the carbonate species in favour of the $CO_{2(aq)}$ (appendix III).

The distribution of cations and anions in Monticchio lakes can be well explained by their dependence on availability and chemical exchange capability. Obviously, both the conditions are dependent on water-rock interactions, minerals precipitation and biological processes. In natural waters, magnesium, sodium and potassium are relatively conservative due to their low chemical reactivity and their small biotic requirements. The HCO_3^- is the main anion in Monticchio Lake waters, followed by chloride and sulphate (fig. 4.5). The cationic ternary diagram (fig. 4.5 b) shows the low relative amounts of Mg compared to Ca and Na+K, for both lakes; the deep waters of two lakes have similar concentrations.

Calculates using PHREEQC code indicated the oversaturation of dolomite and calcite for LPM and LGM. The precipitation of these minerals, in different proportions for the two lakes, could explain the different chemical evolution of shallow water of the two Monticchio lakes from a similar groundwater (fig. 4.5 b); a prevalent decrease of Ca and Mg in LPM and of Ca in LGM. The Monticchio lakes waters are mostly of HCO_3^- - Na^+ - Ca^+ type.

The ionic ternary diagrams (fig. 4.5 a, b) also show that lake waters fall in the range of ground waters of Mt. Vulture, with the exception of few shallow water samples of LGM. The cationic concentrations move away from local rocks composition (red line field fig. 4.5 b).

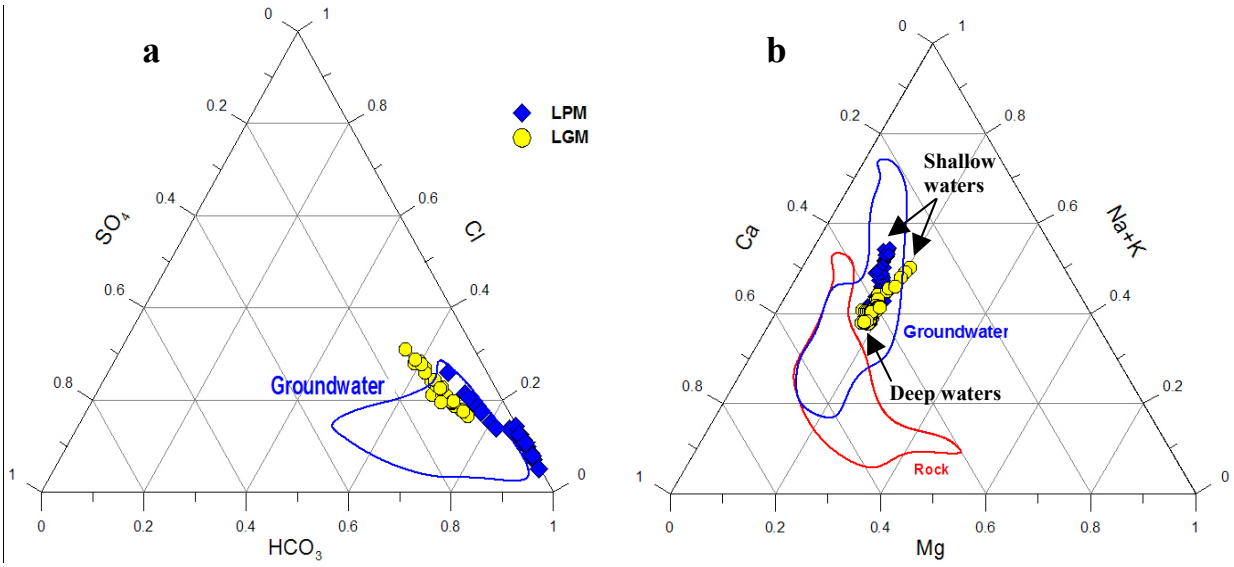

Figure 4.5 - Ternary plot of relative HCO_3, SO_4 and Cl contents (a) and Mg, Ca and Na+K contents (b) in Monticchio lakes waters. The blue and red line circumscribes the range of groundwater and rock composition, respectively (from Gambardella et al., 2006).

The Monticchio lakes are affected by intense biological activity (Robinson, 1994; Mancino et al., 2009), which is able to modify the water chemistry of the lake water (e.g., Brakke et al.,

1987; Van Loon and Duffy, 2005). Our data are characterized by a charge imbalance of major elements, with an excess of positive (cationic) charge (figure 4.6). In our opinion it could be caused by organic acids in solution, as often observed in natural waters (Oliver et al., 1983; Eshleman and Hemond, 1985; Brakke et al., 1987; Tipping et al., 1991; Tipping, 2002; Van Loon and Duffy, 2005) (see also appendix I). The difficult evaluation of organic matter contributes in the water chemistry certainly outsides the aims of this work.

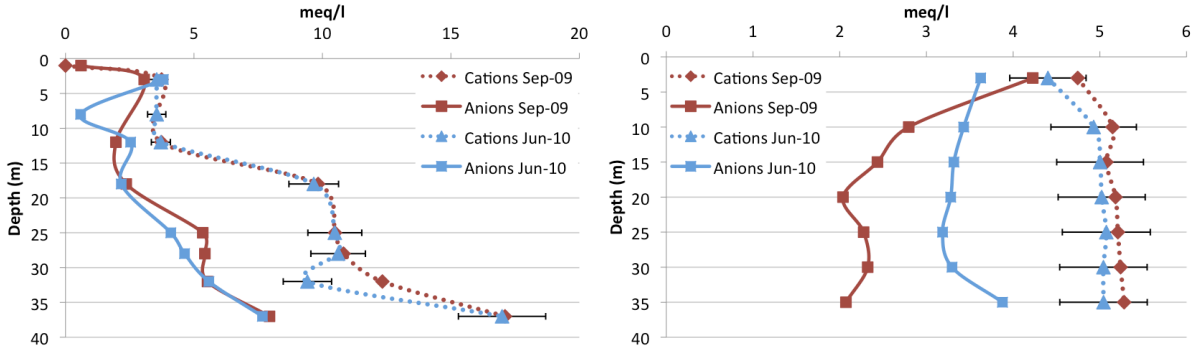

Figure 4.6 - Concentration of cations and anions with depth for LPM (a) and LGM (b), for the month of September 09 and June 10. In the deepest waters the unbalance is close to 54% in LPM and variable from 60 to 23% in LGM.

4.2.2 Trace elements

Both concentration and vertical distribution of trace elements are different between the two lakes (fig. 4.7, 4.8; tab. A2 in appendix I). A first distinction can be made on the basis of vertical distribution; three groups of trace elements are noticed: i) those with low concentrations in epilimnion, but with an increasing concentration towards the bottom (hypolimnion); ii) those with relative high concentration values in epilimnion and a concentration decreasing in the hypolimnion; iii) the trace elements with low variations with depth (fig. 4.7 and 4.8). There is a good correspondence between the behaviour of these three groups of trace elements in the two Monticchio lakes, but in the LPM the distinction appears more evident than in the LGM.

In the LPM, Si, B, Al, Ti, V, Cr, Fe, Mn, As, Se, Rb, Sr, Cs and Ba concentrations, have the same variation with depth as Co. In addition to the Mo, Cu also has lower concentrations in hypolimnion compared to the epilimnion (shallow waters). Finally, Zn and Pb have a less regular distribution and less defined in time. The peculiarity of this lake is the good agreement of data of samplings that are two years apart, in particular for the first two groups of trace elements.

In the LGM, the general behaviour of the analyzed trace elements is similar to that discussed for the LPM, even if in September 09 and June 10 there was a considerable flattening on

concentration differences between epilimnion and hypolimnion, for all elements. The trace elements concentrations of both lakes are within the range of values of Mt. Vulture groundwater (data from Parisi 2010), but some important exceptions are noted (fig 4.9).

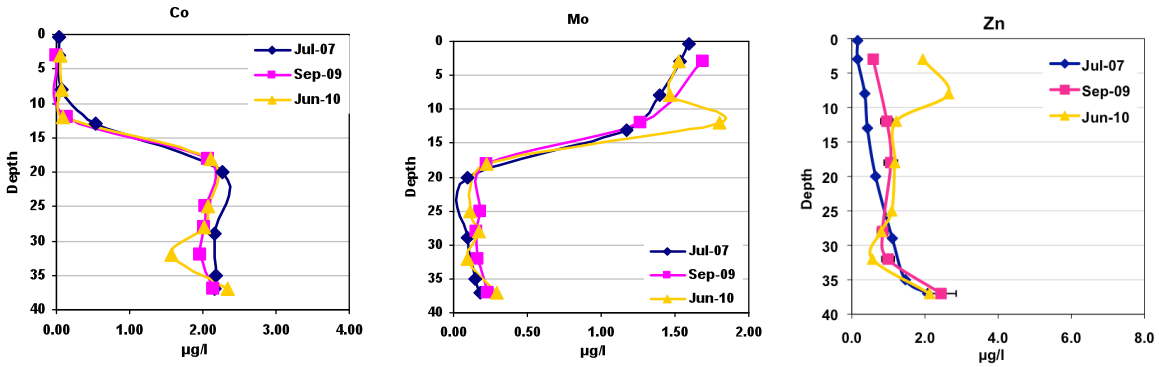

Figure 4.7 - Vertical distribution of Co, Mo and Zn in the LPM, for three different periods (Jul-07, Sep-09, Jun-10). These elements are representative of the three behaviour categories (see text). Data of July-07 result from a sampling campaign preceding the doctorate period.

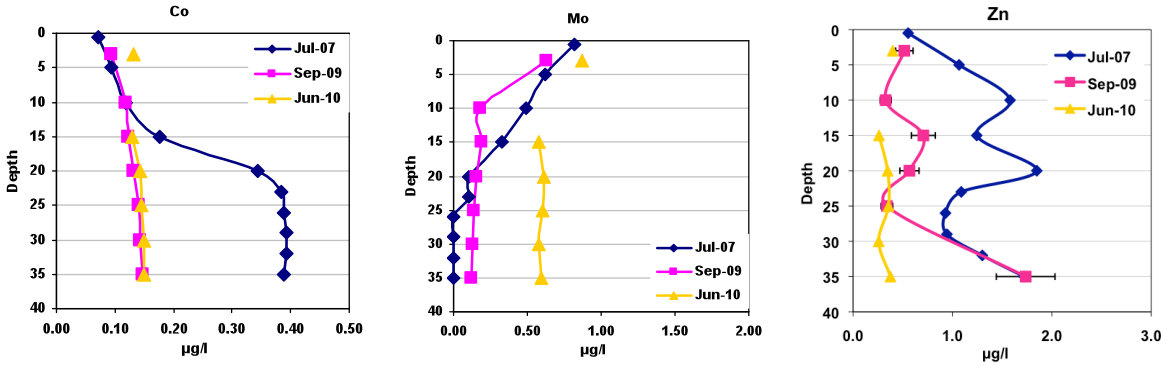

Figure 4.8 - Vertical distribution of Co, Mo and Zn in the LGM for three different periods (July-07, September-09, June-10). These elements are representative of the three behaviour categories (see text). Data of July-07 result from a sampling campaign preceding the doctorate period.

In the epilimnion of LPM the As, Co, Pb and Se have concentrations lower than groundwater values. Instead, the meromictic zone has higher concentrations of Ba, Fe and Mn and lower concentrations of Cu, Pb and Se (fig. 4.9).

In the epilimnion of Lago Grande there are lower concentrations than Mt. Vulture groundwater for As, Co, Cu, Pb and Se and higher only for Mn. The hypolimnion reaches higher values of Ba and Mn.

Assuming that lake waters derive from groundwater, because similar in chemical composition (see major elements), many trace elements suggest that shallow and deep lake waters are subject to inside lake enrichment/impoverishment processes.

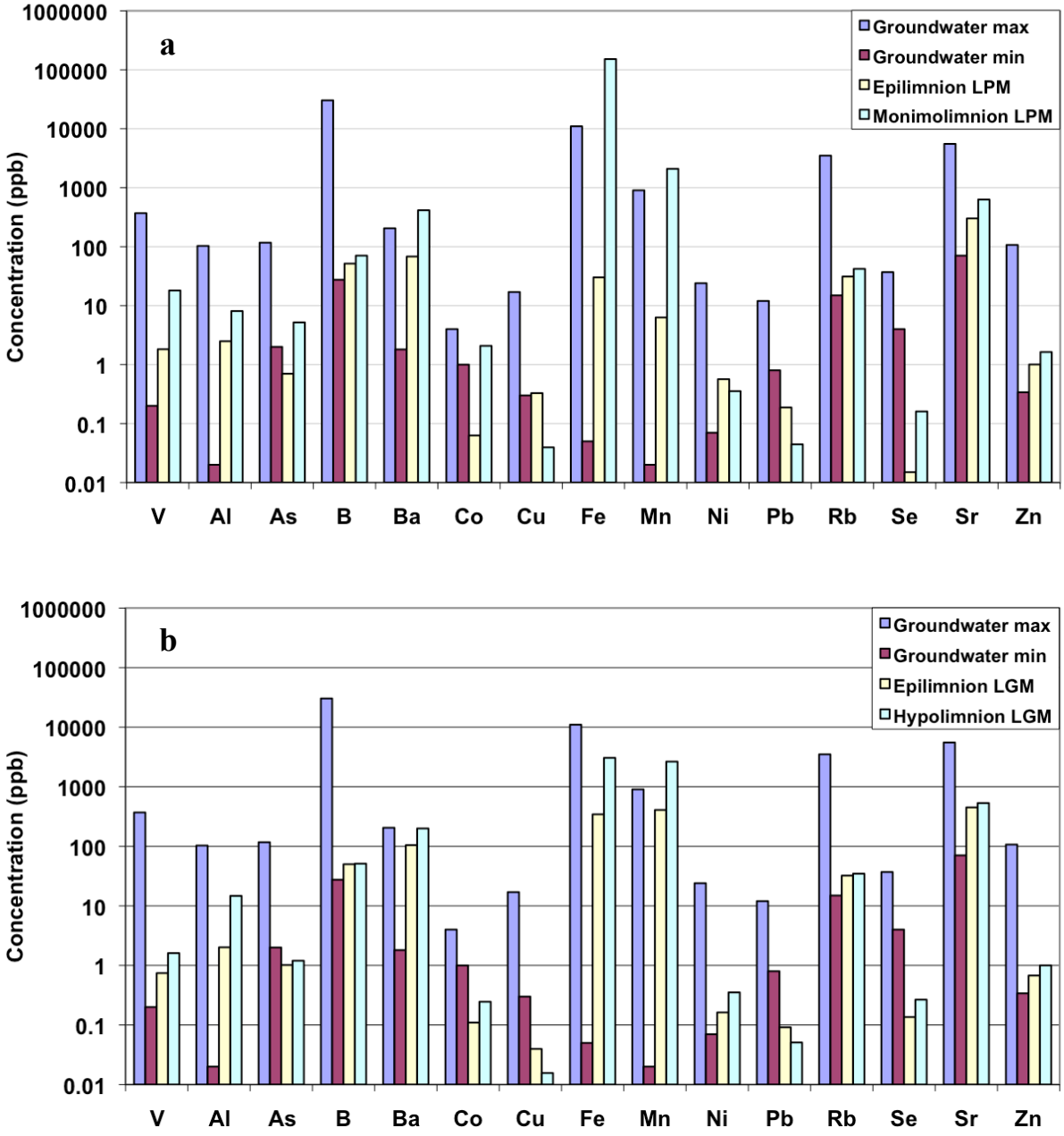

Figure 4.9 - The mean values of trace elements in epilimnion and monimolimnion of LPM (**a**) and epilimnion and hypolimnion of LGM (**b**), compared to minimum and maximum concentrations in groundwater (groundwater data from Parisi, 2009)

4.2.3 Total Dissolved Solids

The total dissolved solids (TDS) of springs and wells of Mt. Vulture show an interesting correlation with altitude (fig. 4.10). Broadly, the waters of springs and wells of high elevation have relatively low TDS values probably due to low residence times in the aquifer. Decreasing the altitude of springs and wells so increase the variability on TDS values (fig. 4.10); this could be explained by a water feeding by groundwater both of superficial or deep aquifer, with less or more residence time, respectively. Effectively it seems clear that the

content of TDS of water is indirectly linked with residence time in the aquifer and so with water-rock interaction time.

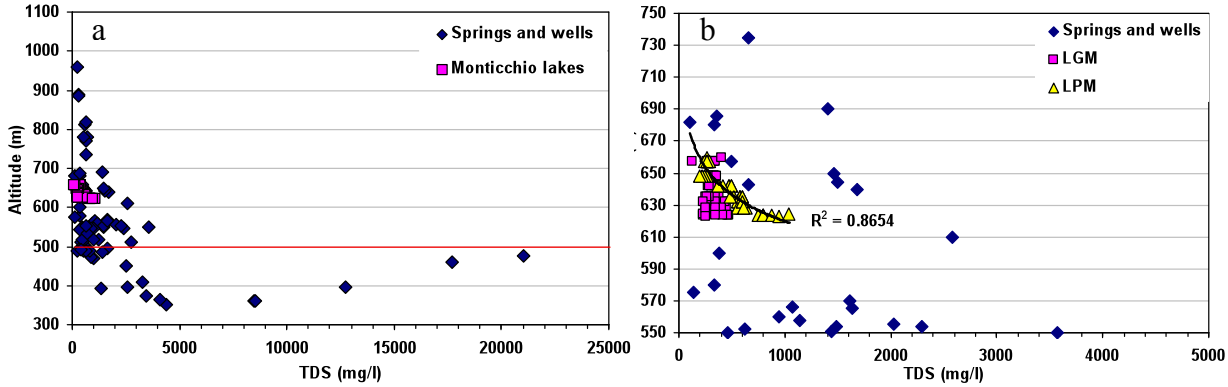

Figure 4.10 - Plots of TDS vs Altitude of springs and wells waters of Mt. Vulture and Monticchio lakes waters. Mt. Vulture data from Paternoster (2005) and Parisi (2010).

The TDS vs altitude plot shows a sudden increase of values and a high dispersion of data below the altitude of 500 meters. Below this elevation the sedimentary rocks crop out and hence more soluble components may be leached out in comparison with volcanic rocks; the last are ubiquitous above about 500 meters of altitude (fig. 4.11).

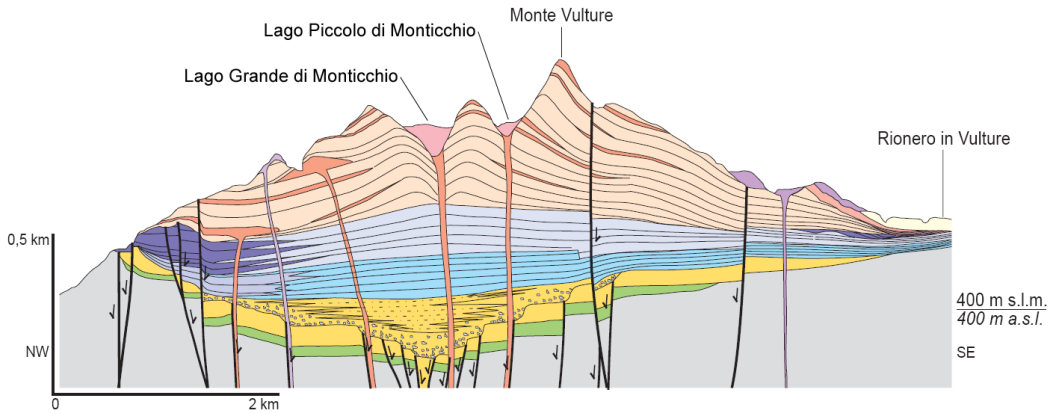

Figure 4.11 - Geological section of Mt. Vulture (modified by Giannandrea et al. 2006). The sedimentary rocks (surfacing below ~ 500 m a.s.l.) are in grey; all the others colours represent the volcanic rocks.

An additional factor that can increase the dissolution of aquifer rocks is the presence of CO_2 in solution (see also section 4.3); this gas is largely present in the whole area of Vulture, preferentially in the waters of deep aquifers. However, the possibility that shallow groundwater can be reached by deep CO_2 can not be ruled out, thanks to deep faults (i.e., short-circuit pathways between groundwater of different depths) or by multistep degassing in deep aquifer (the gas phase can dissolve in shallow groundwater).

In this hydrogeochemical setting the waters of Monticchio lakes perfectly fall in the TDS range of the groundwater of equal elevation (fig. 4.10 b). The distribution of data depends on the depth of lakes waters; the shallow waters have a lower content of TDS, the deeper ones a higher content. In the LPM, which is permanently stratified, the correlation between TDS and altitude coincides with the relation found for groundwater of Mt. Vulture with $R^2 = 0.86$. Moreover, the lakes deep waters are the richest in dissolved CO_2. That being so, once more the geochemical data show a clear relation between lake waters and groundwater.

4.2.4 Isotopes and water evaporation

In δD vs $\delta^{18}O$ graph (fig. 4.12), the deep waters of LPM fall on local meteoric water line (LMWL - Paternoster et al., 2008, see also appendix II), whereas shallow waters of the LPM, and all waters of LGM, show a linear relationship with a typical evaporative slope (fig. 4.12). For each lake, the shallow waters have a higher evaporative shift if compared to deeper waters. This is true to form and in accord with Mongelli et al. (1975) and Marini (2006). Moreover, isotopic data show that LGM has a higher evaporation than LPM (fig. 4.12).
Mongelli et al. (1975) drew an evaporation line on the base of 15 data (from LPM, LGM and springs). Marini (2006) updated the evaporation trend by using data of Mongelli et al. (1975) and data of spring by Ciet and Tazioli (1981), with a total amount of 30 water samples. In this work, the abundance of data (over 130 samples, of LPM and LGM, which are spread over 11 sampling campaigns from 2006 to 2010) permitted to better define and update the evaporative linear relation (fig. 4.12):

$$\delta D = 5.2\delta^{18}O - 8.3 \qquad \text{Mongelli et al. (1975)}$$

$$\delta D = 5.36\delta^{18}O - 7.8 \qquad \text{Marini (2006)}$$

$$\delta D = 4.59\delta^{18}O - 14.0 \qquad \text{this work}$$

$$\delta D = 4.60\delta^{18}O - 13.82 \qquad \text{this work plus Mongelli et al. (1975)}$$

As shown in fig. 4.12, the data of Mongelli et al. (1975) fall close on the trend of this work, but always slightly above the linear regression. Using our data together with the data of Mongelli et al. (1975), the resulting evaporative linear regression is roughly the same than that one obtained with our data (see above equations). Anyway, we are not ruling out that evaporative process in Monticchio lakes was subjected to a small variation in about 35 years.
Indeed, the linear regression of our data (fig. 4.12) does not represent an actual evaporation, rather it is a mixing line between surface waters (more or less evaporated) and groundwater. In fact, it is difficult to believe that deep waters (below the epilimnion, e.g., 10, 15, 20 m) can be directly involved in an evaporative process (proper of under air conditions)

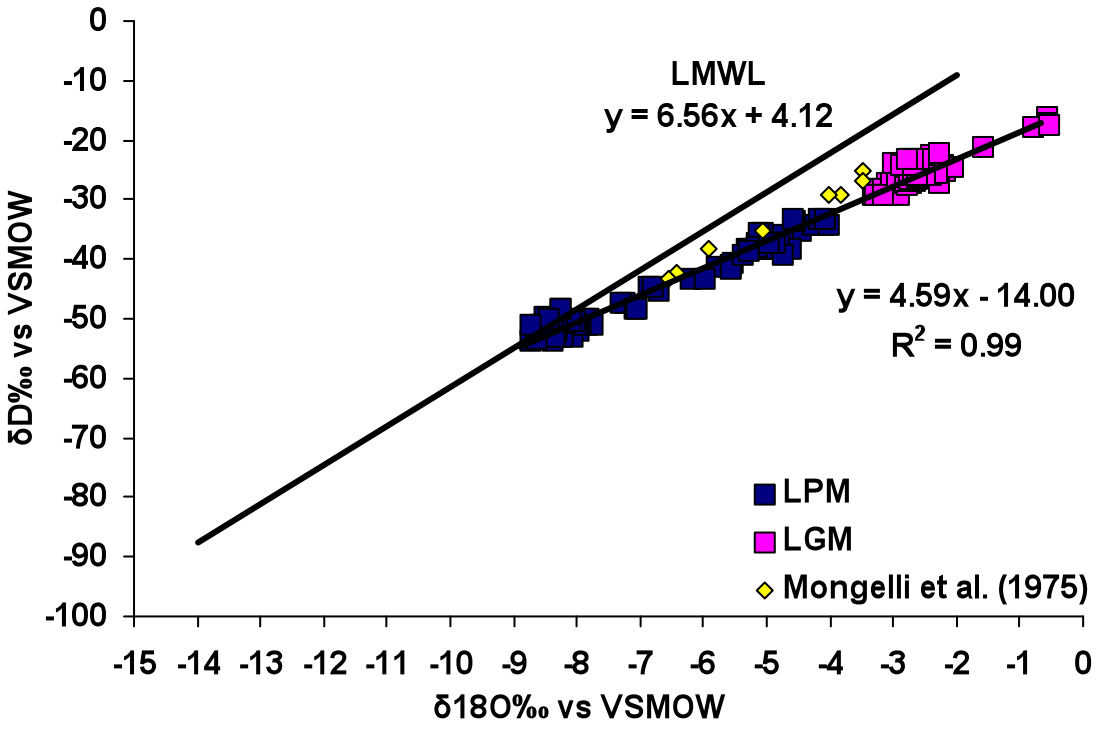

Figure 4.12 - δD vs. $\delta^{18}O$ plot for Monticchio lakes waters. Most of the samples fall on the evaporation line (y = 4.59x-14.0). The data of Mongelli et al. (1975) are very close to evaporation line built with our data. The local meteoric water line (LMWL) was defined by Paternoster et al. (2008) (see appendix II).

The isotopic composition of lake waters is plotted against depth in figure 4.13. The relative behaviour of δD and $\delta^{18}O$ is the same. Both isotopes highlight that deep waters of LPM have a low variability in time and are within the isotopic range of groundwater (fig. 4.13). The shallow waters (down to 12m depth) have small variations due to the change on evaporation rate. The deep waters of LGM are close on more positive and evaporated values than LPM (Fig. 4.12, 4.13), they show a slight variability in time. The shallow waters of LGM do not move much away from deep water values and have a more elevated variability in time, reflecting variability of evaporation rate.

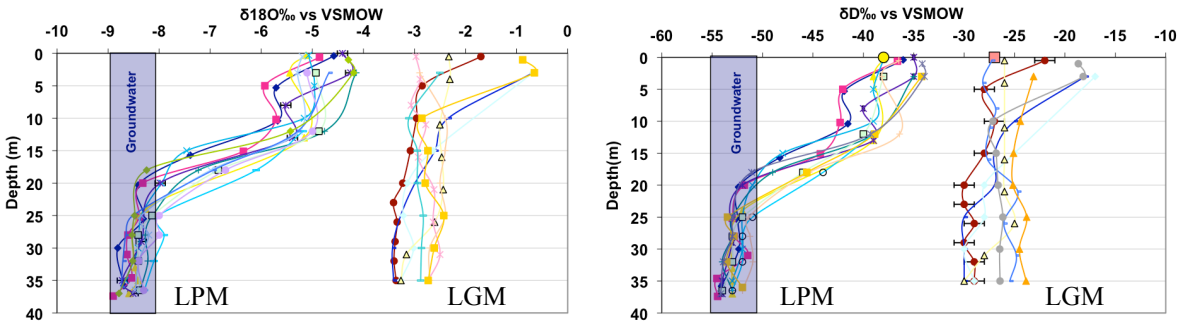

Figure 4.13 - Isotopic data of δD and $\delta^{18}O$ versus depth of LPM and LGM. The shaded area represents the groundwater isotopic values near the Monticchio lakes (see also fig 4.11).

In this isotopic distribution the water dynamics characterize the distribution of values, as we shall see in section 5.2. Nevertheless, the time regularity of the mixing processes and the constancy of groundwater inflow allowed LGM to reach a dynamic equilibrium, which is less stable for shallow waters due to the variability on the evaporation rate.

The intersection of LMWL with evaporation line gives $\delta^{18}O$ = -8.8‰ and δD = -54‰; they can be considered the mean values of groundwater feeding the lake. Since the isotopic shift of groundwater in comparison to the meteoric values is negligible (Paternoster et al., 2008), it is possible to evaluate the recharge altitudes of Monticchio lakes waters by means of linear regressions (isotopic value of rainfall versus altitude) proposed by Paternoster et al. (2008). These authors, using the data of Mongelli et al. (1975), firstly estimated the recharge altitude of LPM of about 1130 meters a.s.l..

The mean recharge altitudes estimated with our data are about 894 and 952 meters for $\delta^{18}O$ and δD, respectively. These values are reasonably coinciding (considering an error of about 50 m over each estimation) and a mean recharge altitude of about 925 meters can be considered (Monticchio lakes are located at 660 m a.s.l.).

Also in this case the abundance of data permits us to better define the mean recharge altitude of Monticchio lakes.

4.2.5 δD vs. Chloride

The isotopic data of lakes waters (see section 4.2.4) show that LPM is fed by groundwater and that shallow waters are subjected to an evaporative process.

A water body exposed to the atmosphere, under ordinary conditions, will become enriched in the heavy water species ($^{1}H^{1}H^{18}O$, $^{2}H^{1}H^{16}O$) rather than the more common and light water specie ($^{1}H^{1}H^{16}O$); so fractionation between water and atmospheric vapour during evaporation occurs. This fractionation is affects by atmospheric conditions, including relative humidity, temperature and the isotopic composition of atmospheric moisture. The water stable isotopes were widely used in lake environments for evaporation study. The main applications concern the isotope-mass balance (e.g., Gonfiantini 1986; Gibson et al. 1996; Saxena et al. 1999; Gibson 2002).

The isotopic composition of a water body from which the water is removed only by evaporation can be described by the formulation of Rayleigh type distillation (Longinelli & Deganello, 1999):

$$\delta - \delta_0 = -\varepsilon \ln f \qquad (4.2.5\text{-}1)$$

where δ and δ_0 are the final and initial isotopic composition of the water, ε is the isotopic enrichment factor between the two considered phases (in our case between water and vapour phases) and *f* is the volumetric residual fraction of the water. This theoretical formulation does not consider the atmospheric conditions (e.g., relative humidity and isotopic composition of moisture), therefore this formula has applicability limits on a natural environment.

Craig & Gordon (1965) and Gonfiantini (1986), studied and theorized the evaporation of free water body to atmosphere and described the variation of the isotopic composition of an evaporating water body as:

$$\delta_0 = \left(\delta - \frac{A}{B}\right) f^B + \frac{A}{B} \tag{4.2.5-2}$$

$$A = \frac{h\delta_a + \varepsilon k + \frac{\varepsilon}{\alpha}}{1 - h + \varepsilon k} \tag{4.2.5-3}$$

$$B = \frac{h - \varepsilon k - \frac{\varepsilon}{\alpha}}{1 - h + \varepsilon k} \tag{4.2.5-4}$$

where *h* is the atmospheric relative humidity ($0 \leq h \leq 1$), δ_a is the isotopic composition of atmospheric moisture, εk is the kinetic isotopic enrichment factor and α is the equilibrium fractionation factor ($\varepsilon = (\alpha\text{-}1) \times 1000$). A mean annual relative humidity of 0.8 (80%) was used (see section 5.1 and fig. 5.3), anyway a variation of 10% of relative humidity does not affect much the result of computation. The δ_a values were estimated on the basis of assumed isotopic equilibrium between atmospheric moisture and precipitation (Gibson et al., 2008 and reference therein) as follows:

$$\delta_a = \frac{\delta_p - \varepsilon}{\alpha} \tag{4.2.5-5}$$

where δ_p is isotopic value of precipitation. The εk (in ‰) can be evaluated with relationships presented by Gonfiantini (1986): εk (^{18}O) = 14.2 (1 - *h*); εk (^{2}H) = 12.5 (1 - *h*).

The evaporation process not only modifies the water isotopic signature, but also influences the saline content of residual water. The increase of ionic concentration is inversely proportional to the volumetric residual fraction of water (*f*). Linking the residual fraction, obtained by isotopic formulations, with ionic content is possible to better constrain the evaporative process that occurs in lake waters. For this purpose was chosen the chloride concentration, because this is a conservative ion that does not participate much in geochemical and biochemical processes. The formulation that links volumetric residual fraction with chloride is the follow:

$$Cl = \frac{Cl_0}{f} \qquad (4.2.5\text{-}5)$$

where Cl is the chloride concentration at the end of evaporative step and Cl_0 is the initial chloride concentration.

In the isotopic modelling of evaporation, deuterium rather than ^{18}O was used because the first one is less subject to chemical interactions that can increase the interpretation difficulty.

Since the LGM has, even in deeper layers, more evaporated waters then LPM (fig. 4.12), firstly we check the possibility that shallow waters of LPM flow towards LGM, through the connecting channel between the two lakes, and continue the evaporative process in the LGM as suggested by Mongelli et al. (1975). As the fig. 4.14 shows, not only a pure evaporation is not able to produce the most values of shallow waters of LPM starting from groundwater, but also the entire shallow waters of LGM cannot derive from a simple evaporation of the groundwater or of the shallow waters of LPM.

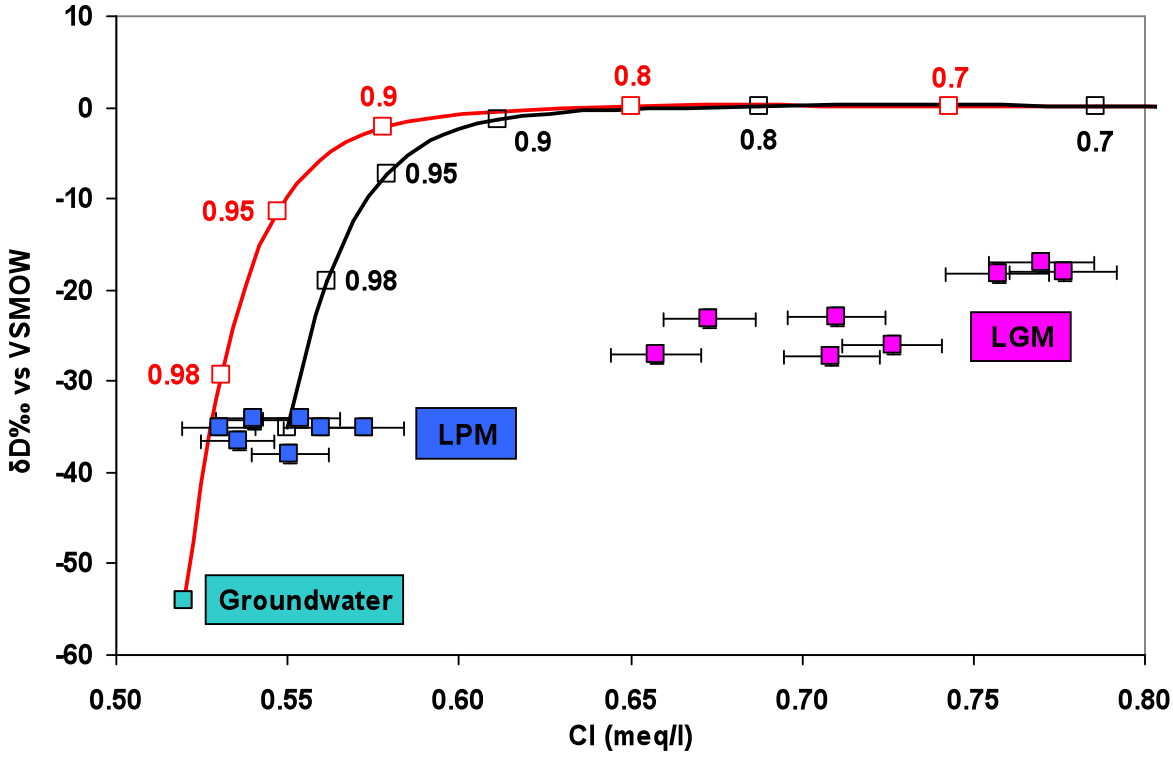

Figure 4.14 - δD versus Cl plot; the groundwater was fixed at δD = -54‰ and Cl= 0.52 meq/litre; the values of LPM and LGM are referred to shallow waters (~3m of depth). The red and black curves represent the trend of the water values during an evaporation (using the equations in text) starting from a groundwater and a shallow water of LPM, respectively. The numbers along the curves show the residual fraction of water during the theoretical evaporation. The error bar of δD (± 1‰) for plotted values is within the symbol.

Therefore there is the necessity to set up a more complex theoretical scheme to explain the deuterium and chloride values in the shallow waters of Monticchio lakes.

The evaporating water of the lakes is localized in the epilimnion, the upper portions of a stratified lake, where lake waters are more chemically homogeneous and well mixed. A box model was applied to the chemical and isotopic balance of the epilimnion. The main inflow and outflow were considered:

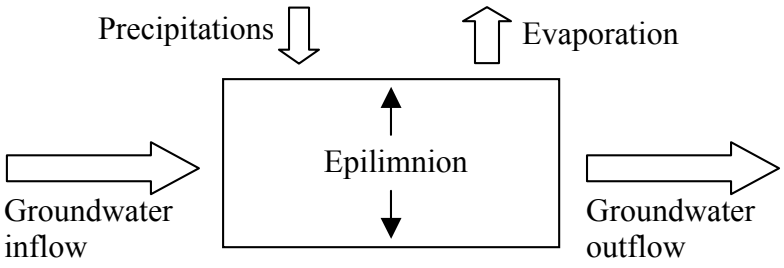

The isotopic and chemical data of lake waters confirm the chemical homogeneity of epilimnion and also consent to verify the nearly steady state of water chemistry in both lakes. This is a necessary condition to apply the box model.

The groundwater outflow does not affect the chemical data (δD and Cl) changing in the considered box, therefore this can be neglected (used chemical parameters have intensive characteristics). The rainfall on the surface of Monticchio lakes can be neglected because its amount is evermore lower than 2.7% of epilimnion volume (this percentage influence the final estimation within the error of data). That being so, the box balance of Monticchio lakes is more simplified because only the groundwater inflow and the evaporation are considered.

The starting water of the model is a groundwater, because this is the water that feeds the lakes (e.g., Chiodini et al., 2000; Celico & Summa, 2004; Paternoster et al. 2008); the following values of the starting groundwater were used: δD = -54 ‰; Cl = 0.52 meq/l. As discussed above, the deuterium value (-54 ‰) represents the intersection between the regression line of lake waters and the local meteoric water line (LMWL) (fig. 4.12).

The data of a well (three time sampled, see Pozzo Maria in tab. A1 - Appendix I) near the lakes (~300 m from LPM and LGM) has a chloride concentration between 0.51 and 0.53 meq/l, which well agree with data of springs and well water in the area (Paternoster, 2005 and Parisi 2009). The fixed value of chloride (0.52 meq/l) was also chosen considering that evaporating water of epilimnion has values always over this value (± 0.01), so the starting value of simulations have to be ≤0.52.

The box model takes into account that a constant groundwater inflow and evaporation are always present, so the chemical value is a result of the dynamic equilibrium of these two balance components. The calculation is based on a succession of evaporation and mixing with

groundwater. Any simulation reaches a steady state value that can be roughly considered the theoretical value of the epilimnion water.

Several simulations display that all values of shallow waters (~3 m of depth) of Monticchio lakes fall in plausible ranges both of evaporation and groundwater inflow (fig. 4.15).

As seen before, the simulations of theoretical model presume the attainment of an isotopic and chemical steady state. The data of February and March of 2009 cannot be plotted in figure 4.15 because in these periods the mixing of lake waters does not allow a steady state condition.

The data, plotted in the theoretical grid (fig. 4.15), show that in LPM the highest groundwater inflow (over the 60%) occurs in the periods with highest evaporation (September and October with relatively low residual fraction, f = ~ 90%). In May and June the evaporation is relative low as the groundwater inflow (97-99% and 30-40%, respectively). Still in the plot of fig. 4.15, September 2008 and September 2009 have the same value (within the error bar) as for June-09 and June 2010, it suggest a seasonal variability of evaporation and groundwater inflow which is repeated in similar manner every year. For the LPM, unfortunately the nearness of groundwater contribute curves do not permits an accurate evaluation of relative groundwater inflow.

The figure 4.15 also shows that in LGM the residual fraction of evaporating water does not change much over time, it is always between 81÷88 %; is interesting that in June 2010 the evaporation is noticeably higher than June 2009. The interesting trend of LGM values highlights a seasonal variability in the groundwater inflow (between 30% and 50%). Moreover September 2008 and September 2009 samples have the same value of groundwater inflow (within the error bar) as for June 2009 and June 2010, suggesting that this parameter has an annual cyclic character.

Probably the groundwater feeding the epilimnion of Monticchio lakes is subject to little seasonal variations; the main variation involves winter and spring periods when rain and snow thawing (both with more negative isotopic values) lower the groundwater isotopic values (Paternoster et al., 2008).

The box model suggests that the mean annual deuterium value of superficial groundwater (~54%), used as inflow value, explains well the deuterium vs chloride data of all periods near to a steady state.

Taking into account the approximate nature of the method, however it is possible to assert that roughly, the LPM has bigger groundwater inflow compared to LGM, which has a mean evaporative rate greater than the LPM. These characteristics cause a major variability of

chemical and isotopic datum in the LGM and comparable values in the LPM over time. Furthermore, from the theoretical simulations of the model it was possible to show that waters of LGM, and in particular the shallow waters, have a considerable contribution from groundwater and do not derive only from waters of LPM that have been more evaporated, like until now believed (Mongelli et al., 1975; Chiodini et al., 2000; Celico & Summa, 2004; Paternoster et al., 2008). This model gives an approximate semi-quantitative estimation, anyway this is a good result considering the use of a small amount of data.

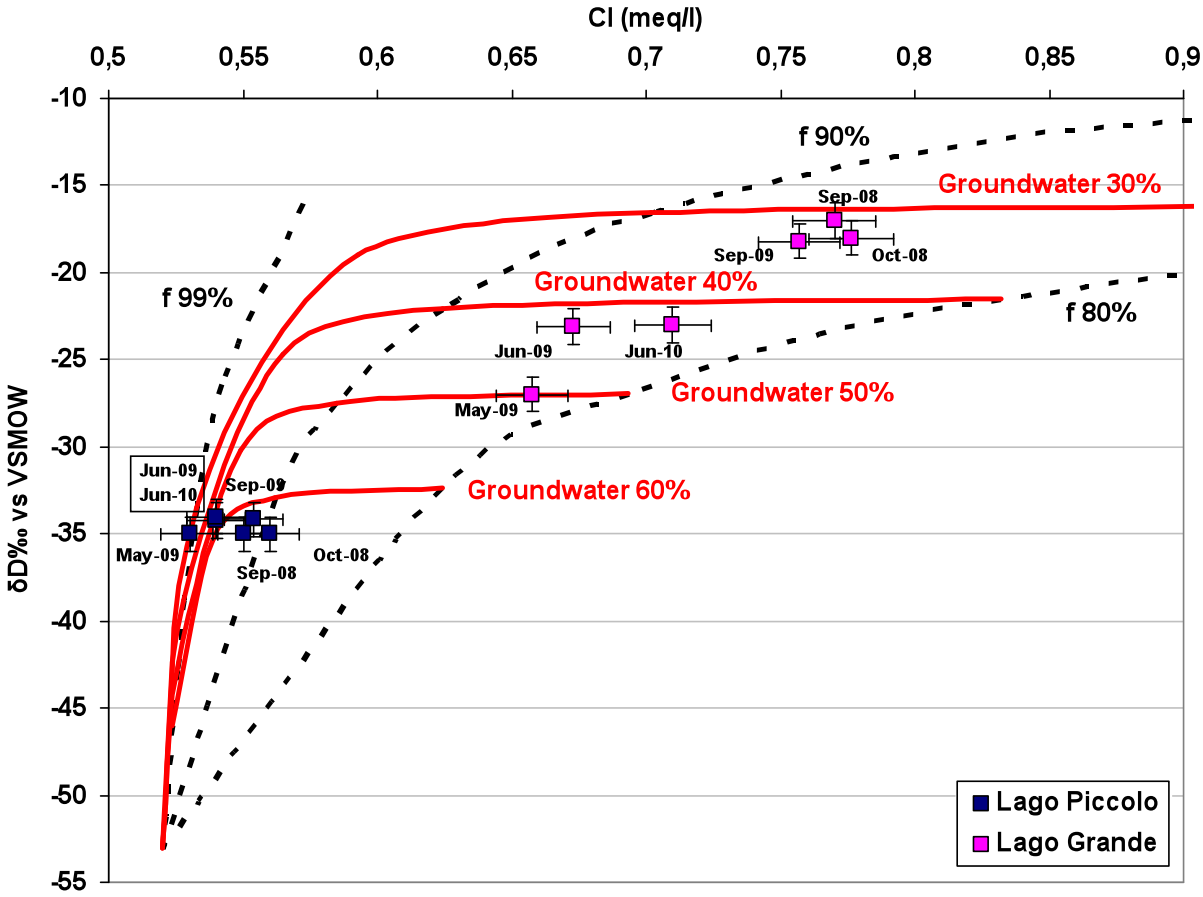

Figure 4.15 - δD versus Cl plot; the groundwater was fixed at δD = -54‰ and Cl= 0.52 meq/litre; the values of shallow waters of LPM and LGM are shown (~3m of depth). All the percentage values are referred to the box volume, which practically is the epilimnion. Each red curve is composed by the theoretical values of steady state with the same groundwater inflow (e.g., 30, 40, 50, 60%) and different residual fraction (*f*); each dashed curve is composed by the theoretical values of steady state with the same residual fraction (*f*) (e.g., 80, 90, 99%) and different groundwater inflow.

4.3 Carbonate system

4.3.1 Carbon dioxide

The dissolved gases in Mt. Vulture waters were mainly reported in recent literatures (e.g., Paternoster, 2005; Gambardella, 2006; Paternoster et al., 2009), but only the study of Gambardella (2006) deals with carbon species with a particular attention for the origin of dissolved CO_2. Many authors investigate the dissolved gases of Monticchio lakes with detail only for LPM (e.g., Fornai, 1992; Chiodini et al., 2000; Cioni et al., 2006; Caracausi et al., 2009).

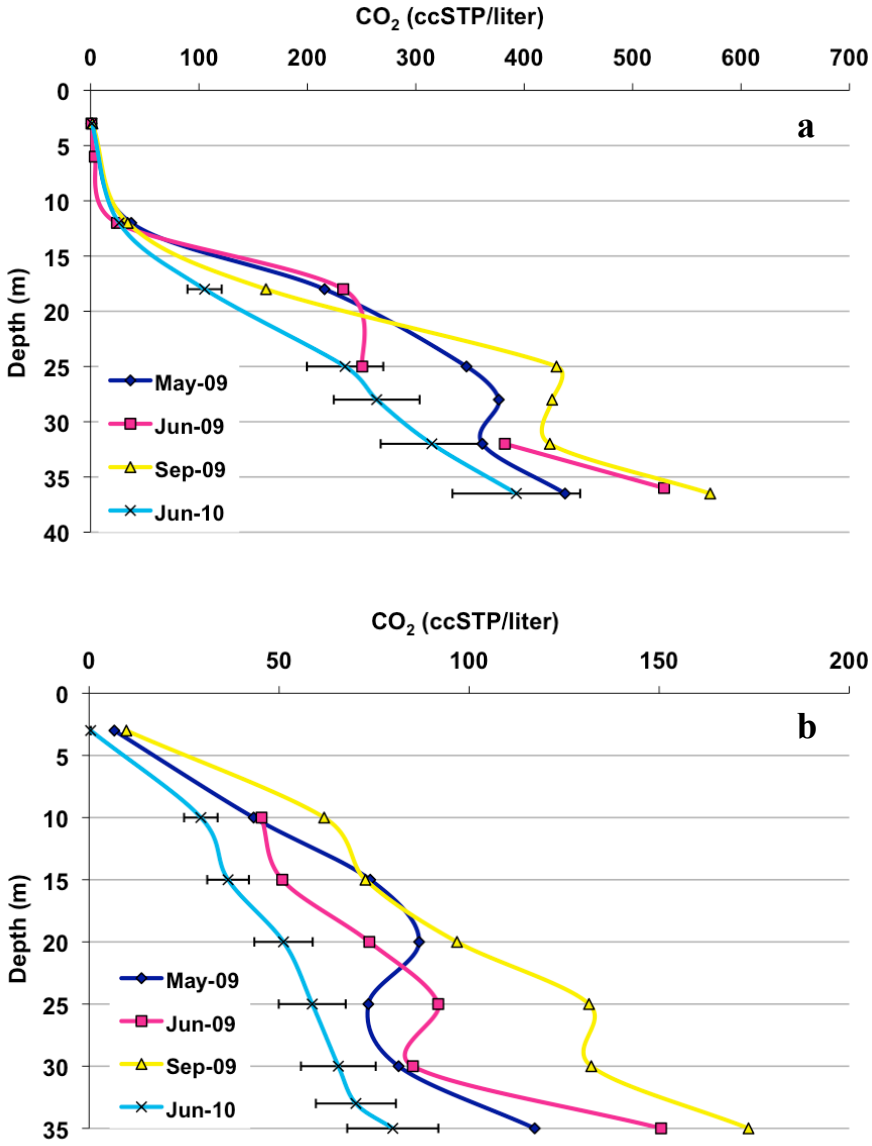

Figure 4.16 - Concentrations of dissolved carbon dioxide (cc STP/liter) versus depth (m) in LPM (a) and LGM (b). The inserts show the data of pH versus depth for the some months of CO_2 profiles.

The dissolved carbon dioxide (as H_2CO_3*) was evaluated on the basis of TDIC values and pH measured in situ by multiparametric probe (appendix III). The gradients of dissolved CO_2 concentration are normally high in both lakes (fig. 4.16). The near bottom water reaches a concentration of dissolved CO_2 close to three orders of magnitude (LGM) and over three orders of magnitude (LPM) higher than air saturated water ($H_2CO_3*_{ASW}$≈0.245 cc/l at 660 m a.s.l. and 25°C). Similar trends are shown by vertical distribution of TDIC.

In a CO_2-H_2O system the pH variations are related to carbonate speciation: high concentrations of dissolved CO_2 tend to reduce the pH values and vice versa. This behaviour is evident in the LGM (fig. 4.16 b) where with high variations of CO_2 concentration over time, the pH variations are well over the error range. In the LPM the pH and $CO_{2(aq)}$ variations, from month to month, are both very low, so the relation pH-dissolved CO_2 are less appreciable.

Ca and Mg carbonate precipitation has been inferred by means of PHREEQC code for shallow waters in both lakes. In fact, as mentioned in section 4.1, the superficial waters are involved in photosynthesis processes, which are able to increase the pH values, leading to conditions of carbonate oversaturation and precipitation (which sinks down to the lake bottom). Furthermore this process justify both the wide variations of Ca in shallow waters of LGM and the low concentrations of Ca and Mg of shallow waters of LPM in comparison to the deep ones (fig. 4.4 b, d; fig. 4.5 b).

The relative low pH values of deep waters (about below 15m for LPM and 20 m for LGM) give conditions of Ca and Mg carbonate undersaturation; therefore in the epilimnion the amount of TDIC is reduced due to carbonate precipitation. In agreement with Schettler & Albéric (2008), in LPM monimolimnion and LGM hypolimnion, increase in Ca, Mg and TDIC is related to a pH decrease, which favour dissolution of settling carbonate particles. Simulations with PHREEQC code suggest the oversaturation and probably precipitation of siderite, below 18 m (high content of Fe was found in the sediments; Schettler and Albéric, 2008).

When the probe was accidentally in contact with sediments the pH value sharply decreased. At this relatively low pH the settling carbonate particles could dissolve more rapidly near the lake bottom. This can represent a source of recycled CO_2 from bottom, in addition to the main carbon dioxide input from the external source, as observed in lake Cuicocha by Gunkel et al. (2009).

4.3.2 CO_2 and water rock-interaction

Gambardella et al. (2006) identified two families of groundwater in Mt. Vulture: i) TDIC > 500 mg/l, high CO_2 concentrations and low values of pH (5.4 < pH < 6.8) ; ii) TDIC < 500 mg/l, low CO_2 concentrations and high pH values (6.6 < pH < 8.3). In figure 4.17 it is possible to note that the lake water samples fall perfectly in the two families of Vulture waters but only the deep waters of LPM fall in the family with high CO_2 concentrations. Furthermore, this plot shows a good correlation between pH and $f\ CO_2$ suggesting that pH variations are mainly controlled by dissolved CO_2. In both lakes the pH values decrease as $f\ CO_2$ increases (fig. 4.17 a) down to a pH of about 5.8, when the pH remains almost constant in spite of both TDIC and $f\ CO_2$ increases; it suggests the possibility that a buffering process is acting.

The water acidification, which is induced by high f CO2, increases the acid attack power of water and consequently the rock dissolution. H^+ ions can be neutralized by hydrolysis of base cations (e.g.: Ca, Mg, K, Na), that are released by rock dissolution. The dissolution of most minerals that constitute volcanic rocks (e.g., Biotite, Kaolinite, Muscovite) starts below pH ≈ 6, so the abundant availability of base cations produces a pH buffering process (Fig. 4.17 b) (Stumm & Morgan, 1996). As a result, the dissolution of magmatic rocks buffers the pH of water, carrying in solution minerals more soluble in waters with pH < 6 (e.g. silicates, Fe and Mn minerals). The pH stop close to this value (~ 6) due to the equilibrium between: acidification by CO_2 and H^+ consumption by base cations. The acidification and the buffering mechanism cause an increase of TDS and electrical conductivity of water, as also observed in section 4.2.3 and in accord with the pattern suggested by Paternoster et al. (2009).

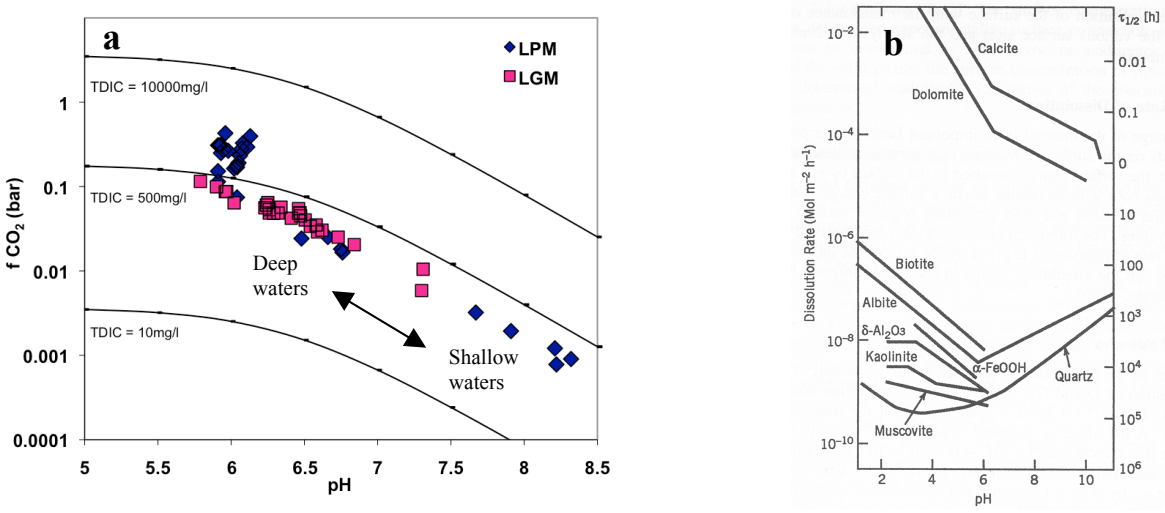

Figure 4.17 - a) Data relative to months of May, June and September of 2009. b) Dissolution rate of different minerals as a function of pH (25°C)(from Stumm & Morgan, 1996, modified).

4.3.3 TDIC isotopic composition

In the LPM the $\delta^{13}C_{TDIC}$ of shallow waters varies periodically (from -3.3 to 1.9 ‰ vs. PDB), but there is a general decrease towards the depth of about 15 meters. Below this depth, for all considered months, $\delta^{13}C_{TDIC}$ values increase towards the bottom (fig. 4.18). In LGM the $\delta^{13}C_{TDIC}$ values of shallow waters have a similar behaviour than LPM ones, instead in the hypolimnion waters the values are constant, with small variations from month to month (fig. 4.18).

All the Monticchio lakes values get close to the inorganic $\delta^{13}C$ range (from -7‰ to +4.5‰ vs. PDB, e.g., Allard et al., 1997; Chiodini et al., 2000; Caliro et al., 2008; Caracausi et al. 2009) (fig. 4.18). In addition to the inorganic carbon source, that includes magmatic and thermo-metamorphic origin, also the atmospheric CO_2 ($\delta^{13}C$= -7‰ vs. PDB) must be considered as carbon source in a lake system due to atmospheric CO_2 exchanges in water-air interface (Chiodini et al., 2000). The high concentrations of TDIC (over two orders of magnitude than $TDIC_{ASW} \approx 0.95$ mg/l; fig. 4.19) are reached in deep waters of Monticchio lakes (>12 m of depth) insomuch as, for these waters, the atmospheric contribute can be neglected. The shallow waters have concentrations of TDIC higher than air saturated water (from one to two orders of magnitude). Moreover the $\delta^{13}C_{TDIC}$ of the shallow waters shows a trend toward values more positive than $\delta^{13}C$ of atmospheric CO_2 (fig. 4.18, 4.19), it suggests that atmospheric contribution is negligible also for shallow waters.

PHREEQC code simulations indicate that conditions for $FeCO_3$ and $MnCO_3$ precipitation (siderite-rhodochrosite solid solutions) below the depth of 18 m in LPM are reached. Experimental investigations showed that carbon isotope shift of TDIC ($\delta^{13}C_{TDIC}$) related to siderite precipitation is limited to a decrease of about 0.2 ~ 2‰ (Jimenez-Lopez & Romanek, 2004). At the lake bottom, the low pH conditions of sediment (see above) could cause the partial dissolution of settling carbonates (carbonates of Fe, Mn, Ca and Mg, all with a higher isotopic signature than TDIC), increasing both the TDIC amounts and $\delta^{13}C_{TDIC}$ at the bottom, as it occur in LPM (fig. 4.18 a; 4.19).

The high biological activity of lake systems suggests the presence of a carbon component of organic origin. The high isotopic values of TDIC in Monticchio lakes indicate a low contribution of the organic source ($\delta^{13}C$ from -24‰ to -28‰; Chiodini et al., 2000; Caliro et al., 2008; Gambardella, 2006). Nevertheless, the difference of the carbon isotopic signature of TDIC between the bottom water of LPM and LGM can be reasonably explained by different amounts of organic carbon in the carbon cycle of the two lakes (Fig. 4.18).

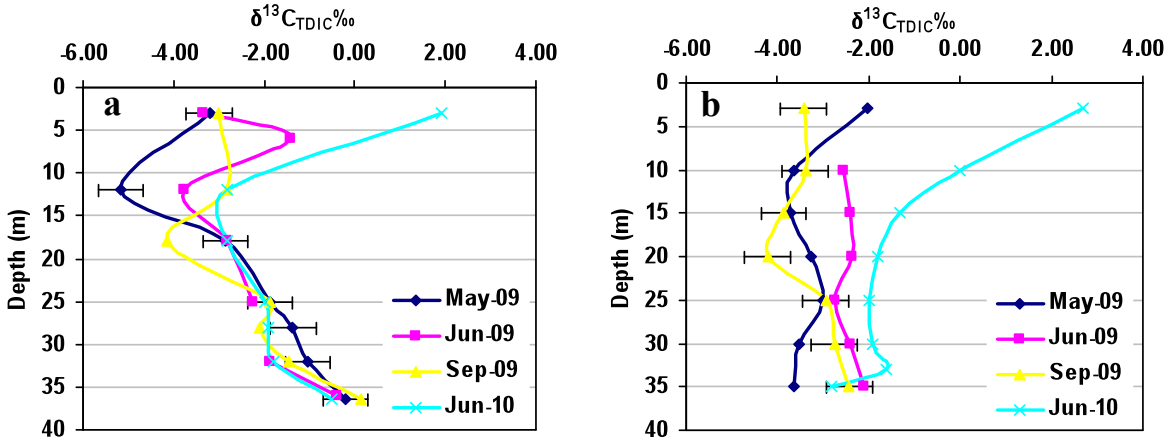

Figure 4.18 - Distribution of $\delta^{13}C_{TDIC}$ (vs PDB) with depth (m), for LPM (a) and LGM (b). The considered months are May, June and September of 2009 and June 2010.

The plot in figure 4.19 shows an interesting trend for LPM, the monimolimnion samples decrease both in $\delta^{13}C_{TDIC}$ and in TDIC towards the lake surface; the shallow waters have a trend that heads for more positive values (see also fig. 4.18). The monimolimnion trend not only suggests that the carbon inorganic source in LPM has a $\delta^{13}C \approx 0$ ‰, but also a CO_2 flux high enough to support the elevated TDIC values of LPM is present. In figure 4.19 the hypolimnion waters of LGM are plotted on a limited range of $\delta^{13}C_{TDIC}$ and TDIC values, about between -2 ÷ -4 ‰ and 250÷500 mg/l, respectively. The shallow waters of LGM have the same behaviour of LPM ones.

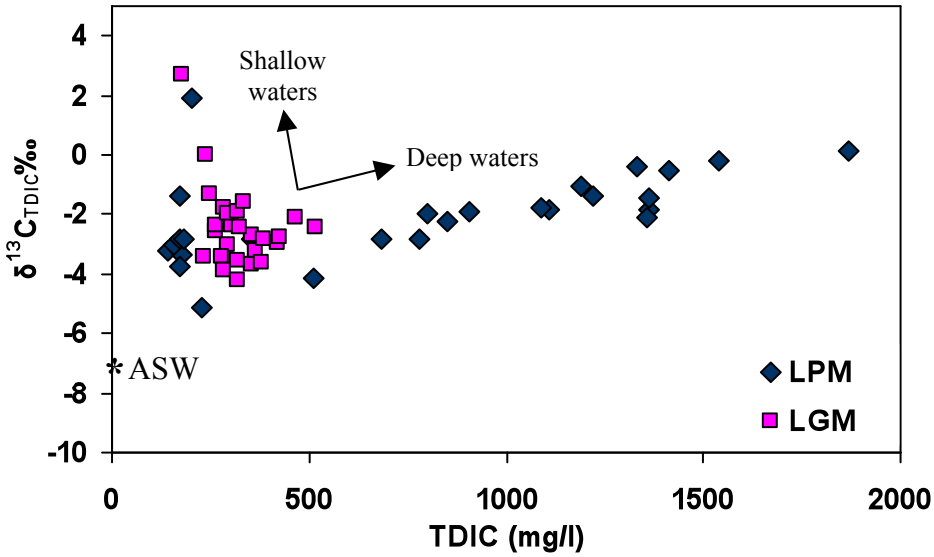

Figure 4.19 - Plot of $\delta^{13}C_{TDIC}$ versus total dissolved inorganic carbon (TDIC) concentrations of Monticchio lakes. The values are representative of May-09, June-09, September-09 and June-10. ASW is the value of air saturated water.

Looking for an explanation for the increase of $\delta^{13}C_{TDIC}$ in shallow waters (fig. 4.18, 4.19), other processes are able to modify the isotopic carbon signature, i.e.: CO_2 consumption by

photosynthesis and CO_2 production by respiration, carbon loss by calcite precipitation, carbon derived from dissolution of carbonate minerals and CO_2 degassing.

The photosynthesis produces light carbon CO_2 consumption and can increase the isotopic signature of TDIC up to about 7‰ δ units (McConnaughey et al. 1997), as also observed for others lakes (Myrbo & Shapley, 2006). Another process linked to the biological cycle is the respiration, able to decrease the $\delta^{13}C_{TDIC}$ values, oppositely to the observed variation in shallow waters of Monticchio lakes. Moreover, the photosynthesis causes larger ^{12}C depletion than respiratory ^{12}C enrichment in TDIC (McConnaughey et al. 1997).

As previously discussed the CO_2 consumption by photosynthesis increases the pH and can induce the carbonate precipitation. This process enriches the carbonates of ^{13}C, with fractionation between solid carbonate and bicarbonate of 1.85±0.23‰ at 20°C (Emrich et Al. 1970), decreasing the $\delta^{13}C_{TDIC}$, in an opposite direction than the observed increasing trend of superficial waters. So, even if carbonate precipitation occurs in shallow waters of both lakes, this process is not able to counterbalance light carbon CO_2 consumption by photosynthesis, as also suggested for the Lake Averno by Caliro et al. (2008).

CO_2 degassing is precluded due to the undersaturation of dissolved CO_2 in both lakes, it is confirmed by relative high pH values in shallow waters (see section 4.1). Nevertheless, the CO_2 degassing could cause only a small increase in $\delta^{13}C_{TDIC}$, in the order of 0.5 δ units (Chiodini et al., 2000).

4.4 Gas chemistry

4.4.1 Major gases

Previous works on the water geochemistry of LPM (i.e., Fornai, 1992; Chiodini et al., 1996; Chiodini et al., 1997; Chiodini et al., 2000; Cioni et al., 2006; Caracausi et al. 2009), highlight that CO_2 and CH_4 are the main dissolved gaseous species. Our data confirm that the amount of dissolved gases in the shallow waters of LPM reflects the equilibrium with atmosphere (Cioni et al., 2006 and references therein). Deep waters of LPM are dominated by CO_2, CH_4 and N_2, in order of abundance (N_2 data of Nicolosi (2007) were used); the low concentrations of O_2 and the presence of CO denote characteristics of an anoxic and reducing ambient. The CO_2 has been discussed in section 4.3 (carbonate system), so in this section it will be treated marginally.

In the LPM waters, the dissolved CH_4 does not vary much seasonally; the lower concentration has been measured in shallow waters and it increases towards the lake bottom in the monimolimnion, reaching the concentrations up to 160 cc STP/litre (fig. 4.20 a; tab. A4 appendix I). The dissolved CH_4 in the waters of LGM increases with depth and the highest concentrations in the entire hypolimnion have been measured during summer-autumn time. The dissolved methane in deep waters of LGM drastically decreases during winter-spring time (fig. 4.20 b; tab. A4 appendix I).

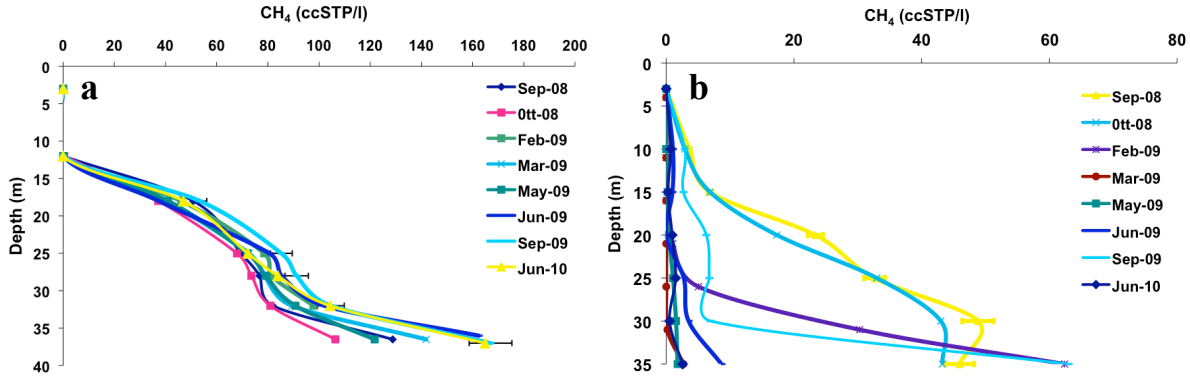

Figure 4.20 - CH_4 concentrations versus depth for LPM (a) and LGM (b), from September 2008 to June 2010.

By means of the methane isotopic investigation (δD and $\delta^{13}C$), it was possible to constrain the genetic processes leading to the formation of dissolved methane in the waters of Monticchio lakes.

In LPM, the $\delta^{13}C_{CH4}$ values range from -60.8‰ to -61.9‰ vs. PDB, while a slightly ^{13}C-enrichment is observed in methane dissolved in LGM lake (from -58.8‰ to -57.4‰). The

δD_{CH4} values range from -291‰ to -298‰ vs. SMOW, while in LGM methane is slightly enriched in heavy isotopes, displaying values from -241‰ to -257‰ (fig. 4.21).

All the LPM samples lie in the field of methane produced by Bacterial methyl-type fermentation, while LGM samples fall in the field of transition between methyl-type fermentation and carbonate reduction (Schoell, 1980; Jenden and Kaplan, 1986; Withicar 1986 and 1999) (fig.4.20). Methane thermogenically produced seems to be absent or negligible compared to methane bacterially produced (Fig. 4.21).

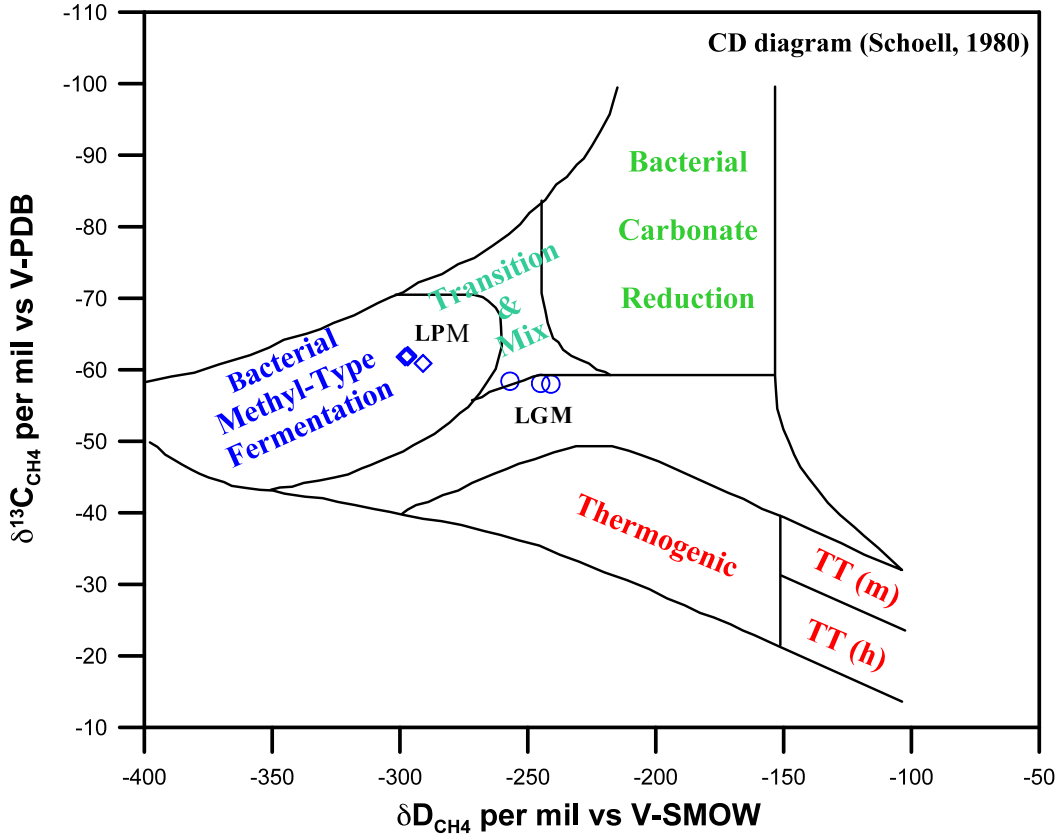

Figure 4.21 - δD vs $\delta^{13}C$ plot (midified by Schoell, 1980). The values of methane in dissolved gases of LPM and LG are plotted. The error of values is within the graphic sign.

Gutsalo (2008) developed an advanced thermodynamic approach to distinguish methanogenic pathways between CO_2-reduction and acetate fermentation. On the basis of new experimental data, he stated that the CH_4-H_2O and CH_4-CO_2 systems approach thermodynamic isotope equilibrium in the case of methane derived from CO_2-reduction while hydrogen and carbon isotope fractionations proceed under non-equilibrium during methane formation by acetate fermentation (see application in appendix IV).

Assuming that the biocenosis of bacteria responsible of the acetate fermentation in both Monticchio lakes is similar to those ones present in Lake Wuermsee (Northern Germany, Whiticar et al., 1986; Woltemate et al., 1984), the obtained δD_R values (methane through

CO_2-reduction) are -210‰ and -229 ‰ for LGM and LPM respectively while δD_F values (methane through acetate fermentation) are -307‰ and -317 ‰ for LGM and LPM respectively (see appendix IV for calculations). The measured δD_{CH4} values (Fig. 4.21) fall within the range of values found for CO_2-reduction and acetate fermentation. By applying a simple hydrogen isotope balance equation, the relative methane contribution from acetate fermentation and CO_2-reduction were estimated. At LPM, production of methane is dominated by acetate fermentation with the fraction of about 70% (range 67-78%), while in LGM waters acetate fermentation and CO_2-reduction operate in almost equal proportion at around 45% (range 32-54%), This could be reflect a different nature of sediments between LPM and LGM.

4.4.2 Noble gases

Dissolved Ar in shallow waters of Monticchio lakes is in equilibrium with atmosphere, showing seasonal variations (fig. 4.22) due to the change of Ar solubility with temperature (Aeshbach-Hertig et al. 1999a). Along the water column of the two lakes, the values have a low variability in the different months, often within the error. The deep waters of LPM show a decrease in dissolved Ar concentration. It cannot be explained by variations of its solubility on the basis of temperature, salinity and recharge altitude (pressure); the Ar concentration in deep waters of LPM are always lower than Ar in air saturated water at a temperature of ~10°C (mean annual temperature at water recharge altitude)(fig. 4.22 a).

The atmospheric $^{40}Ar/^{36}Ar$ ratio is about 295.5 (Fisher, 1982), the Ar isotopic ratio in the waters of Monticchio lakes is close to this value, even in the deep waters of LPM.

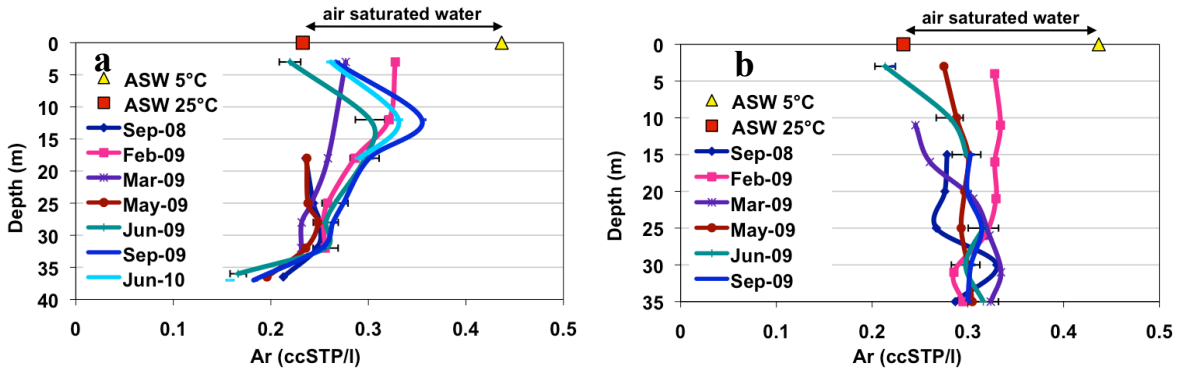

Figure 4.22 - Distribution of dissolved Ar amounts (cc STP/l) with depth (m) in LPM (a) and LGM (b), for different months. The dissolved Ar values of water in equilibrium with atmosphere are reported (in the range of temperature of 5 and 25°C and at altitude of 660 meters a.s.l., Aeshbach-Hertig et al. 1999).

The Ar profiles in LPM (4.22 a) display the lowest Ar concentration in the deepest waters and an increase towards the thermocline (10-15 m). The dissolved Ne of Monticchio lakes waters have a similar behaviour of Ar. Therefore, their concentrations in the deep portion of the lake, well below the air saturated water at T- P conditions of the water recharge altitude, are related to stripping of atmospheric noble gases by outgassing processes which probably occur in groundwater. The uotgassing can be triggered by high concentrations of dissolved CO_2 (the Vulture area is well-known for sparkling waters).

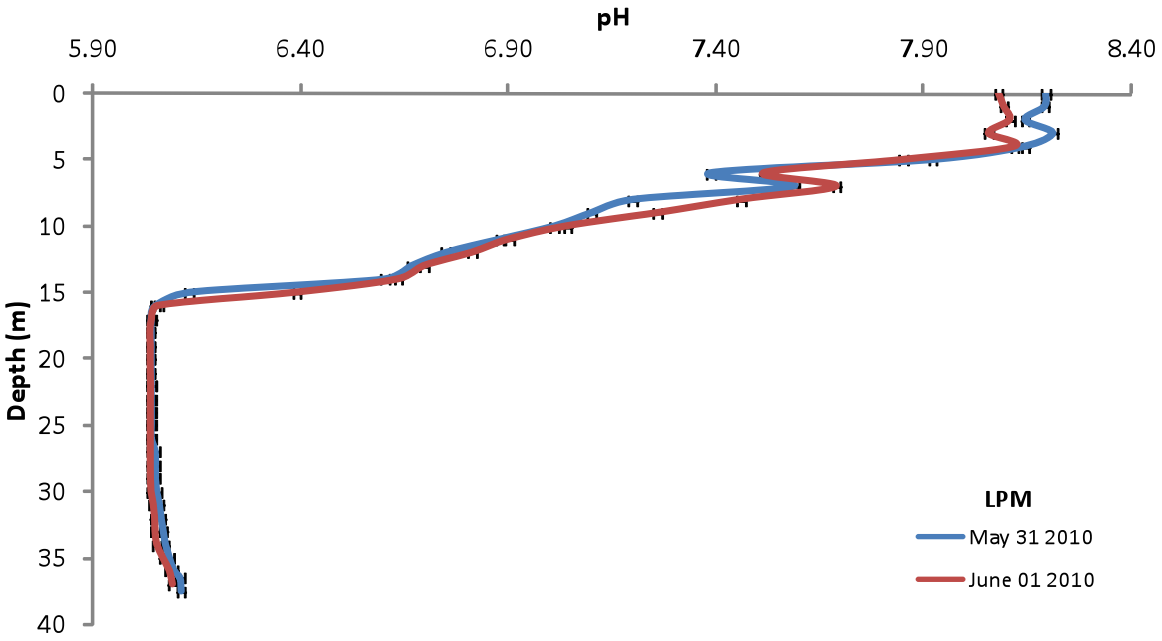

Figure 4.23 - LPM high resolution pH (±0.01units) profiles clearly showing a sharp inversion of the pH trend, peaking at depth of about 7 m. That suggests, together with the observed Ar variations, a lateral groundwater inflow at shallow depth.

The recurrent high concentration measured at about 12 meters of depth could suggest a water input at shallow depth, which carries noble gases in equilibrium with air at the water recharge altitude (T≈10°C). This shallow water inflow could also explain the pH variation measured with a high resolution pH probe at a depth of ~7 m in May and June 2010 (fig. 4.23). The wide sampling intervals of dissolved gases do not allow the best fitting between depths supposed by Ar data (~12 m) and pH data (~7 m).

The dissolved helium in LPM waters reaches concentrations up to two orders of magnitude more than air saturated water (4.5×10^{-5} cc STP/liter at the lakes altitude of 660 meters and an annual mean temperature of 14°C). The highest concentration has been measured in the monimolimnion at a depth of 28 meters (fig. 4.24), where He abundance displays a relatively narrow range of variations over time, then it strongly decreases towards the surface, down to

the equilibrium with atmosphere. The dissolved helium profiles suggest a major He supply at about 28 meters of depth most probably by a groundwater inflow through the lake wall (as supposed by Nagao et al. 2010 in Lake Nyos) (fig. 4.24). This implies a decoupling of volatile inflow into to the lake waters between the CH_4 and CO2 (coming from the bottom) and helium (mainly coming from 28m and secondly from bottom).

Furthermore, the dissolved He concentration gradient at depth interval of 28-36 m is lower than those between 28 m and shallower depths. The noble gas gradients (He, Ne, Ar) are probably related to lateral inflow at 28 m of almost undegassed groundwater, which mixes in proportions of 1:4 with degassed water inflow from the lake bottom.

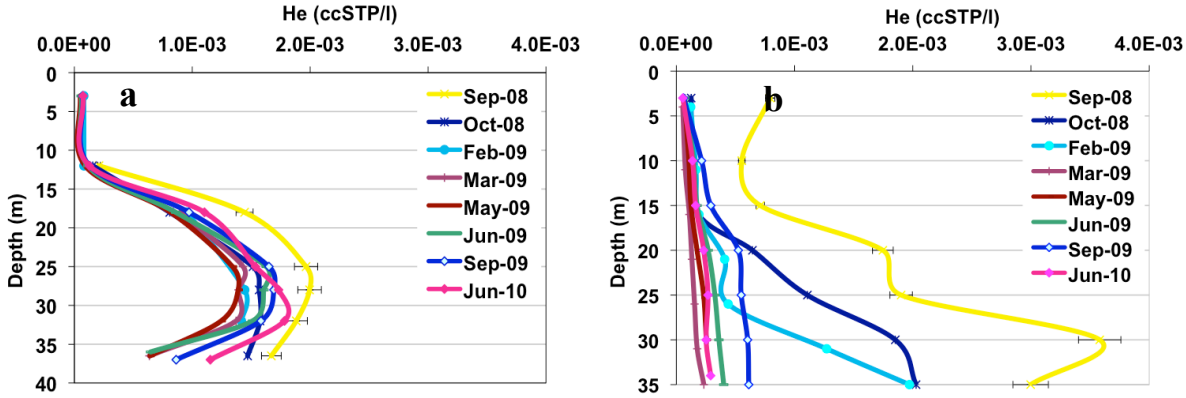

Figure 4.24 - Distribution of dissolved He amounts (cc STP/l) with depth (m) in LPM (a) and LGM (b), for different months.

An alternative model (with only one groundwater inflow from lake bottom) could explain a similar depletion of noble gases in the deepest waters by bubble degassing from bottom (bubbles would strip the less-soluble gases such as He, Ne, Ar; Evans et al. 1993; Aeschbach-Hertig et al. 1999). In LPM the methanogenesis in the bottom sediments could lead to bubble formation and CH_4-rich bubbles could escape into lake water. These bubbles also contain the gases carried by the groundwater inflow from bottom (i.e, CO_2, He, Ar, Ne), which equilibrate with CH_4 during the circulation within the sediments. The bubbles will dissolve as they rise through the water column, transferring the He, Ar and Ne to shallower depths (e.g., 28m). The repartition of volatiles between gaseous and water phases (during a rising up of bubbles) in deep waters of LPM is not easy to control, therefore this model is difficult to demonstrate. We prefer to consider the double groundwater inflow model to explain the data of dissolved gas.

The dissolved helium concentrations in LGM are usually lower than those in LPM. In September 2008 the abundance of helium in LGM waters was significantly high, being twofold the maximum value in LPM waters. In LGM, the high concentration of He and other gases are reached in deep waters, it suggests a groundwater inflow from the bottom (more

probably the water is the carrier of dissolved gases). Moreover, the He concentrations undergo seasonal variations due to water mixing (similarly to those noticed for CH_4 and CO_2; see also section 5.2), it suggests the opportunity of studying the water lake circulation by means of dissolved gases monitoring.

The three main helium sources on earth are: mantle (MORB: 8±1 Ra), atmosphere (1 Ra) and radiogenic decay in the crust (~0.02 Ra) each of them with a distinct R/Ra, where Ra is the $^3He/^4He$ ratio in the atmosphere (~1.39×10^{-6}) (Craig and Lupton , 1978; Mamyrin and Tolstikhin, 1984; Sano et al., 1998). ^3He can be generated in water by ^3H decay and used for determination of water-age. In Monticchio lakes the abundance of tritium is very low (between 0 and 2.6 TU, see appendix I), precluding the ^3H-^3He dating use, as reported for other lakes (Kipfer et al., 1994; Aeschbach-Herting et al., 2002). Due to low tritium concentrations the contribution of tritiogenic ^3He in the evaluation of mantle-derived ^3He is negligible; in fact in a volcanic area mantle-derived gases are relatively enriched in ^3He with respect to the other sources (Aeschbach-Hertig et al., 1999b, and references therein).

The He isotope ratios (expressed as R/Ra_c: values corrected for the atmospheric component, see appendix V), below 15 meters of depth, show seasonal variations in both lakes ranging between about 5.3 and 6.1 R/Ra_c (fig. 4.25; tab. A4 in appendix I). These values indicate a significant contribution of mantle-derived helium component. If we consider values reported in previous works (Chiodini et al., 2000; Nicolosi, 2007), the minimum value of R/Ra_c found in lake waters is 4.4.

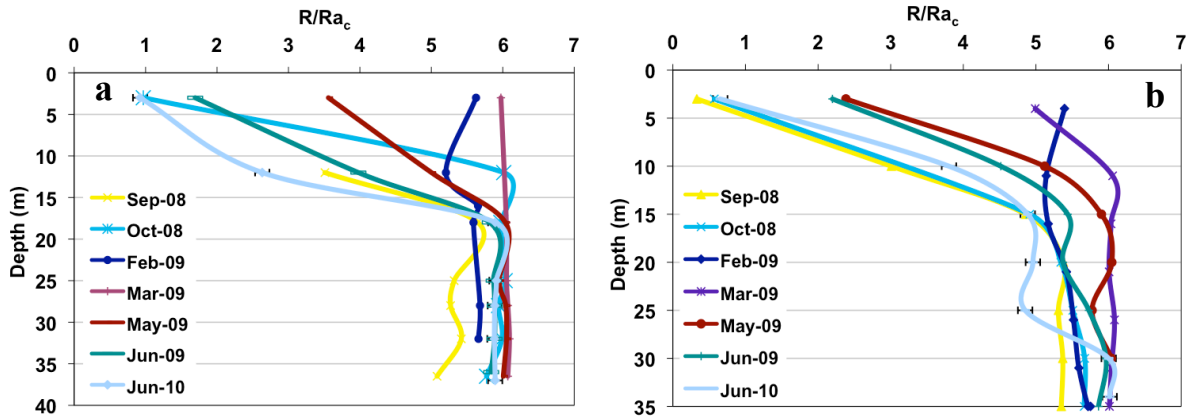

Figure 4.25 - The R/Ra values corrected for the atmospheric contamination (R/Ra_c) versus depth (m), in LPM (a) and LGM (b), for different months.

Although MOR mantle signature is characterized by He isotope ratio of 8±1 Ra (Porcelli and Ballantine, 2002), helium isotope ratios in fluids inclusions of olivine, from maar ejecta of Laghi di Monticchio Syntem (Giannandrea et al., 2006), range between 6.1 and 4.4 Ra

(Paternoster, 2005). The highest value of 6.1 Ra, also measured in mantle xenoliths (lapilli tuff) of the same ejecta formation, was assumed by Paternoster (2005) as the He isotopic signature of under Mt. Vulture mantle. The He isotope ratio of 4.4 Ra has been discussed by Caracausi et al. (in preparation) as the possible consequence of: i) magma aging by radiogenic ^{4}He ingrowth from U-Th decay within magmas prior and during phenocrystal crystallization of olivine and pyroxene; ii) post eruptive radiogenic ^{4}He in-growth; iii) contamination of magmas by assimilation of crustal rocks or fluids prior or during phenocrystal crystallization of olivine and pyroxene. Taking into account the mean U and Th contents in Vulture lavas (13 and 34 ppm respectively; De Fino et al., 1986) an olivine-melt partition coefficient of 0.008 (Marty et al., 1990) and a magma storage time of 20 Ka, we calculated that the initial 6.1 Ra He isotope ratio can decline down by only 0.5 Ra units. This suggests that process " i " is ineffective to explain the measured 4.4 Ra values. Also, the process " ii " can be discarded, as the radiogenic ^{4}He produced after the olivine and pyroxene crystallization mainly accumulates in crystal lattice and does not enter the fluid inclusions and the "vacuum crushing" technique does not release lattice components (Caracausi et al., in preparation). Even though the process " iii " seems to be a plausible explanation, we would note that also Mt. Vulture mantle heterogeneity can not be ruled out. Hence, we plot our data on a R/Ra versus ^{4}He/^{20}Ne graph (fig. 4.26), where the main helium sources are: atmosphere (1 Ra: ^{3}He/^{4}He = 1.39 x 10^{-6}; Craig and Lupton, 1976; Mamyrin and Tolstikhin, 1984; Sano et al., 1998); radiogenic helium (~ 0.02 Ra); Mt. Vulture magmatic He, which has been separated in two He sources (6.1 Ra and 4.4 Ra), in accordance with the values measured in fluid inclusions of Monticchio maar ejecta.

We note that the isotope ratios of helium dissolved in deep waters of Monticchio lakes falls between the mixing trends among atmospheric, radiogenic and mantle derived He. In addition, the helium isotope ratios show an inverse relation with the He isotope concentration in both lakes: at high R/Ra_c ratios we found low helium concentrations and vice versa (fig. 4.27). This relation is valid at the depth of ~ 28 m in LPM and at the bottom (35 m) in LGM (these are the supposed depths of the main groundwater inflow).

A comparison between He isotope data of the two lakes (fig. 4.28) shows that the measured values (corrected for the air component) lie on a line with 1:1 slope.

The above relations suggest: i) groundwater inflow at ~ 28 m in LPM and at the bottom (35 m) in LGM; ii) a common supply of the main helium inflows in both lakes; iii) a variable contribution of two mantle derived He sources, one with low helium concentration and high isotopic value ($R/Ra \geq 6.1$), another with high helium concentration and low He isotope ratio;

vi) a seasonal change in their helium contribution; this suggests a link between dissolved helium and groundwater hydrology (see also fig. 4.24 and 4.25).

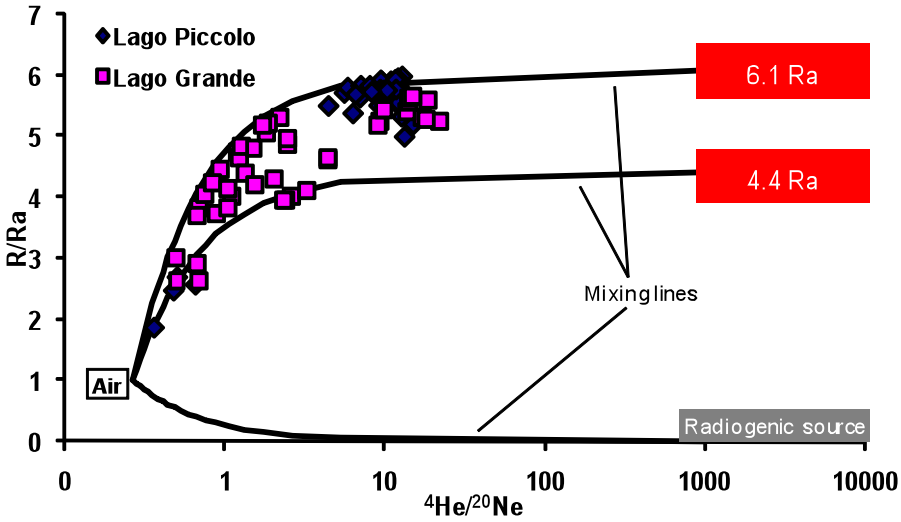

Figure 4.26 - Helium isotope ratios, expressed as R/Ra not corrected for the atmospheric contamination), and $^{4}He/^{20}Ne$ ratios of dissolved gases in Monticchio lakes waters. Solid lines show the mixing between atmospheric derived helium (air), radiogenic helium and mantle derived He (6.1 and 4.4 Ra).

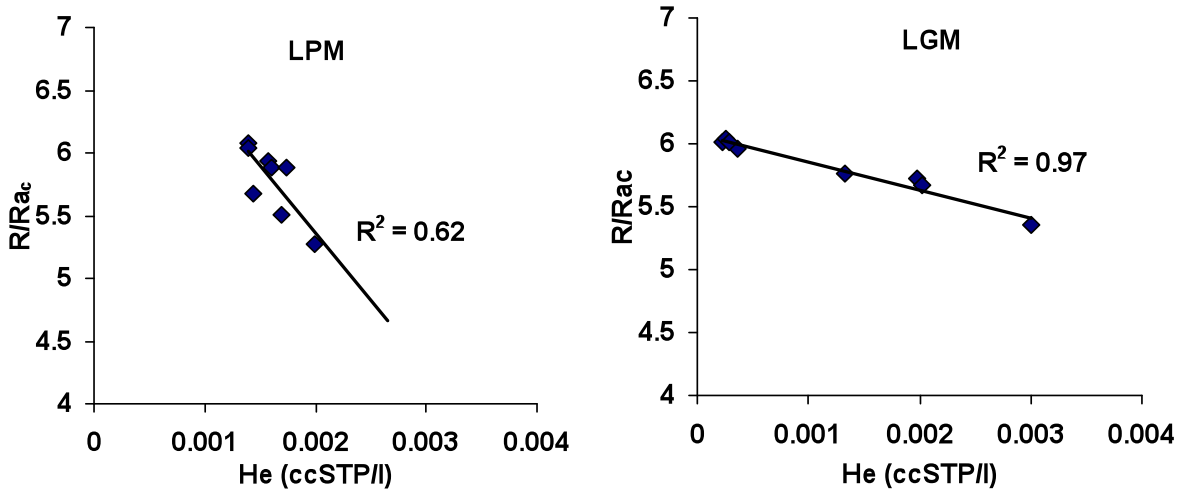

Figure 4.27 - Plot of helium concentrations versus R/Ra_c in Monticchio lakes. Each point of both graphs represents the value of a single sampling campaign at the depth of 28 and 35 meters (the depths of the main helium inflows), for LPM and LGM respectively.

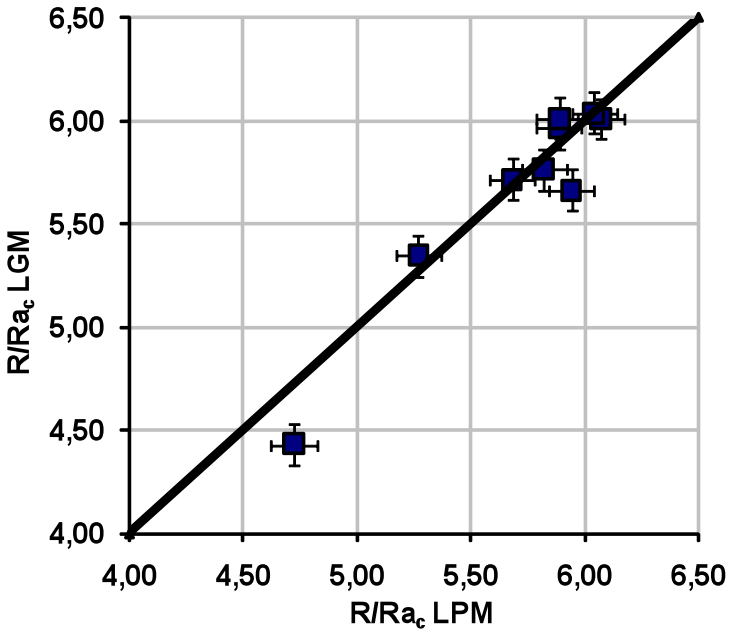

Figure 4.28 - Helium isotope ratios (R/Ra_c) of the main He inflow in the lake waters (depths 28 m at LPM and LGM bottom). The measured values for waters sampled in the two lakes within a few days apart are close a line with 1:1 slope in the graph.

5.0 Fluid circulation in Monticchio lakes

5.1 Water inflow/outflow

In geochemical study of a lake can be relevant the study of fluids dynamic. A first approach is related to the local hydrological cycle in terms of water balance. The water balance (also called water budget) of a lake is summarized by the following equation:

$$I + P - O - E = \Delta W \qquad (5.1\text{-}1)$$

I = inflow into the lake
P = precipitation onto lake surface
O = output from the lake
E = evaporation from the lake surface
ΔW = water volume that makes the change in water level

In lake systems the estimation of I and O values is more difficult because both components depend on complex interactions with other systems (e.g., groundwater, rivers, anthropic drainage and withdrawals). Commonly it is easier to measure or estimate the evaporation instead of the input or output that are calculated by water budget equation (Lewis 1983).
The evaporation is useful not only to close the water budget equation, but also to better constrain the evaporative process, previously highlighted by δD and $\delta^{18}O$ isotopes.
The evaporation from Monticchio Lakes has been computed for one or more month's intervals and during 2008-2010 years. The meteorological parameters used to evaluate the evaporation were not measured on Monticchio lakes, but in stations about 10 kilometres away, then few approximations were used (see Appendix VI).
The evaporation rate (E in m/s) on Monticchio lakes was determined with the Bowen-ratio energy budget (BREB); this is one of the most accurate methods to estimate evaporation (Drexler et al., 2004; Rosenberry et al., 2007; appendix VI). The BREB is reported in the form of Gianniou and Antonopoulos (2007):

$$E = \frac{R_s - R_{sr} + R_a - R_{ar} - R_b - S}{\rho_w L_v (1 + \beta)} \qquad (5.1\text{-}2)$$

S = change of the thermal content of the water body (W/m^2)
R_s = short-wave (solar) radiation incident at the lake water surface (W/m^2)
R_{sr} = reflected short-wave radiation from the water surface (W/m^2)
R_a = long-wave radiation (atmospheric diffuse radiation) incident at the water surface (W/m^2)
R_{ar} = reflected long-wave radiation from the water surface (W/m^2)
R_b = back (long-wave) radiation emitted from the lake water (W/m^2)
ρ_w = water density (Kg/m^3)

L_v = latent heat of vaporization of water (J/kg)
β = Bowen ratio

Each single parameter is treated in appendix VI, in more details.

The difficult estimation of Bowen ratio (β) make this method not easy to employ, so to verify the consistency of the obtained results, we also used two empirical methods, the Priestley-Taylor and the DeBruin-Keijman methods, which are easer to apply, although they give lees accuracy than BREB.

The Priestley-Taylor equation is an empirical formulation; it is a modification of Penman formula presented by Priestley and Taylor in 1972, in the following form:

$$E = \alpha \frac{s}{s+\gamma} \frac{R_N - S}{\rho_w L_v} \tag{5.1-3}$$

α = 1.26, Priestley-Taylor empirically derived constant
s = slope of saturation vapour pressure, temperature curve
R_N = net radiation ($R_s - R_{sr} + R_a - R_{ar} - R_b$)
γ = 66 Pa °C^{-1}, psychrometric constant

The DeBruin-Keijman method is similar to the previous one, but uses different constants, as follows (Rosenberry et al. 2007; see also appendix VI):

$$E = \frac{s}{0.85s + 0.63\gamma} \frac{R_N - S}{\rho_w L_v} \tag{5.1-4}$$

A review of estimating evaporation methods is presented in appendix VI with particular attention for the methods used here.

The use of all these methods requires the analysis of solar radiation that influences the thermal balance of the lakes.

As shown in figure 5.1, incoming radiation is dominated by incident either short-wave (R_s) or long-wave (R_a) radiation at the lake surface. Instead the outgoing radiation is mainly represented by long-wave radiation emitted from the lake water (R_b). The reflected short-wave and long-wave radiations (R_{sr} and R_{ar}) are negligible for energy balance. All the radiation components show a characteristic seasonal variation, with the highest values in summer and the lowest in winter. The net radiation (R_n) (Fig. 5.1 c) is evidently positive all year long with a seasonal variation similar to the other energy components. It is interesting to note that in December *Rn* attains a negative value denoting a heat (long-wave radiation) outgoing from water body.

The relative humidity has little influence on some energy components (i.e., R_a, R_{ar} and R_n), as observable in figure 5.1a and even on the final value of evaporation (it has to be reminded that the minimum and maximum values of relative humidity have a fixed difference of 20%, see also appendix VI).

The seasonal variations of the thermal content in the water bodies swing between positive and negative values (fig. 5.1 b). In autumn and winter the heat stored into the lakes is negative so the water bodies are cooling; in spring and summer the positive values indicate the gain of thermal energy, facilitated by increase of net radiation. For the considered period, the stored thermal content of LPM is 5.7 W m^{-2} annually whereas it is 2.5 W m^{-2} for the LGM. Theoretically, S = 0 means that the lake gains and releases heat in the same amount, thereby both Monticchio lakes, in the annual period, can be considered in a thermal quasi steady state (Fig. 5.1 b).

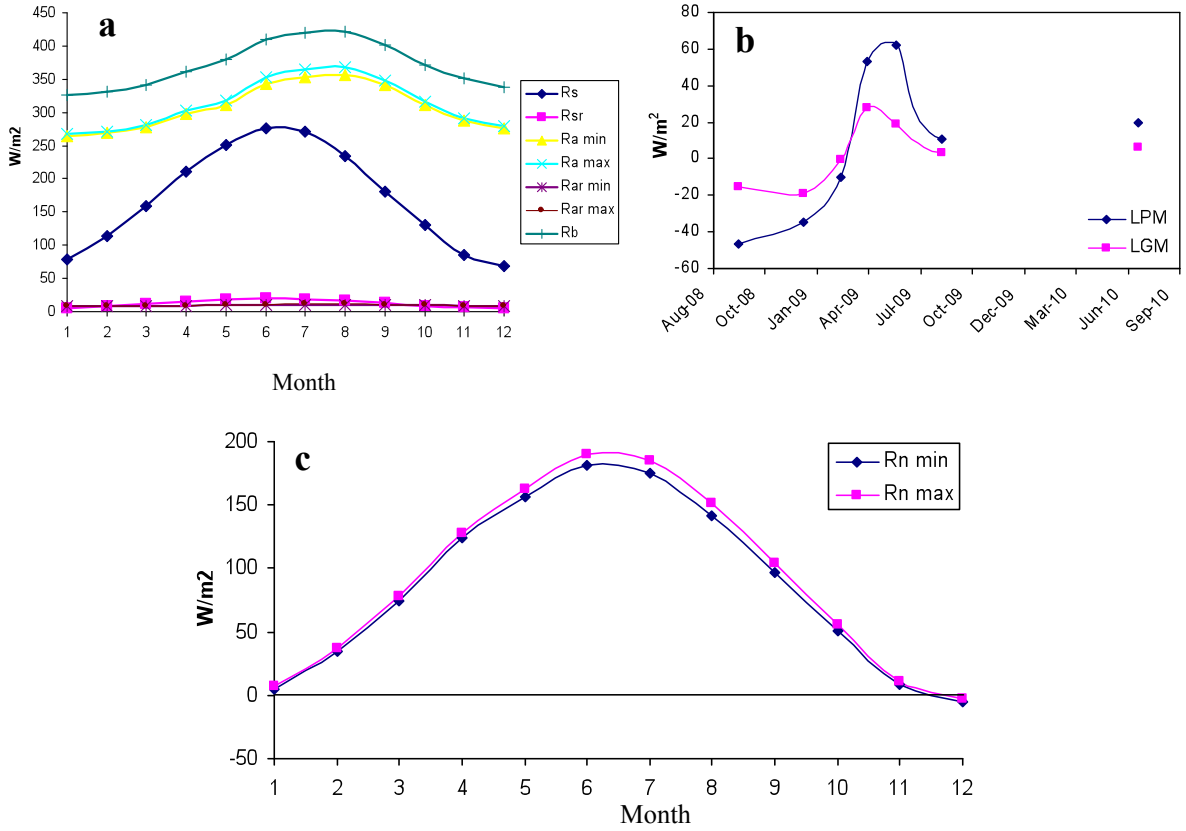

Figure 5.1 - a, c: solar radiation components; the terms min and max represent the estimations with minimum and maximum value of relative humidity; b: the heat storage in the lakes (S).

The Bowen ratio (β) was estimated with equation A40 (appendix VI). The β values have a range depending on minimum and maximum values of relative humidity (βmin and βmax, respectively) and on air temperature.

The two empirical methods give results in agreement with data evaluated with BREB. There is a good agreement between the results obtained by the Pristley-Taylor, DeBruin-Keijman and BREB methods (Appendix VI; fig. 5.2 and tab. 5.2).

Table 5.1: Main estimated data sources.

	Ta	N	rh min	rh max	Rn min	Rn max	Lv	β min	β max	α min	α max	S (LPM)	S (LGM)
Sep-08	**17.8**	**12.3**	**68.8**	**88.8**	**95.51**	**102.45**	**2457280**	**0.16**	**0.37**	**1.31**	**1.10**	**-46.9**	**-15.6**
Oct-08	**14.3**	**10.9**	**74.8**	**94.8**	**51.13**	**56.40**	**2465680**	**0.28**	**0.61**	**1.26**	**1.01**		
Nov-08	**10.2**	**9.8**	**70.4**	**90.4**	**7.86**	**11.63**	**2475520**	**0.27**	**0.50**	**1.41**	**1.19**	**-34.8**	**-19.3**
Dec-08	**5.6**	**9.2**	**75.3**	**95.3**	**-5.01**	**-2.43**	**2486560**	**0.36**	**0.70**	**1.50**	**1.20**		
Jan-09	**5.0**	**9.5**	**78.8**	**98.8**	**4.85**	**7.30**	**2488024**	**0.40**	**0.99**	**1.48**	**1.04**		
Feb-09	**5.3**	**10.5**	**69.6**	**89.6**	**34.59**	**37.12**	**2487256**	**0.36**	**0.58**	**1.51**	**1.30**		
Mar-09	**8.1**	**11.7**	**67.2**	**87.2**	**74.59**	**77.80**	**2480560**	**0.30**	**0.49**	**1.46**	**1.27**	**-10.4**	**-0.5**
Apr-09	**10.3**	**13.1**	**73.6**	**93.6**	**123.59**	**127.44**	**2475280**	**0.28**	**0.58**	**1.39**	**1.13**	**53.4**	**28.1**
May-09	**15.3**	**14.2**	**56.1**	**76.1**	**156.77**	**162.52**	**2463280**	**0.09**	**0.21**	**1.46**	**1.31**		
Jun-09	**19.4**	**14.8**	**57.4**	**77.4**	**180.27**	**188.16**	**2453440**	**0.07**	**0.20**	**1.37**	**1.22**	**61.9**	**18.9**
Jul-09	**22.7**	**14.6**	**51.5**	**71.5**	**174.54**	**184.64**	**2445520**	**0.00**	**0.11**	**1.39**	**1.25**		
Aug-09	**22.6**	**13.6**	**53.4**	**73.4**	**141.44**	**151.45**	**2445760**	**0.01**	**0.13**	**1.38**	**1.24**	**11.0**	**3.2**
Sep-09	**17.8**	**12.3**	**68.8**	**88.8**	**95.51**	**102.45**	**2457280**	**0.16**	**0.37**	**1.31**	**1.10**		
Jun-10	**19.4**	**14.8**	**57.4**	**77.4**	**180.27**	**188.16**	**2453440**	**0.09**	**0.22**	**1.37**	**1.22**	**19.3**	**6.5**
Jul-10	**22.7**	**14.6**	**51.5**	**71.5**	**174.54**	**184.64**	**2445520**	**0.03**	**0.15**	**1.39**	**1.25**		

Ta: air temperature (°C); N: maximum number of sunshine hours per day (h); rh: relative humidity (%); Rn: net radiation (W/m^2); Lv: Latent heat of vaporization (J/Kg); β: Bowen ratio; α: Priestley-Taylor constant; $S_{(LPM)}$, $S_{(LGM)}$: change of the thermal content of the lake for LPM and LGM (W/m^2).

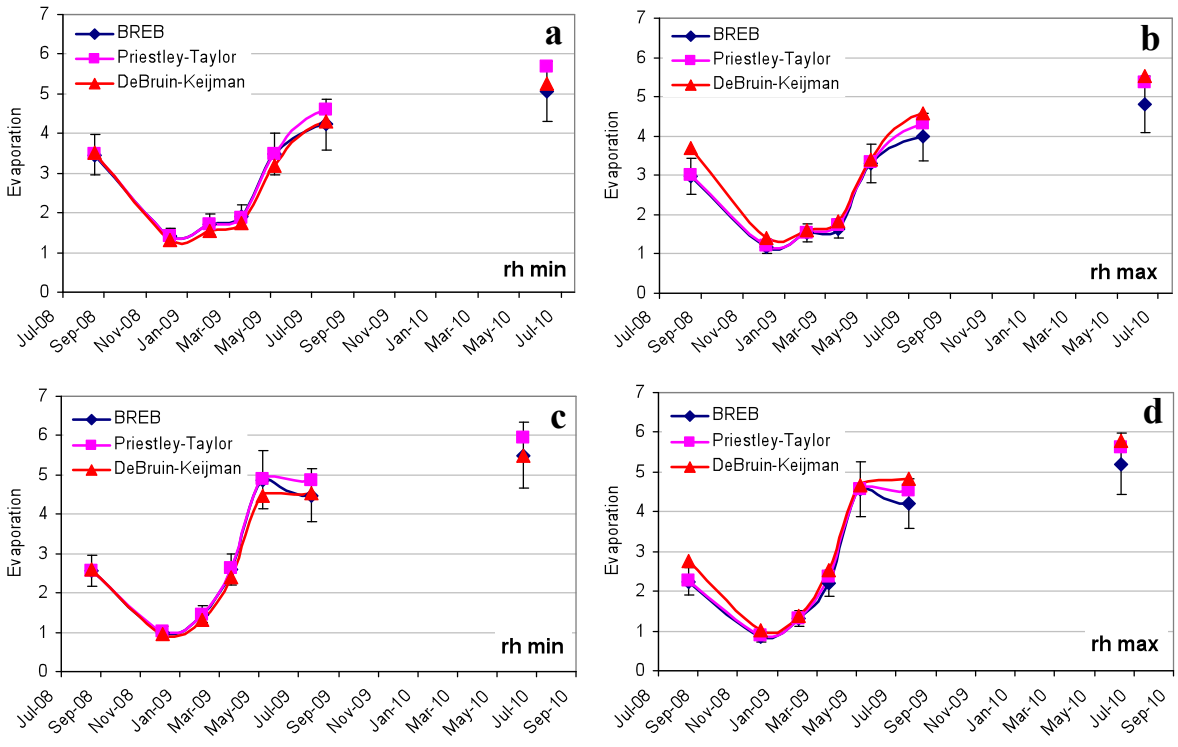

Figure 5.2 - Comparisons of evaporation (mm/day) obtained by different methods. a, b: evaporation with minimum and maximum values of relative humidity for LPM; c, d: evaporation with minimum and maximum values of relative humidity for LGM.

To roughly verify the theoretical estimations, in the month of June-10 was evaluated the evaporation rate by means of floating self-made evaporimeter (see appendix VI, fig. A VI.3) obtaining a rate of about 4.6 and 5.1 mm/day for LPM and LGM, respectively. These values are very close to theoretical values (BREB method).

High evaporation occurs during warm periods (from March to October) when the input energy in the lake is at greatest levels, also in perfect agreement with the data of change in the thermal content of the lake.

In the estimations made by BREB and Priestley-Taylor methods, a decrease of evaporation rate corresponds to an increase of relative humidity (Fig. 5.3, Tab. 5.2). Instead the results from the DeBruin-Keijman method do not follow this trend probably because this method uses energy data and excludes other meteorological parameters. These are used only for theoretical estimation of some energetic parameters (i.e.: R_a, R_{ar}, R_n). In the other methods the relative humidity and the air temperature are considered by means of Bowen ratio and Priestley-Taylor constant (that is not really constant, see Appendix VI).

Table 5.2: Evaporation values (E in mm/day) of Monticchio lakes for different methods and for selected periods. The E min, E max and E mean are the evaporation at minimum, maximum and mean relative humidity considered.

LPM	DeBruin-Keijman			Priestley-Taylor			BREB		
	E min	E max	E mean	E min	E max	E mean	E min	E max	E mean
Sep-Oct 08	3.51	3.69	3.60	3.48	3.00	3.24	3.46	2.98	3.22
Oct 08-Feb 09	1.33	1.41	1.37	1.42	1.21	1.32	1.40	1.18	1.29
Feb-Mar 09	1.55	1.62	1.58	1.71	1.55	1.63	1.72	1.54	1.63
Mar-May 09	1.73	1.84	1.79	1.88	1.73	1.81	1.91	1.64	1.78
May-Jun 09	3.18	3.39	3.29	3.49	3.32	3.41	3.48	3.31	3.39
Jun-Sep 09	4.30	4.57	4.44	4.59	4.32	4.46	4.22	3.98	4.10
Jun-Jul 10	5.25	5.54	5.40	5.69	5.38	5.53	5.07	4.81	4.94

LGM	DeBruin-Keijman			Priestley-Taylor			BREB		
	E min	E max	E mean	E min	E max	E mean	E min	E max	E mean
Sep-Oct 08	2.60	2.77	2.69	2.57	2.26	2.42	2.56	2.24	2.40
Oct 08-Feb 09	0.95	1.03	0.99	1.01	0.88	0.95	0.99	0.86	0.93
Feb-Mar 09	1.31	1.38	1.35	1.45	1.32	1.39	1.46	1.32	1.39
Mar-May 09	2.40	2.52	2.46	2.62	2.36	2.49	2.60	2.21	2.40
May-Jun 09	4.47	4.67	4.57	4.90	4.58	4.74	4.88	4.56	4.72
Jun-Sep 09	4.54	4.82	4.68	4.85	4.55	4.70	4.48	4.21	4.35
Jun-Jul 10	5.50	5.78	5.64	5.95	5.61	5.78	5.50	5.21	5.35

The monthly data, both for LPM and LGM, show seasonal variations: with an increase of air temperature there is a corresponding decrease of relative humidity and an increase of evaporation, and vice versa (Fig. 5.3). These parameters are not only interdependent, but also have a common source of variations that is the solar radiation. In fact, the increase of solar

radiation in spring and summer causes an increase in air temperature and a decrease of the relative humidity. In these relatively high-energy conditions and drier air, evaporation increases, while in autumn and winter, the decrease of sunlight hours and of solar energy radiation causes a cooling down with a raise of relative humidity. This climatic setting does not facilitate the evaporation and, in some extreme cases, can induce condensation. So that it is possible to assert that the parameters, which directly influence the evaporation rate, are mainly: air temperature and relative humidity, as shown in Fig. 5.3.

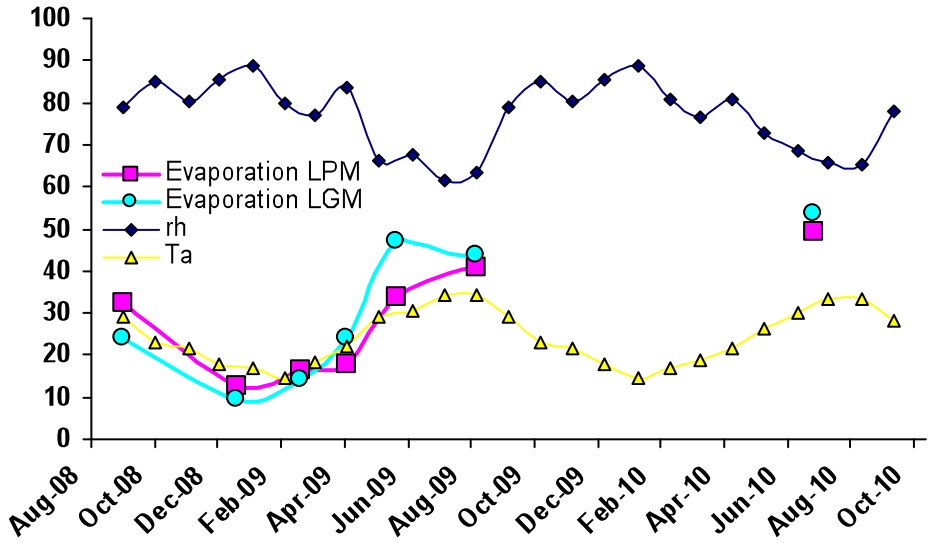

Figure 5.3 - Monthly variations of mean relative humidity (rh in %), BREB mean evaporation of LPM and LGM (mm/day) and mean air temperature (Ta in °C). Evaporation x10 and temperature + 10.

The comparison between the two lakes highlights that the LGM is subjected to a greater evaporation only in spring and summer than LPM. Whereas evaporation is slightly higher in LPM than LGM in autumn and winter. Despite the evaporative rate can be higher in LPM than LGM the residual fraction of evaporating lake water is always lower in LGM (as suggested by isotopic data and δD vs Cl systematics, see section 4.2.4 and 4.2.5) due to the different thickness of evaporating water volume (epilimnion, fig. 5.4). Although the two lakes are subjected to very similar environmental and meteorological conditions, they still show different evaporation behaviours. Analysing the data used for those evaluations, it is possible to note that the parameter, which considerably influence the evaporation of the two lakes is the heat storage in the lake waters (S). Therefore, the different evaporation between the two lakes is caused by a different capacity of the lakes to store and release heat.

The two heat sources of Monticchio lakes are the heat flow from the bottom and solar radiation. In LPM the first one is highlighted by temperature gradient below ~15 m of depth,

constant over time (fig. 5.4 a). In LGM a heat source from bottom has to exist, even if this is not legible from temperature profiles; is also reasonable to assume that this source is constant over time.

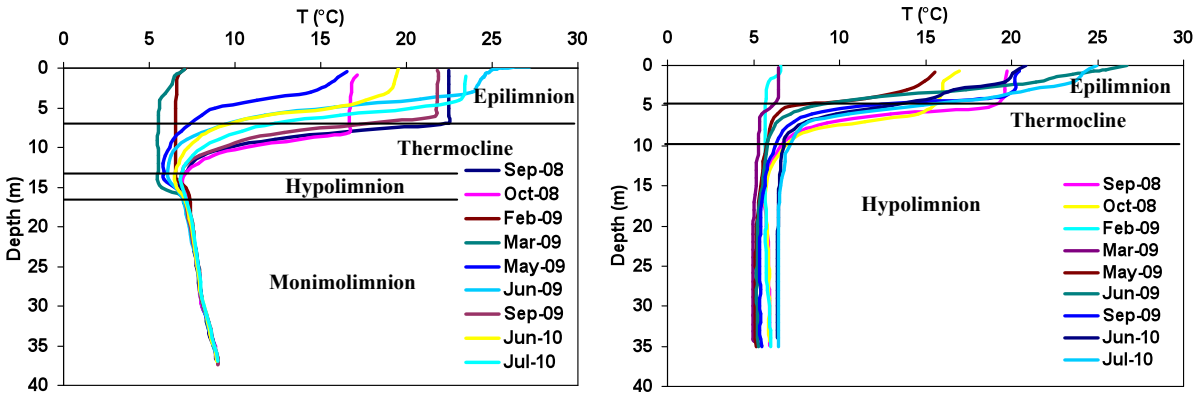

Figure 5.4 - Plots of temperature versus depth for LPM(a) and LGM(b), from September 2008 to July 2010. The thermal stratification is shown; the limits between thermal layers change from month to month, so border lines are approximate. The error on the temperature datum is within the profile sign.

The heat due to solar radiation changes seasonally like the heat storage into LPM and LGM (fig. 5.1a, b), but the different variations between the two lakes can be attributed to the different adsorption of solar radiation by lake water. The water has a high absorption of infrared and red wavelength, which generates a significant heating in the first meters of water. A rapid decrease in absorption is in the low wavelengths down to a minimum in the blue spectrum (see appendix IX). Absorption of low wavelengths of visible spectrum, particularly in UV range, increases in the presence of high turbidity and dissolved organic compounds. The different transparency between the Monticchio lakes (see appendix IX; Schettler and Albéric, 2008; Mancino et al. 2009) can well explain the different amounts of heat storage in the two lakes and therefore the different evaporation. The different heating of shallow waters of LPM and LGM is evident in temperature profiles in figure 5.4, moreover a different thickness of heated water volumes is shown. Another factor that can influence the evaporation and *S* parameter of the two lakes is the different exposition to wind; in fact the LGM is less protected than LPM by crater rims.

It is possible to recognize a trend by plotting evaporation data of other lakes in the world (Borrelli, 2008) versus their latitude, despite of the dispersion points and the limited number of data. The mean annual evaporation values of both Monticchio Lakes, estimated with BREB method, perfectly fall on this trend (Fig. 5.5; Tab A6 in Appendix VI).

With the obtained evaporation values for the considered periods, it is now possible to apply the water balance (equation 5.1-1).

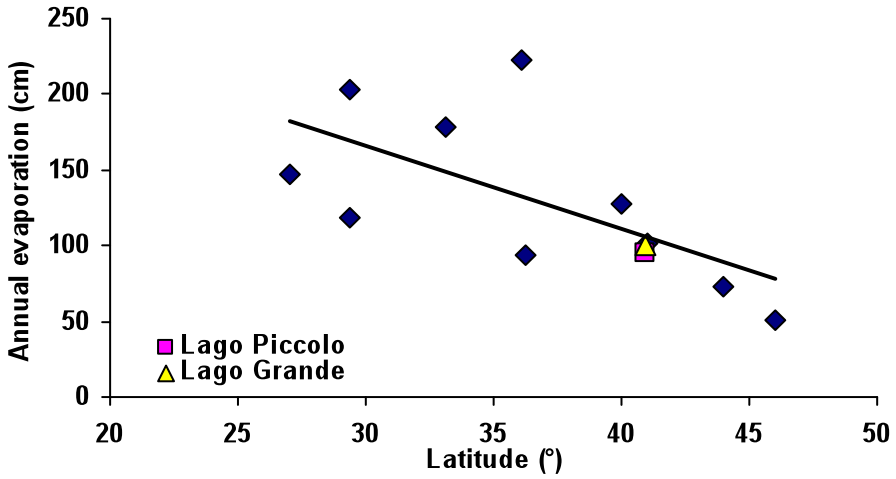

Figure 5.5 - Mean annual evaporation of some lakes (cm) versus latitude (°) (data from Borrelli, 2008). The Monticchio lakes values fall on the highlighted trend.

For Monticchio lakes the equation 5.1-1 was modified to resolve I and O components: groundwater inflow (I_g), superficial inflow (I_s), groundwater outflow (O_g) and superficial outflow (O_s). Since it's not possible to distinguish between I_g and O_g, then the term I_{net} (net groundwater inflow) is considered.

$$I_{net} = E - P \pm \Delta W + O_s - I_s \qquad (5.1\text{-}5)$$

In this formulation the contribution of precipitation that falls on the hydrologic basin of Monticchio lakes is considered within the groundwater inflow; the P component is the precipitation that falls directly on lake surface. With the aim of acquire the rainfall we used the mean monthly precipitation from 1964 to 2006 (fig. 5.6).

LPM does not have I_s; whereas the waters, which flow from LPM to LGM by means of channel, represent the O_s of LPM and the I_s of LGM. The channel that discharge LGM waters into Ofanto River is the O_s of LGM. All the water flows in the channels and water level variations were measured during each sampling campaign.

The data are reported in table 5.3 and the obtained groundwater flows are plotted in figure 5.7. It is interesting to note a well correspondence between the seasonal variations of groundwater inflow estimated by the water balance and the δD versus Cl evaporative model, mainly for LGM (section 4.2.5, fig. 4.15).

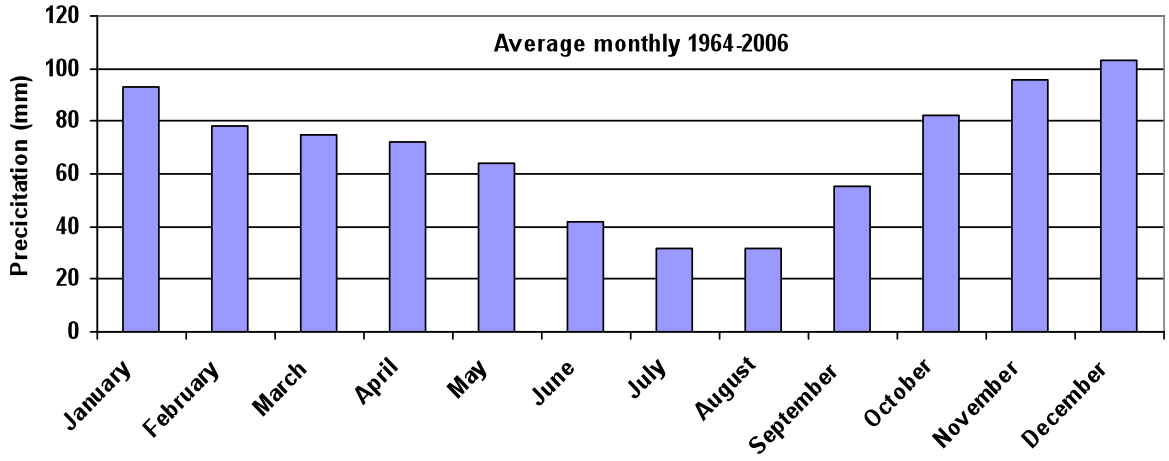

Figure 5.6 - Average monthly precipitation at Melfi gauge station (situated about 8 km from Monticchio lakes at 580 m a.s.l.) for 1964-2006 period. Data from Hydrographic Service of Civil Engineers of Puglia Region.

Table 5.3. Data sources of water balance parameters for Monticchio lakes, all values are in m^3 day^{-1}.

LPM	Channel outflow (O_S)	Water volume linked to change in water level (ΔW)	Mean evaporation (E)	Precipitation (P)
feb-mar 2009	2761.71	12.54	303.16	474.48
mar-may 2009	2704.77	-9.24	332.25	446.57
may-jun 2009	1100.37	-3.65	634.10	328.72
jun-sep 2009	396.85	-15.10	826.44	198.47
jun-jul 2010	585.12	0.00	944.21	229.49

LGM	Channel inflow (I_S)	Channel outflow (O_S)	Water volume linked to change in water level (ΔW)	Mean evaporation (E)	Precipitation (P)
may-jun 2009	1100.37	3181.09	-173.77	1984.34	740.41
jun-sep 2009	396.85	0.00	-131.26	1889.47	447.04
jun-jul 2010	585.12	0.00	-59.68	2300.18	516.89

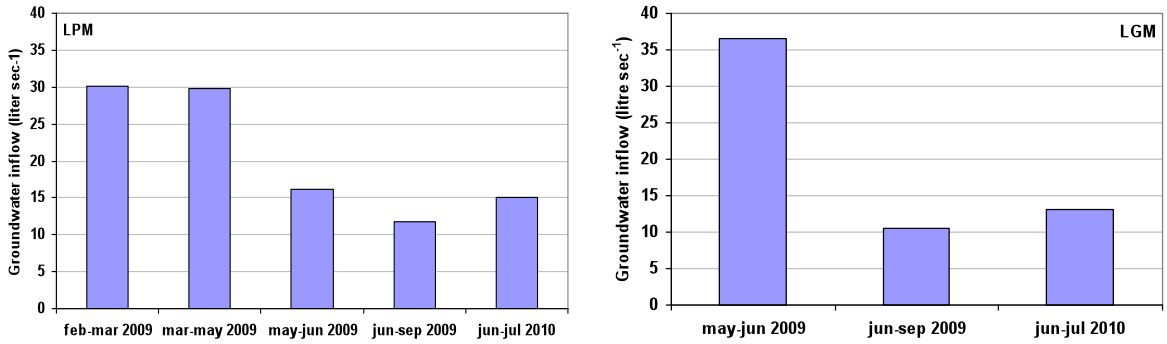

Figure 5.7 - Net groundwater inflows in LPM and LGM for the specified spans. The error on values is about 5%.

From presented data it is evident that LPM has low variations in water level due to an outflow channel, through which the water can flow into the LGM. This channel practically controls

the level of the lake. The evaporation weights more than others balance parameters in summertime. The direct precipitation has a marginal role on the LPM water budget.

The maximum shift of water level measured at LGM is about 60 cm, but variations over one meter are reported in literature (Schettler & Albéric, 2008). The channel of outflow regulates the maximum level of LGM. In warm periods the water level is lower than the channel level so the water flow in this channel is absent. The evaporation value is higher than LPM and heavily affects the water balance, justifying the extreme isotopic shift on the evaporative trend (see isotopic data in 4.2.4 section). Even for LGM the direct precipitations no much affect in the water balance.

The net groundwater inflow (I_{net}) in the LPM is between ~30 litre/sec in winter and spring periods and 12-15 litre/sec in summer. The LGM has higher seasonal I_{net} variations than LPM, the winter/spring groundwater inflow reach over 35 litre/sec, in summer time about 10-13 litre/sec.

5.2 Structure and dynamics

LPM is considered a meromictic lake, having a shallow mixolimnion and a deep monimolimnion, which is characterized by stagnant water (Cioni et al., 2006). The LGM is considered dimictic, with two mixing periods, which are still not well identified (Schettler & Albéric, 2008).

The homogenization and differentiation of chemical and physical parameters in water column of lakes mostly depend on circulation dynamics.

The water of LPM from the surface down to 14 m has a constant EC (Fig. 4.2) so the contribution of dissolved solids on density is almost the same; a similar condition exists for the whole LGM waters (fig. 4.2). In these water volumes, the temperature can heavily influence the density and therefore the mixing processes. In fact, the surface water gets colder in the coldest periods of the year with the increase in density and thus triggers a mixing process, as seen in the first 14 m of LPM and in the entire LGM. In the warmest month of the year a thermal stratification occurs, with cold heavy water in deeper portion and warm light water in shallow layers. In the LPM waters deeper than 14 m the temperature profiles are the same in shape for all measurement periods, compatible to the supposed permanent stratification of this water volume (monimolimnion).

The EC data confirm the circulation scheme deduced by temperature profiles. The mixing processes keep the EC of surface waters of LPM (down to 14m) and whole LGM waters (the volume involved by thermal stratification) homogeneous. Since EC represents the content of total dissolved salts (TDS), an increase of EC implies an increase in density (see appendix VII). So the relevant electrical conductivity gradient in monimolimnion of LPM makes an important density gradient, probably liable of stratification and permanent static condition of monimolimnion of LPM.

The pH variation with depth (fig. 4.3) confirms the seasonal circulation of Monticchio lakes. The water stratification (warm period) induces different values between shallow and deep waters; the cool mixing period causes a partial or total homogenization of pH values in water column. As for temperature and EC, pH variations are valid down to ~15 m of the LPM and for the entire LGM. In the monimolimnion of LPM the pH values are subjected to seasonal variations (fig. 4.3), it is plausible that in periods of superficial turnover (cold periods) a diffusive stripping of gas is triggered with a decrease of deep dissolved CO_2 concentrations and an increase of pH values. Otherwise, in warm period the stratification of the entire lake

allows the accumulation of carbon dioxide in the deep portions, which reach lowest pH values (see also section 4.3.1).

The detail of ion concentration confirms the link of water chemistry with circulation dynamics. Both cations and anions show that shallow and deep waters of LPM are different in concentrations (fig. 4.4, 4.5). The ion profiles suggest a good and permanent stratification of deep volumes (monimolimnion). Homogeneous values of shallow layers (mixolimnion) suggest frequent turnover. The figure 4.4 also shows that the shallow waters of LGM often fall on the same values of the deep waters (both shallow and deep waters have very similar EC values – fig. 4.2), suggesting periodical mixing that involves the entire lake. For mixolomnion (the water volume subjected to periodically mixing) of both lakes, the mixing occurs in a cool period (at least from February to May), resulting in homogenization of all values. In cold periods the stratification facilitates the differentiation of solids in solution between shallow and deep waters, especially for calcium (the least conservative cation), as clearly observed in LGM (fig. 4.4 d).

In the HCO_3-SO_4-Cl ternary plots (fig. 5.8), shallow and deep waters of LPM always fall in a distinct groups and these waters never mix; instead in LGM, during cool periods shallow and deep waters overlap, indicating the water mixing. The same evidences can be noted in Mg-Ca-Na+K plot, for both lakes (fig. 4.5).

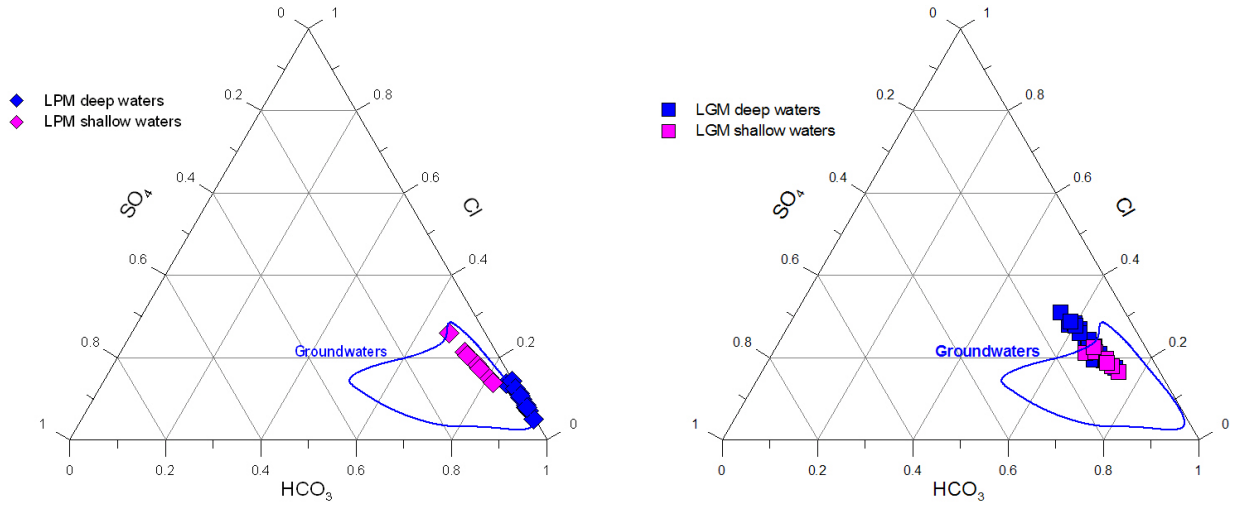

Figure 5.8 - Ternary plot of relative HCO_3^-, SO_4^{2-} and Cl^- contents in the waters of LPM and LGM for months of May, June, September 2009 and June 2010.

Analogously to the chemistry of major elements, mixing processes influences trace elements. Because of their low concentrations, trace elements can be a powerful tool for identification of mixing. Indeed, for LPM, the overlap of data of different months (fig. 4.6) is compatible

with a permanent stratification in the deeper water and turnover of mixolimnion. In the LGM trace elements have a period of very different concentrations between shallow and deep waters, during stratification (July 2007), and have two periods of partial homogenization, probably due to turnovers (fig. 4.7).

Water dynamics strongly control the concentration of dissolved gases in LGM: the highest methane concentrations were measured (up to 60 cc STP/liter) in the deep portion of the lakes during the stratification period (summertime); in periods of turnovers the concentrations along the water column became homogeneous (fig. 4.16 b). Focusing on the periods of methane accumulation and depletion, we found the highest values of dissolved CH_4 in September/October, suggesting that the stratification is maintained at least up to these months. The CH_4 concentrations drastically decrease in February, highlighting the de-stratification process, which persist up to May. A new stratification process starts in June, promoting a new accumulation of CH_4 in deep waters.

Dissolved helium concentrations show the same temporal variations observed for methane, following perfectly the water mixing processes.

Moreover, in the R/Ra versus $^4He/^{20}Ne$ graph (fig. 5.9), the deep waters of LPM (> 18m) always display less atmospheric contribution. Shallow waters are more aerated and the R/Ra values of the two groups are well separated (fig. 5.9 a). In LGM both deep and shallow waters display He isotope ratios in the same range of values during water mixing periods and only in stratification periods the He isotope composition of the deep waters is distinguishable from that of the shallow one. (Fig. 5.9 b).

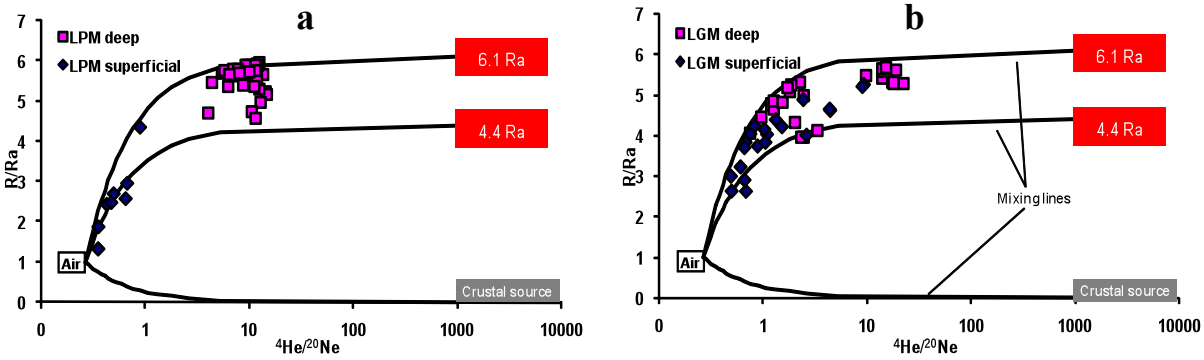

Figure 5.9 - Correlation diagram between the R/Ra (not corrected for the atmospheric contamination) and $^4He/^{20}Ne$ ratios of dissolved gases in LPM (a) and LGM (b) waters. Solid lines show the mixing of atmospheric derived helium (air) with deep sources (4.4 and 6.1 Ra) and with radiogenic helium (crustal source).

The concentration of others dissolved noble gases of atmospheric origin (e.g. Ar and Ne) are also influenced by water motion. In fact, dissolved Ar in LPM decreases towards the bottom down to values lower than that of air saturated water (fig. 4.22). That suggests isolation of

deep waters of the lake, after degassing processes occurred in the feeding aquifers (see section 4.4.2). In contrast, dissolved Ar in LGM is comparable to that of air saturated water at any depth. This different behaviour of Ar content in the two lakes can be explained by the turnover that seasonally occurs in LGM and carries shallow aerated waters towards depth and vice versa.

The obtained results clearly show that dissolved gases are powerful geochemical tools, together with water chemistry. Furthermore, dissolved gases have the advantage of high mobility and large differences in concentration and isotope signature between the various sources.

Our data suggest the circulation of LPM and LGM waters as schematized in figure 5.10. The LPM mixolimnion (i.e. epilimnion, thermocline and hypolimnion) spreads down to ~14 m of depth and mixes in cool periods. LGM mixes entirely in cool periods. As previously suggested by Cioni et al., (2006), our data confirm the meromictic nature of LPM; moreover we observe that mixolimnion of LPM (down to 14 m) mixes with a behaviour of a monomictic lake (mixing of entire lake once a year).

The meromixis of LPM can be related to groundwater inflow that feeds the deep portion of the lake with gases in CO_2 rich and TDS (see section 4.3), which make the waters denser. Therefore, LPM can be termed "crenogenic meromictic" (Boehrer & Schultze, 2008 and reference therein).

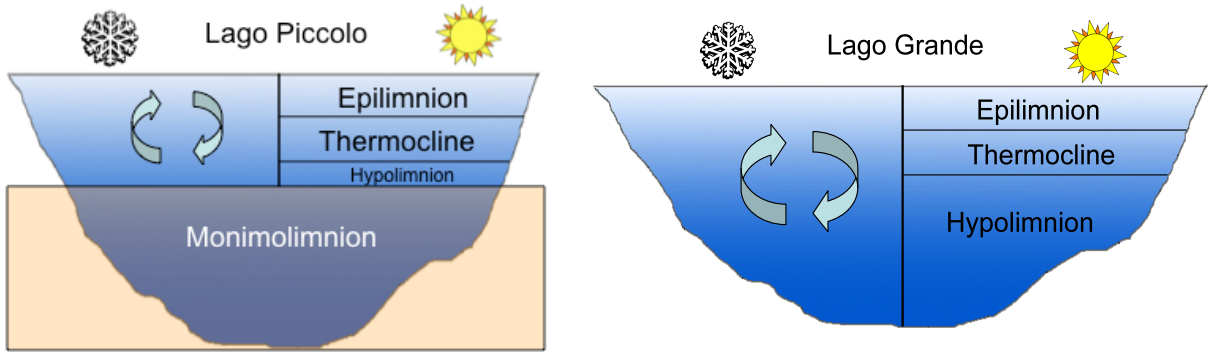

Figure 5.10 - Schematic picture of water dynamic in cold and warm periods for LPM and LGM.

On the basis of water chemistry and computer simulation by PREEQC code, we reasonably inferred the occurrence of endogenic processes (e.g. Ca, Mg, Fe, Mn carbonate precipitation) within the Monticchio lakes; the settling carbonate particles partially or totally dissolve in deep waters contributing to the increase of water density. If meromixis is induced by biological activity it is of biogenic type; if monimolimnion form due to biological activity and

inorganic geochemical processes the meromixis is defined endogenic (Boehrer & Schultze, 2008 and reference therein). LPM is probably both crenogenic and endogenic meromictic lake.

The entire LGM is formed by a mixolimnion that mixes only once a year, even if the turnover period involve some months. Therefore, differently from that reported in literature (Schettler & Albéric, 2008) it can be classified as a monomictic lake.

Although the two lakes are located only one hundred of metres apart, their water dynamics are quite different (fig. 5.10).

The engine of mixing processes is the change of water density between contiguous water volumes. Unfortunately, accurate field measurement of this physical parameter is generally not achievable (Gräfe et al., 2002). According to the approach outlined by Boehrer & Schultze (2008), it was calculated taking into account the available chemical and physical parameters, i.e., temperature, pressure, solids in solution, dissolved gases and suspended particles. Cioni et al. (2006) suggested that LPM monimolimnion is characterized by water having a higher density than the shallow ones, due to high concentration of dissolved solids, so that the considerable heat flux from the lake bottom is not able to destabilize the water stratification. In fact, even if the water density increases towards the bottom, the heat flux from LPM bottom is a factor working in the opposite direction up to ~15m. Therefore, the TDS, dissolved CO_2, and hydrostatic pressure appear have a decisive role on the density of deepest waters. On the contrary dissolved CH_4 has a destabilizing effect, due to its low molar mass and its relatively high partial molar volume (16 g/mol and 36.2 cc/mol respectively; see appendix VII). TDS and Fe^{2+} have an important role, due to the high molar mass and high concentrations in monimolimnion of LPM (up over to 9 meq/l). Fig. 5.11 shows as, the density of shallow waters is lower than that of deep waters during the two considered months (September 2009 and June 2010).

Considering that water and gas chemistry of shallow waters do not change too much in time (see water and gas sections, 4.2, 4.3, 4.4), a cooling of those waters (in figure 5.11 are also plotted the simulations for September 09 and June 10) would increase the density enough to mix them down to about 12 m of depth at LPM, as verified by the estimated density of shallow waters in February. Moreover, the shallow water density at 4°C is lower than densities of monimolimnion waters, preventing any mixing with deep waters. In contrast, in LGM the shallow water density at 4°C is close to values of hypolimnion, but slightly lower (fig. 5.11). Then, a high wind speed could trigger a turnover in LGM in cold periods. Also the organic and inorganic suspended matter can increase the superficial water density. Therefore,

to evaluate the contribution of suspended matter, in June 2010 we sampled a known volume (100 ml) of LGM shallow water (80 cm of depth), which was weighed by a precision balance, obtaining ρ=1.00255 ± 0.002 g/cm^3 (measured datum in fig. 5.11 d). In spite of the large error, this value is much higher than the estimated density of LGM shallow water (considering all dissolved species). This suggests that concentrations of suspended matter can give an important contribution to water density and can be significant to trigger a turnover of LGM (Boehrer & Schultze, 2008 and reference therein). In the LPM, the mixing processes are well explained without the density contribution of suspended matter. Moreover the transparency of LPM shallow water is greater than that of LGM (the transparency as Secchi depth is 5.5m in LPM compared to 0.3m in LGM; Mancino et al. 2009) due to a lower concentration of suspended solids than in the LGM, so the contribution of suspended matter on the density of LPM was considered negligible.

Despite the suspended matter can affect the mixing processes of LGM, the water and gas chemistry suggests that mixing occur in coldest period of the year, thus temperature has a key role in the turnover of Monticchio lakes. If the water temperature decreases below 4°C (highest density of water, see appendix VII), then the cold stratification starts. This is typical of dimictic lakes (mixing of entire lake twice a year) and often accompanied by ice cover. Between warm and cold stratifications there are two periods of mixing. If the water temperature does not decrease below 4°C, the cold stratification cannot be established and the mixing extend for the entire cold months (monomictic lake).

In winter, air temperature in Vulture area (at the Melfi station located at 580 m a.s.l.) reaches monthly mean values between 4 and 5°C (Fig. 5.12). Due to the higher elevation, the air temperature at Monticchio lakes (660 m a.s.l.) is probably lower than at Melfi station, but considering the high specific heat of water (fourfold higher than air value) and that lake waters undergo to the radiant heating by sunlight, we can expect that shallow water temperature can be higher than air temperature. Although we have not data referred to winter months, but continuous records performed 29/05/2010 - 06/06/2010 period confirm that behaviour (fig. 5.12) and display that the mean daily air temperature above the Monticchio lakes are 2°C below than that measured at Melfi station (18.2°C and 20.3°C, respectively). So the monthly mean temperature in shallow waters of Monticchio lakes in colder period can be considered above 4°C, then LGM is a warm monomictic lake and LPM is a meromictic lake, but his mixolimnion behaves as a warm monomictic lake.

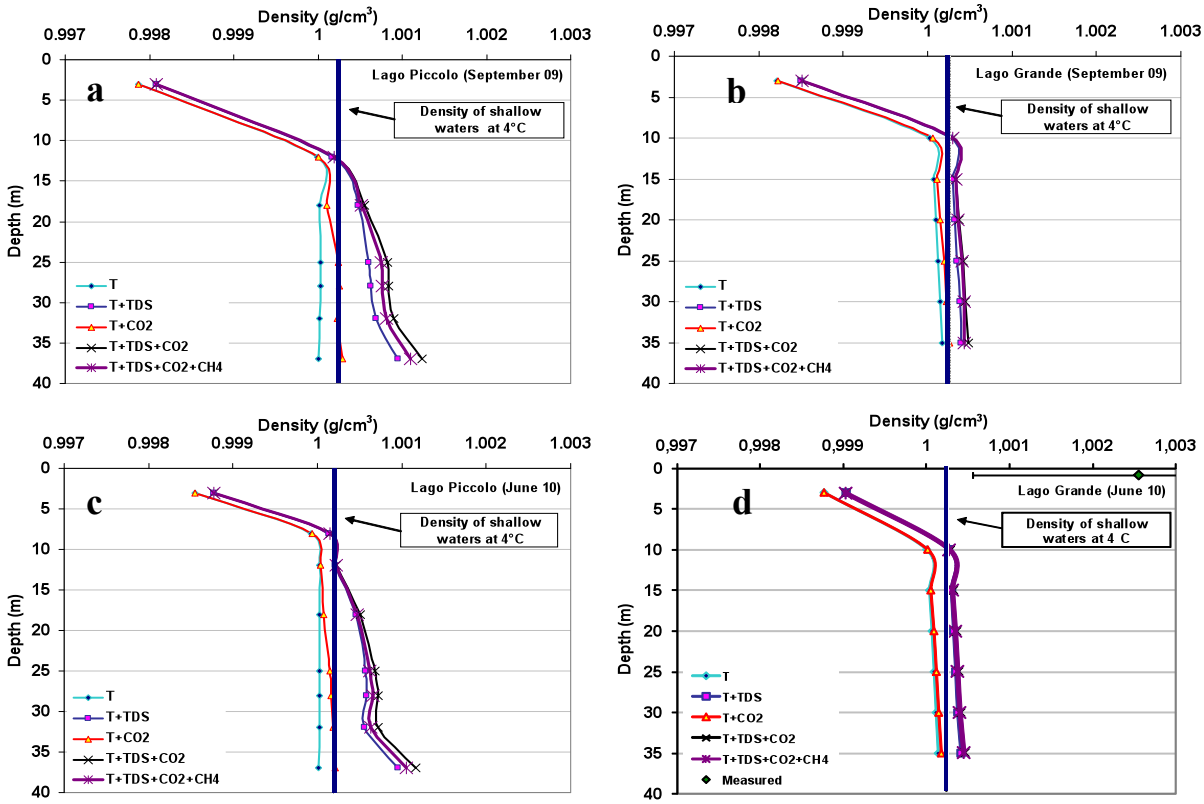

Figure 5.11 – Plots of water density versus depth for LPM (a, c) and LGM (b, d) in months of September 09 (a, b) and June 10 (c, d). The strip around the value of 1.0002 g/cm^3 indicates the shallow water density at 4°C. The measured value in plot d is relative to the water sample weighed by precision balance. See Appendix VII for calculations.

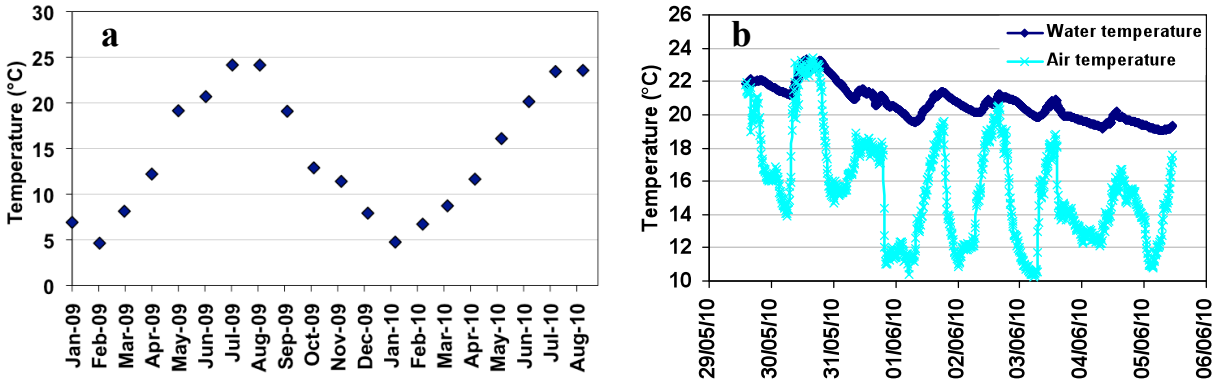

Figure 5.12 - a) Air temperature at the Melfi station (580 m a.s.l.; 10 Km away from lakes); b) Water and air temperature at the floating station on the LGM (the acquisition of data is every 15 minutes). The water temperature is meanly higher than air ones (see text).

By means of estimated densities it is possible to evaluate the stability along the water column of Monticchio lakes. Many parameters are used in literature to compute the stability: Schmidt stability (S), Birge stability (B), total work (G=S+B), Brunt-Väisälä- frequency (N) and E* stability (e.g. Idso, 1973; Kling et al. 1988; Kling et al., 1994; Wüest et al., 1996; Ambrosetti & Barbanti, 2002).

The evaluation of stability using S, B and G, allows to estimate the energy needed to de-stratify the water column. These methods consider the contribution of gases on density, but they do not take into account the saturation degree of gases. In fact, gas exsolution is able to destroy the local stability. The carbon dioxide has two behaviours: i) in undersaturation conditions it increases the water density and stabilizes deep layers (as previously discussed); ii) if P_{CO2} exceeds the ambient hydrostatic pressure, the exsolution can trigger a turnover (Kling et al 2005). The formulation proposed (Kling et al., 1988 and 1994) allows to consider the saturation degree of gases as follows:

$$E^* = \left[\left(\frac{1}{\rho}\right)\left(\frac{d\rho}{dz}\right)\right] \times \left[\left(\frac{P_{amb}}{P_{gas}}\right) - 1\right] \times \left(\frac{1}{P_{gas}}\right) \qquad (5.2\text{-}1)$$

where E* is the local stability (m^{-1} bar^{-1}), ρ is the density, z is the depth (m), P_{amb} and P_{gas} are the ambient hydrostatic pressure and the dissolved gases pressure (bar) respectively.

The first term [(1/ρ)(dρ/dz)] of equation (5.2-1) is a standard measurement of stability with the Brunt-Väisälä-frequency (N^2), but expressed in m^{-1} rather than s^{-2} because the acceleration of gravity (9.81 m s^{-2}) is not considered. Even if the values of E* cannot be converted in energy units (as for S, B and G), it is easy to evaluate the stability: negative values indicate unstable conditions and positive values correspond to stable conditions (Kling et al., 1988 and 1994).

The N^2 and E* values for Monticchio lakes are plotted in figure 5.13 and 5.14. All values are referred to the immediately superior layer (for example the local stability at 10 m was computed considering a *dρ* between 10 and 3 m). For both lakes it is evident that in the layer of maximum density gradient the stability is high (between surface layer and 10-15 m layer); more probably in winter period these layers are characterized by instability because the density gradient is near zero.

The LPM has local stabilities for the only contribute of density (N^2) higher than LGM except for 28m depth; the deeper value of LGM is even negative, denoting a local instability. Taking into account the gas pressure, the local stabilities (E*) of LPM (more reach in dissolved gases then LGM) lower drastically because near to exsolution, especially in near bottom waters (fig. 5.14, 5.15). In the LGM the dissolved gases, distant to exsolution line (fig. 5.15), increase the stability mainly thanks to high molar mass and low molar volume of CO_2. The graphs in figures 5.13 and 5.14 are referred only to September 2009; the other month estimated is June-10 and has a similar trend than the plotted one.

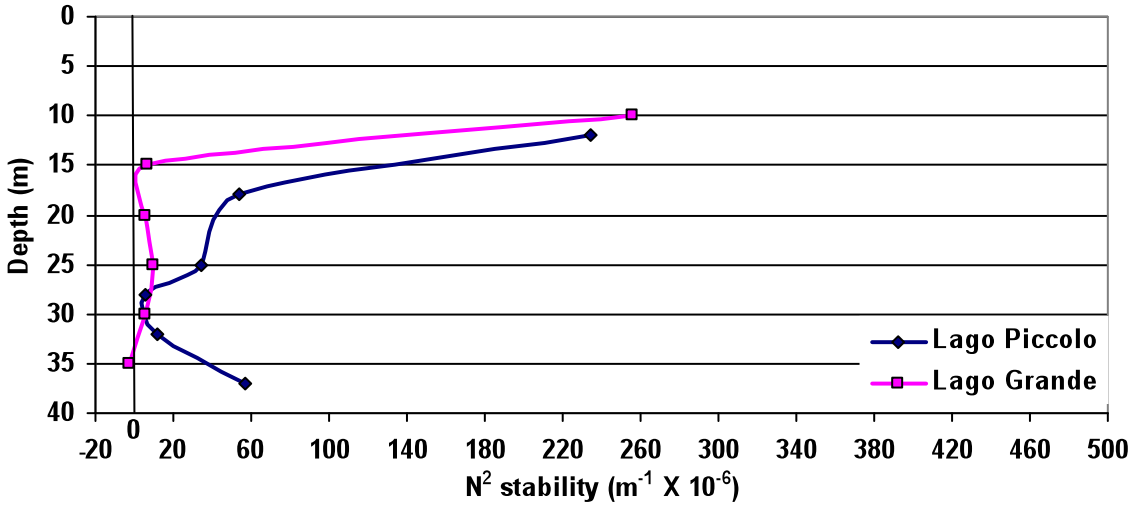

Figure 5.13 - Distribution of local water column stability ($m^{-1} \times 10^{-6}$) with depth (m) in LPM and LGM (N^2, see text). The plotted data refer to September 2009.

The stability data shows the importance of dissolved gases on the lake water stability. Looking at the figure 5.15, LGM is always undersaturated (over 2.4 bars below saturation line) due to the periodic turnovers that gradually release the accumulated gases of deep water volumes to the surface. Whereas the near bottom waters of LPM are slightly undersaturated (in the range of 0.4÷1.26 bars: fig. 5.15).

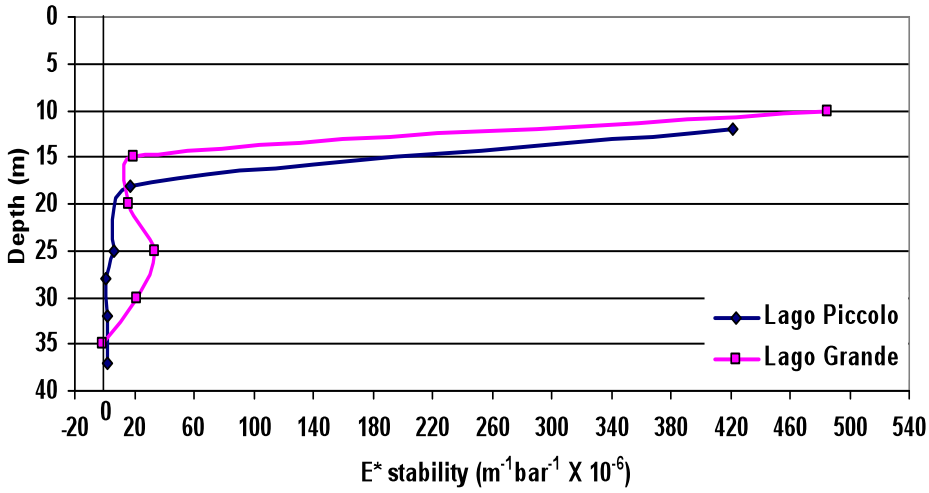

Figure 5.14 - Distribution of local water column stability (m^{-1} $bar^{-1} \times 10^{-6}$) with depth (m) modified for the effects of dissolved gas (E*, see text) in LPM and LGM. The plotted data refer to September 2009.

In the case of LPM, the oversaturation (degassing) can be easily reached by a forced rise of deep waters to shallow depth (lower hydrostatic pressure) as a consequence of, e.g., landslide, earthquake, internal wave. These processes were proposed to explain the disastrous outburst of CO_2 from Lake Monoun in 1984 (Sigurdsson et al. 1987) and Lake Nyos in 1986 (Kling et al. 1987; Evans et al. 1994), that caused the loss of lives (37 and 1746, respectively). Other

possible explanation can be found in a sudden gas injection in the lake bottom from a CO_2 accumulation in the crust (accumulations of CO_2 near the Earth surface were already observed; Chivas et al., 1987; Lockwood and Rubin, 1989).

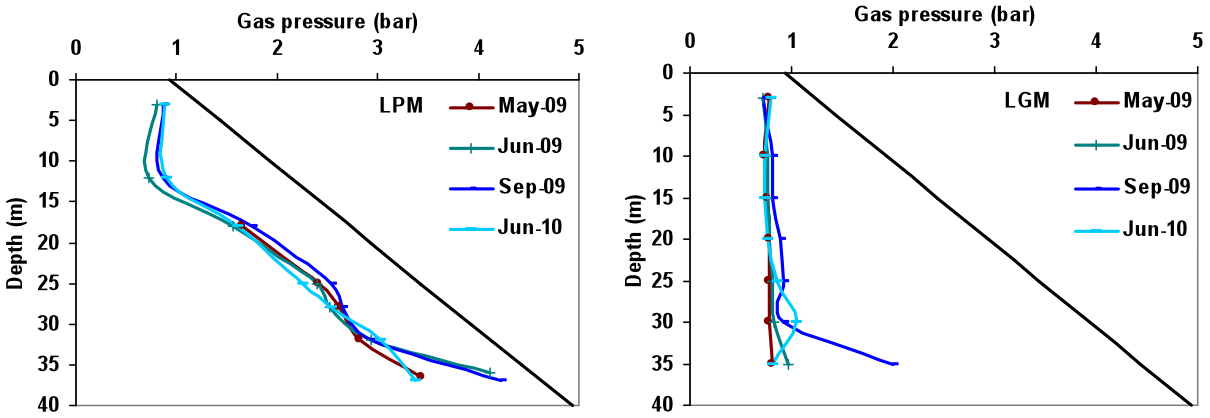

Figure 5.15 - Distribution of total in situ gas pressure (bar) with depth (m) in LPM and LGM, over time (from May 2009 to June 2010). The black solid line represents the gas saturation line (total hydrostatic plus atmospheric pressure), over this limit the dissolved gas will form bubbles.

Considering the concentrations of dissolved CH_4 and CO_2 in the deep waters of LPM, an amount of about 84 tons and 814 tons respectively were stored in the lake, with an equivalent released gas volume of about 5.8×10^5 m^3 (at 1 bar). The corresponding thickness of that lethal gas mixture would be about 3.5 m over the entire lake surface. Those figures confirm previous estimate (Caracausi et al., 2009). Despite it is an approximate estimate, the LPM has a relatively high potential of gas hazard. It should be noticed that particularly during touristic periods, there are about 30000 visitors throughout the summer (Hansen, 1993). The scenario is further complicated by the crater topography with high rims, which does not facilitate the dispersal of lethal gases.

The possibility of a gas eruption, even called limnic eruption (Sabroux et al., 1987), becomes more realistic considering historical documents (Tata, 1778; Palmieri and Scacchi, 1852; Ciarallo and Capaldo, 1995) that reported events of massive gas release from LPM.

5.3 Thermal and mass transport

The water circulation of Monticchio lakes highlighted the high stability of deep waters of LPM and the seasonal mixing of waters of entire LGM.

The diffusive/advective processes in lake waters can be better understood by means of mass diffusion coefficient/heat diffusivity coefficient (e.g., Jassby and Powell, 1975; Imboden et al., 1983; Benoit and Hemond, 1996).

The law that defines the fluxes (J_i) is the Fick's First Law:

$$J_i = -D_i \frac{\partial x_i}{\partial z} \tag{5.3-1}$$

where D_i is the diffusion coefficient of i-esim substance (cm^2 s^{-1}), $\partial x_i/\partial z$ is the gradient of concentration of i-esim substance in the z space. In conditions of molecular transport the D_i (D_{iMOL}) is well known for various substances, so that it is possible to estimate the flux Ji, if the gradient is known.

A similar theoretical formulation defines the heat flux by means of Fourier postulate:

$$H = -K \frac{\partial T}{\partial z} \tag{5.3-2}$$

where K is the heat diffusivity coefficient (cm^2 s^{-1}) and $\partial T/\partial z$ is temperature gradient in the z space.

Unfortunately, the transfer process governing the distribution of mass and energy in lakes is normally not the molecular diffusion, so it is not possible to know a priori both D_i and K. These two parameters are conceptually different because one is referred to a mass transport, another to an energy transport, practically they have an analogous meaning. In the case of molecular diffusion the D_i assumes a specific value for any substance and is different from K. In conditions of turbulent water movement the eddy diffusion coefficient ($D_{i\ EDDY}$) must be considered and this assumes the same value both for chemical substances and heat. Therefore, the $D_{i\ EDDY}$ is the same for all substances and also applies to thermal diffusion as Kz because the turbulent transport is an in mass movement, orders of magnitude more rapid than molecular diffusion.

The evaluation of vertical Kz could allow an estimation of fluxes by the use of gradients, as seen above. There are many attempts in the Kz evaluation (e.g., Powell & Jassby, 1974;

Katsev et al. 2010). The commonly used method for calculating the vertical eddy diffusion coefficient makes use of temporal and spatial temperature variations of lake waters (e.g., Powell & Jassby, 1974; Imboden et al., 1983; Benoit & Hemond, 1996). The method is largely explained in Powell & Jassby (1974) and Jassby & Powell (1975).

Benoit and Hemond (1996) rearranged the flux gradient method of Powell & Jassby (1974) introducing thermal exchange with sediments. The modified method takes into account the temperature variations due to the effect of: eddy diffusive transport, radiant heating by sunlight ($R_{(z)}$) and thermal exchange with sediments ($H_{(z)}$), as follows:

$$K_z = \left[-\int_z^{z_{max}} \rho C_p \frac{dT}{dt} F_{(z)} dz + R_{(z)} F_{(z)} - \int_z^{z_{max}} H_{(z)} l_{(z)} dz \right] \cdot \left[\left(\rho C_p \frac{dT}{dt} \right) F_{(z)} \right] \qquad (5.3\text{-}3)$$

where, T is the temperature (°C), t is the time (s), z is the depth (cm), $F_{(z)}$ is the lake area at depth z (cm^2), $l_{(z)}$ is the wetted perimeter of the lake at depth z (cm), ρ is the density (g cm^{-3}) and C_p is the heat capacity (cal $g^{-1}°C^{-1}$).

The terms related to the radiant heat by sunlight and the thermal exchange with sediments are difficult to estimate because they depend on several parameters, which are not easy to evaluate. For this reason often they are not considered (e.g., Li, 1973; Imboden et al., 1983; Wuest et al., 2000). Also in our case these terms are not considered, mainly because they are negligible in the context of Monticchio lakes. We refer to Appendix IX for more explanation about that.

The used method provides the comparison of thermal gradient with time. The LPM monimolimnion is in a quasi thermal steady state, therefore small temperature variation over time (< 0.05 °C/month) imposes the use of temperature data at least of one month apart (in agreement with our sampling campaign intervals). Moreover, considering the conditions of quasi thermal steady state of LPM (permanent stratification) the range of estimated eddy diffusion coefficient for June-July 2010 was extended to all investigated months.

The rapidity of temperature variation over time at LGM is higher than at LPM (fig. 4.1). For this reason is not advisable the use of data with monthly interval (with rapidity in temperature changes, in a month can alternate increase and decrease of temperature, which would alter the *Kz* estimation). We measured the temperatures of LGM waters every few days; this dataset is more difficult to elaborate (the study is still in progress). Anyway the estimated K_z values for LGM cannot be extended to all investigated months.

Thus we estimated the values of vertical eddy diffusion coefficient only in LPM, they are shown in figure 5.16. Taking into account a maximum error of about 40% for smaller values, the deeper waters of LPM (≥ 30 m) have a K_z ranging between 8.9×10^{-4} and 2.3×10^{-3} cm^2 s^{-1}, close to molecular thermal diffusivity (1.4×10^{-3} cm^2 s^{-1}). This suggests a high stability of LPM deep water. For the same lake, in the remaining part of monimolimnion (> 15 m) the K_z values are higher with a peak at 25 m. In the shallow depths of LPM the values increase and stay unchanged (fig. 5.16).

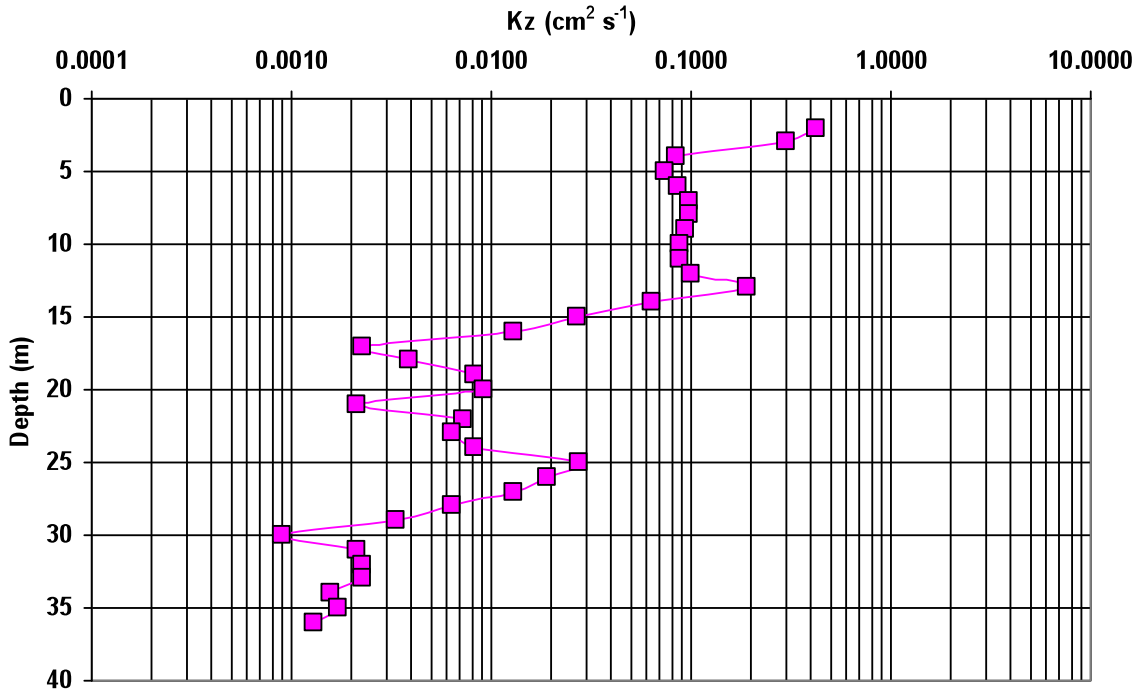

Figure 5.16 - Vertical eddy diffusion coefficients (Kz) during the period May 31-2010 – July 12-2010 in LPM. The error bar of Kz can reach the 40% in lower values. The most reliable values are restricted to the thermocline, hypolimnion and monimolimnion (5-10, 10-15, 15-36 m of depth, respectively; fig. 4.1 and 5.10), where can be assumed that vertical transport via advection and horizontal currents are negligible (Jassby and Powell, 1975).

The water motion can be triggered by a groundwater inflow, so the K_z of deep water (below 30 m) could suggests a low groundwater inflow; the increase of eddy diffusion coefficient between 25-30 meters can be related with a high groundwater inflow. Even the vertical eddy diffusion coefficients confirm that the LPM is meromictic.

5.3.1. - Gas fluxes

with equation (5.3-1) it was possible to evaluate the gases flux using the estimated diffusion coefficient and the concentration gradients.

The total diffusion coefficient of i-esim substance ($D_{i\,TOT}$) is:

$$D_{i\,TOT} = D_{i\,MOL} + D_{i\,EDDY} \qquad (5.3\text{-}4)$$

where $D_{i\ MOL}$ is the molecular diffusion coefficient and $D_{i\ EDDY}$ is the eddy diffusion coefficient. The mean heat diffusivity coefficient for deeper layer of LPM is 1.73×10^{-3} cm^2 s^{-1} (from 30 to 36 meters of depth; fig. 5.16); considering an error of about 40%, this value can be approximated to the value of thermal diffusivity in water (1.43×10^{-3} cm^2 s^{-1}). So the deeper water layer of LPM (from 31 to 36 meters of depth) the mean diffusion coefficient ranges from molecular (for $CH_4 = 1.24 \times 10^{-5}$ and for $CO_2 = 1.26 \times 10^{-5}$ cm^2 s^{-1} at 10°C) to eddy (1.43×10^{-3} cm^2 s^{-1}).

The methane fluxes from the bottom of LPM (37 meters of depth) range between about $1x10^{-3}$ and $1x10^{-1}$ g m^{-2} day^{-1}, using the molecular and eddy diffusion coefficient, respectively (fig. 5.17). Considering the error of ~30%, these fluxes are constant over time. Probably the methane production mainly occurs in monimolimnion because it is in anoxic conditions.

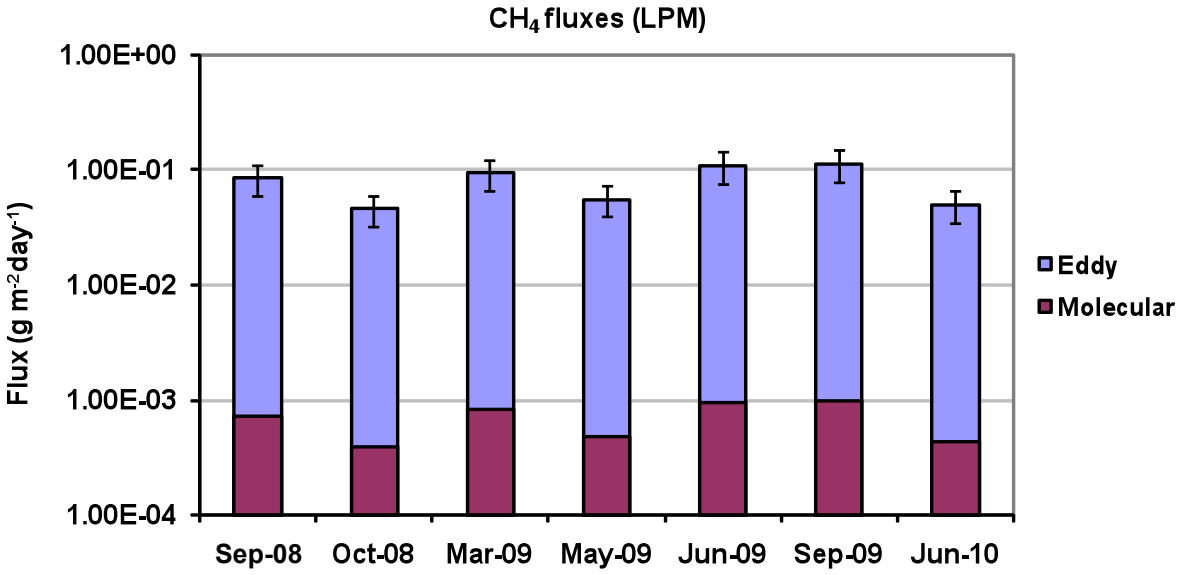

Figure 5.17 - Histogram of methane fluxes in LPM for sampled months. The values are both referred to Eddy and Molecular diffusion in water. The error is about 30%.

In LGM the eddy diffusion coefficients are not available, therefore we estimate the CH_4 fluxes using a molecular diffusion coefficient (1.24×10^{-5} cm^2 s^{-1}), obtaining values very variable over time (from 0.033 to 7.9×10^{-4} g m^{-2} day^{-1}). Certainly, this is a rough estimation, so considering the high water circulation of LGM, probably the actual fluxes are in the range of 2÷5 order of magnitude higher than estimated ones (as suggested by eddy diffusion

coefficients in other lakes; Li, 1973; Jussby and Powel, 1975; Imboden et al., 1983; Robarts and Ward, 1978; Katsev et al., 2010). However, unlike LPM, the methane flux is variable over time. Even in LGM the CH_4 production more probably involves the entire lake bottom, with a widespread contribution of anoxic sediments (in the deeper portion).

The CO_2 flux come from the bottom of both Monticchio lakes and its inorganic signature implies an external inflow, more probably a groundwater inflow, riches in dissolved carbon dioxide (see also chapter of carbonate system.

For the CO_2 fluxes estimations we considered the gradients and the eddy diffusion coefficients of bottom water layer (32 to 37 m) for LPM. Considering the values above discussed, the eddy fluxes are between 0.4 and 0.7 g m^{-2} day^{-1} over time. The fluxes with molecular diffusion are about two orders of magnitude lower than eddy ones (fig. 5.18 a). The variations from month to month are in the error range (~30%), so the carbon dioxide flux in LPM can be considered unchanged over time.

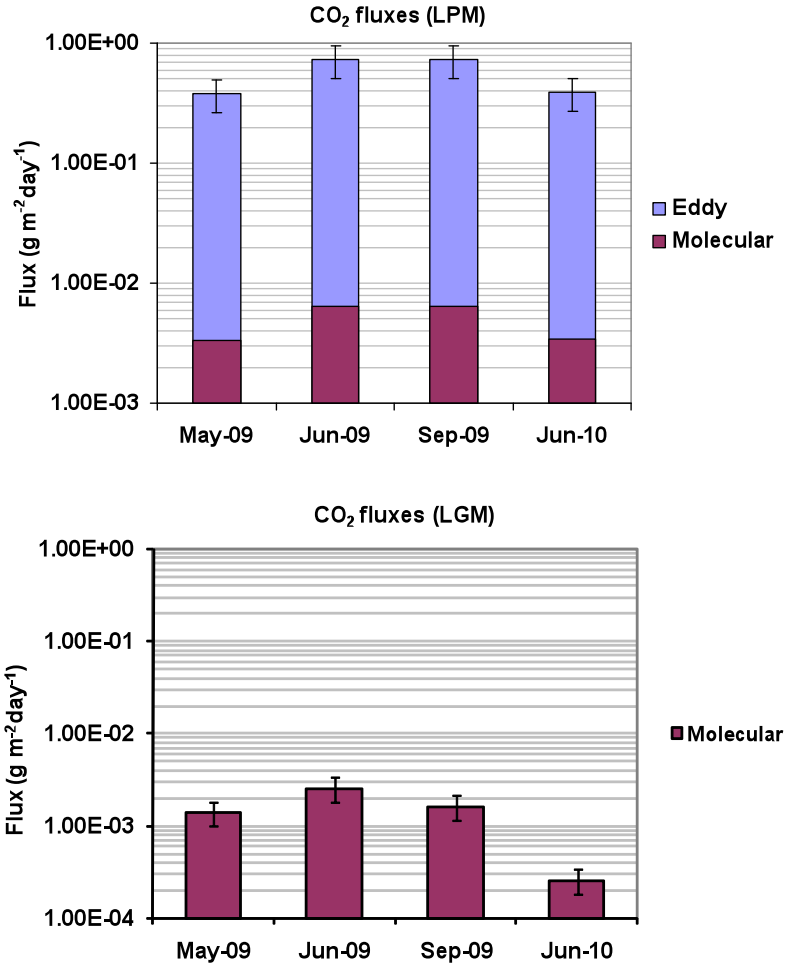

Figure 5.18 - Histogram of carbon dioxide fluxes in LPM and LGM for sampled months. The LPM values are both referred to Eddy and Molecular diffusion in water; the LGM values were evaluated assuming a molecular diffusion. The error bar is about 30%.

As for the methane fluxes, for CO_2 we used a molecular diffusion coefficient (1.26 x 10^{-5} cm^2 s^{-1}) and we obtain values between 0.26 and 2.5 × 10^{-3} g m^{-2} day^{-1} in LGM (fig. 5.18 b). More probably the values are underestimated, but a clear variation over time exists.

The main inflow of mantle-derived helium in LPM is localized at about 28 m, therefore two flux directions are recognized, one towards the bottom the other one towards the surface (fig. 5.19 a). For the upward fluxes, helium gradients in the range of 18 and 25 m of depth were used, whereas helium gradients from 32 to 37 m were used for downward flux. As show the figure 5.19 a, the flux towards the surface, for different months, ranges from 6.3 × 10^{-7} to 1.4 × 10^{-6} g m^{-2} day^{-1}, these values are always higher than the fluxes towards the bottom that range from 4.7 × 10^{-8} to 4.3 × 10^{-7} g m^{-2} day^{-1}. As known, the carbon dioxide is normally a carrier of helium (and other gases) in volcanic systems, so the possibility that there is also some helium inflow from the lake bottom (about 37m) cannot be ruled out.

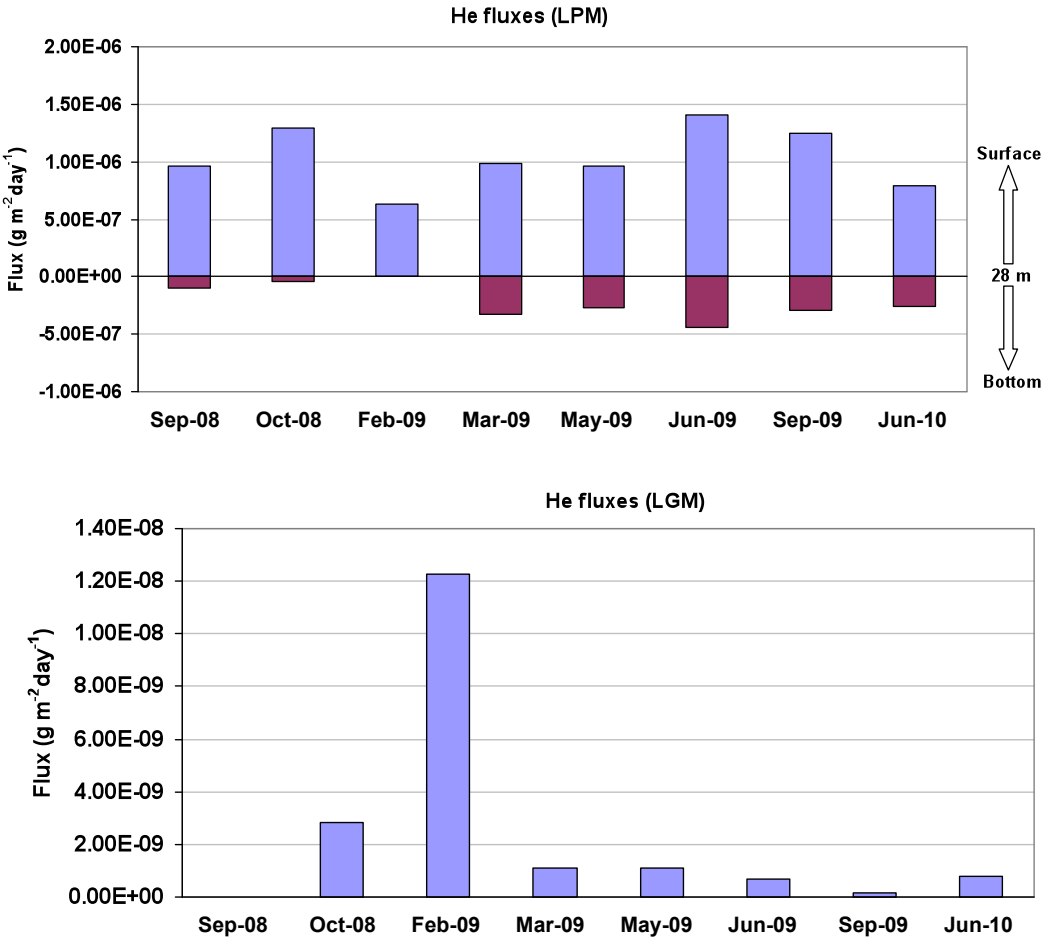

Figure 5.19 - Histogram of He in LPM and LGM for sampled months. The LPM values are referred to Eddy diffusion in water also considering the 28 meters input, two fluxes forms: towards surface and towards bottom. The LGM values was evaluated assuming a molecular diffusion. The error bar are about 30%.

The helium flux in LGM comes from the bottom and we considered gradients between 30 and 34 m of depth (fig. 5.19 b). Assuming that the diffusion coefficient is molecular one (5.67 × 10^{-5} cm^2 s^{-1} at 10°C), the resulting fluxes are meanly close to 1 × 10^{-9} g m^{-2} day^{-1} with a peak of 1.2 × 10^{-8} g m^{-2} day^{-1} in February 2009. Even the helium fluxes in LGM change from month to month, this can be explainable with seasonal variations on water dynamic (see section 5.2). It is worth of note that our gas fluxes estimations at LGM are largely underestimated, we have evidences that the diffusion is well above the molecular one. For example, an eddy diffusion coefficient of 0.03 cm^2 s^{-1} was adopted for Lake Mashu (Igarashi et al., 1992); using this value with our data of LGM, the evaluated fluxes would increase by two orders of magnitude.

5.3.2.-Heat flow

As discussed in section 4.1, temperature profiles of LPM show clear gradients below 16 m of depth and temperature increases towards the bottom (37 m) (details of the temperature profile is shown in figure 5.20).

By means of the Fourier postulate (eq. 5.3-2), the temperature gradients and the eddy diffusivity coefficients (K_z), we can obtain the heat flow in deep water layers. The thermal diffusivity in water used was 1.43x 10^{-3} cm^2 s^{-1}. The mean estimated deep heat flow is 75 mW m^{-2}, which has been almost constant during the 3 years of investigations.

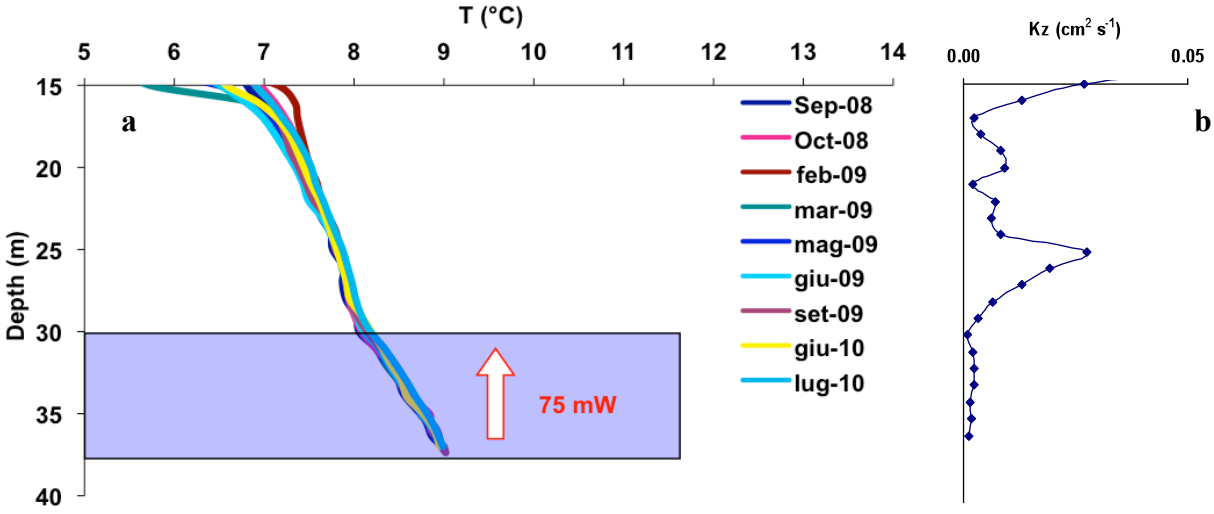

Figure 5.20 - Detail of Temperature profile versus depth (from 15 m to bottom) in LPM for different months (a); eddy diffusion coefficients (Kz) as in figure 5.16 (b). Below the 30 m of depth there is a change on temperature gradient ad on Kz.

Previous geophysical investigations measured a regional heat flow in the Mt.Vulture area (Mongelli et al.,1996) of about 50 mW m^{-2} (fig. 5.21). Taking into account that heat produced

by the decay of U, Th and K contained in Mt. Vulture volcanic rocks is at most 5-6 mW m^{-2} (see Appendix VIII), a clear heat excess of about 20 mW m^{-2} is present in LPM (75-50-5=20 mW m^{-2}).

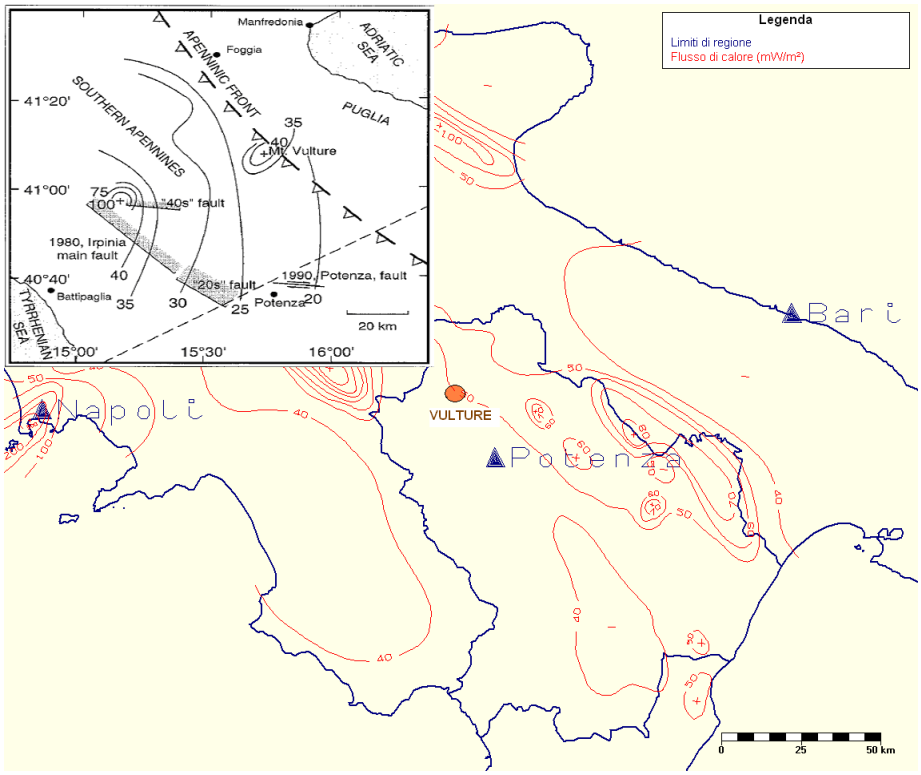

Figure 5.21 – Heat flow in Southern Italy. The Mt. Vulture falls in the curve of 50 mW m^{-2} (Banca Nazionale dati geotermici – I.I.R.G.-C.N.R. Pisa). The square above shows a high spot gradient on Vulture area of 40°C/Km (modified from Mongelli et al., 1996).

5.4 Origin of He and CO_2

The observed synchronous variations in both lakes of He abundances, He isotope ratios and CO_2, strongly indicate that a relevant gas transfer from the depth of Mt. Vulture is still active. Consequently, two important questions arise about the actual origin of CO_2 and He: i) are they extracted from deep and hot solidified igneous intrusions? ii) in spite of the extremely long time lapse (about 140 ka) from the volcanic eruption forming the Monticchio *maars*, some degassing melt is present at depth?

With the aim of investigate the subject, we tried to reconstruct the pristine isotope composition of CO_2 and the concentration of both CO_2 and He. Those were transported into the lake through the groundwater.

Having this in mind, we focussed our attention on TDIC data of LPM bottom (at depth of 36 m). The total inorganic carbon (TDIC) dissolved in the deepest waters of LPM is 0.023 mol/l, having an isotopic signature $\delta^{13}C$ = -0.5‰ (vs. PDB), while dissolved CH_4 is 0.00625 mol/l. 70 % (0.004375 mol/l) of the latter is generated by acetate-type fermentation and the remaining 30% (0.001875 mol/l) is produced by CO_2 reduction (see section 4.4.1). Taking into account that an equal amount of CO_2 and CH_4 are produced during the process of acetate fermentation, we estimated that 0.004375 mol/l of CO_2 are generated with a $\delta^{13}C$ down to -20 and -28 ‰ (Pearson and Friedman, 1970; Deines at al., 1974; Rose and Devisson, 1996). At the same time the carbon isotope composition of CO_2 is shifted towards more positive values ($\Delta\delta \sim 6‰$; Botz et al., 1996) during its reduction to form methane.

1) CH_3COOH (acetate fermentation) $\longrightarrow$ { CH_4 (70% of the total); CO_2 (lowest $\delta^{13}C_{(CO2)}$ = -20 ‰ ÷ -28 ‰) }

2) CO_2 reduction process $\longrightarrow$ CH_4 (30% of the total) leads to a positive shift of CO_2 isotope composition ($\Delta\delta \sim 6‰$).

We can consider two different pathways:

i) the CO_2 generated by acetate fermentation is added to deep CO_2 entering into the lake;
ii) deep CO_2 entering into the lake is partially reduced to form methane and is mixed with CO_2 generated by acetate fermentation process.

In the first case, the deep inorganic CO_2 (equal to 0.023-0.004375 mol/l) entering into lake is admixed with 0.004375 mol/liter of organic CO_2, produced by acetate fermentation. Then the

carbon isotope composition of that CO_2 mixture will be shifted towards less negative values ($\Delta\delta\sim$ 6‰, as a consequence of CH_4 production by CO_2 reduction process). Bearing in mind that the resulting CO_2 has a $\delta^{13}C$ value -0.5‰, then the carbon isotope composition of deep inorganic CO_2, entering into the lake, should have a $\delta^{13}C$ no lower than -3‰.

In the second case, deep inorganic CO_2 is shifted by ~ 6‰ after CO_2 reduction process and then it is mixed with CO_2 produced by acetate fermentation process, which has a carbon isotope signature in the range of -20 ‰ ÷ -28 ‰. This would lead a isotope composition of deep CO_2 entering into the lake no lower than -3.8 ‰.

Taking into account that in the lake deep waters we measured 0.023 mol/l as TDIC and that the CO_2 consumption during methanogenesis processes is equivalent to 0,006 mol/l of dissolved CH_4, of which 0.004375 mol/l are produced via acetate and 0.001875 mol/l are produced via CO_2 reduction), we estimate the TDIC content in groundwater was of 0.029 mol/l (= 0.023 + 0.006).

However, we have to take into account that atmospheric noble gases clearly indicate that degassing process had already affected groundwater that carried the deep inorganic CO_2. We estimated a residual fraction of Ar (F_{Ar} = 0.7) as a result of that degassing, by comparison of the Ar content in the deep water of the lake with the expected amount in a meteoric water equilibrated with atmospheric gases at T and P conditions of groundwater recharge (about 10°C).

Therefore, we can assess to both the deep inizial CO_2 /Ar and He/Ar ratios (before groundwater degassing), being known the final CO_2 /Ar and He/Ar ratios. Assuming a Rayleigh process, the following relationship is used:

$$\left(\frac{i}{Ar}\right)_{final} = \left(\frac{i}{Ar}\right)_{inizial} F_{Ar}^{\left(\frac{K_i}{K_{Ar}}-1\right)}$$

where $\left(\frac{i}{Ar}\right)_{final}$ and $\left(\frac{i}{Ar}\right)_{inizial}$ are the final and initial ratios of dissolved volatile specie (CO_2 or He) respectively. F_{Ar} is the residual fraction of dissolved atmospheric Ar, K is the Henry constant.

As reported above, the TDIC content (final) in groundwater, before CO_2 consumption by methanogenesis processes, was of 0.029 mol/l. The resulting initial concentration of CO_2 , dissolved in groundwater before degassing occurs, are about 0.04 mol/l.

With the aim of assessing the effect of degassing on the initial, we evaluated the carbon isotope shift assuming that degassing of groundwater occurred at pH values in the range of 5.0÷6.5 and at temperature of about 10°C (fig. 5.22 a and b).

As a result, the carbon isotope composition of residual TDIC would shift towards more positive values by +1.0 ‰ (at maximum for pH=6.0) than the calculated initial TDIC in groundwater of 0.04 mol/l. Therefore, the initial concentration (0.04 mol/l) of TDIC in groundwater would have a carbon isotope signature of $\delta^{13}C_{(TDIC)}$ ranging between -4.0 ‰ and -4.8 ‰ (vs PDB).

It is worth of note that these calculated isotope signatures are surprisingly close to that of carbonatitic matrix (-4.8 ‰) of LPM maar ejecta (Rosatelli et al., 2000).

Analogously, the calculated initial content of mantle helium (6.1 Ra) dissolved in groundwater is 1.28 x 10^{-2} cc STP/l, with a corresponding ^{3}He amount of 4.8 x 10^{-12} cc STP/l. The resulting pristine $CO_2/^{3}He$ ratio of deep-seated gas is 8.3 × 10^{9}, which is not distant from the ratio 2.9 × 10^{9} (Costa, 2010) by mofete gases of Maschito site (located at South-East of Mt. Vulture, along the same tectonic discontinuity crossing the Monticchio lakes). However the ratio is higher than the typical value of ~ 2 × 10^{9} reported for mantle gases (e.g., Marty et al., 1994; Sano and Marty, 1995; van Soest et al., 1998).

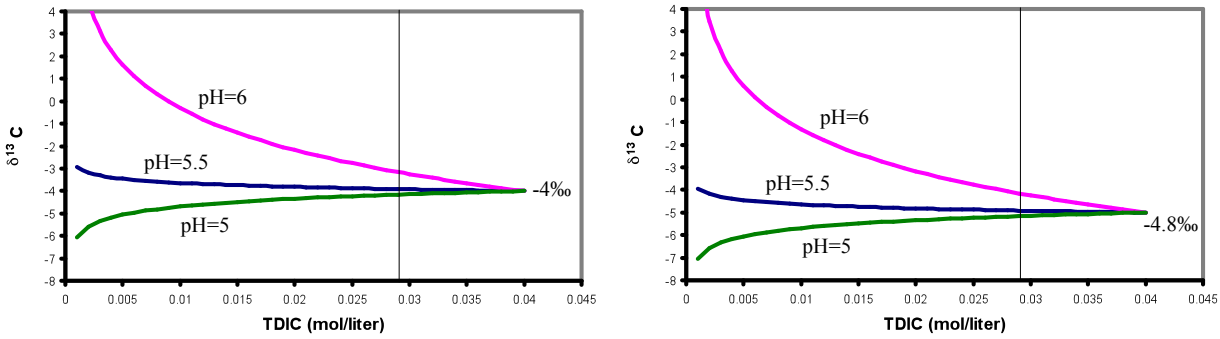

Figure 5.22 - Carbon isotope shift after degassing fractionation at different pH values and referred to the calculated residual TDIC in groundwater of 0.029 mol/l. a) is related to a $\delta^{13}C_{(TDIC)}$ = -3‰ (vs PDB); b) is related to a $\delta^{13}C$ near -3.8 ‰ (vs PDB); the pristine isotope signature are -4 and -4.8 ‰. (carbon isotope fractionation from Deines at al., 1974).

5.5 ^{3}He/Heat and C/^{3}He

Assuming helium and heat coming from by a common deep source, by means of discussed fluxes we evaluate in LPM a ^{3}He/heat ratio of about 2.13 x 10^8. This value is in the range of others maar lakes and confirms that this lake-type has higher ^{3}He/heat ratio compared to others crater lakes of different origin as Kipfer et al. (2002) pointed out (fig. 5.23). The ^{3}He/heat ratio in LPM is also higher than values found in submarine hydrothermal systems of the ocean (Baker and Lupton, 1990; Jean-Baptiste et al., 2004). Aeschbach-Hertig et al. (1996) suggest a decreasing of ^{3}He/heat ratio in maar lakes with age, but this relation consists of only two data (Lake Nyos and Laacher See), as declared by the authors. The datum of lac Pavin (Aeschbach-Hertig et al., 1999) and our value, certainly enrich the worldwide dataset, but not enough to constrain the relation ^{3}He/heat versus age of last volcanism.

Anyhow, the ^{3}He/heat ratio in LPM is comparable to values of Lac Pavin and Laacher See, which are characterized by a younger volcanism (6600 and 11000 years, respectively) than LPM genesis (140000 years). If a relation of ^{3}He/heat ratio with age of volcanic activity had to exist it would be reasonable to think that ^{3}He amounts and heat measured in LPM came from a magma source very younger than 140000 year.

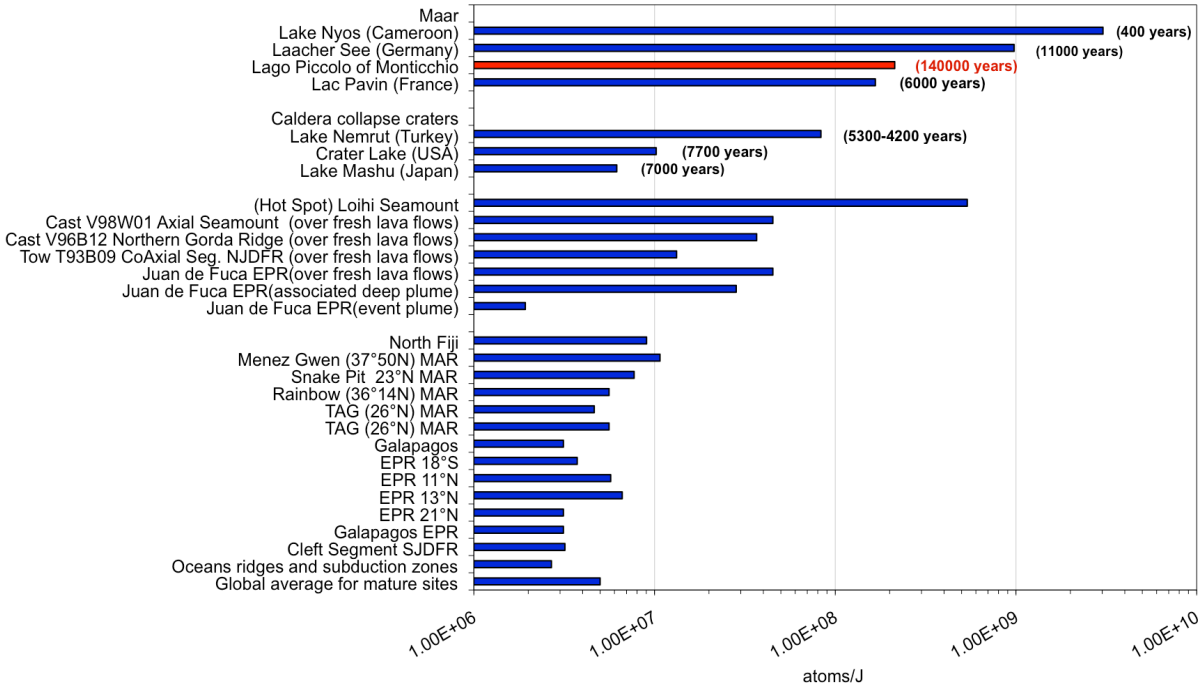

Figure 5.23 - Comparison of ^{3}He/heat ratio (atoms/J) of many volcanic systems. The value of LPM (2.13 × 10^8) falls in the range of maar-type lakes. The years in brackets are referred to the last volcanic activity. Data from Kipfer et al. (2002) and reference therein, Baker and Lupton (1990) and Jean-Baptiste et al. (2004).

A more systematic variation with age than ^{3}He/heat ratio was found for the ratio C/^{3}He using data of Lake Nyos, lac Pavin and Laacher see (Aeschbach-Hertig et al., 1999b; Kipfer et al. 2002; fig. 5.24); the C/^{3}He ratio decrease with increasing of the maar formation age. However, the value of Lake Monoun (1.7×10^{10}, Nagao et al. 2010) does not fit in the provisional relationship.

The pristine C/^{3}He ratio of gases feeding LPM (8.3×10^9) is near the value of Laacher see (9×10^9, 11000 years), therefore a magma source younger than 140000 year can be hypothesized.

In the C/^{3}He vs. ^{3}He/^{4}He (as R/Ra) plot (fig. 5.25), the maar lakes and the caldera collapse crater lakes fall in distinct areas. The maar lakes have lower values both of C/^{3}He and R/Ra than caldera collapse crater lakes. The two groups of lake are out of mixing between MORB and Crust end-members, this could result from addition of CO_2 derived from marine limestone and sedimentary rocks (Marty et al., 1994; Nagao et al., 2010).

LPM fall within the values of maar lakes and get close to the values of Etna and Vulcano, the most active volcanic areas in Southern Italy. This suggests a prevalent magmatic origin of CO_2 and He (as already highlighted by isotopic data both of CO_2 and He).

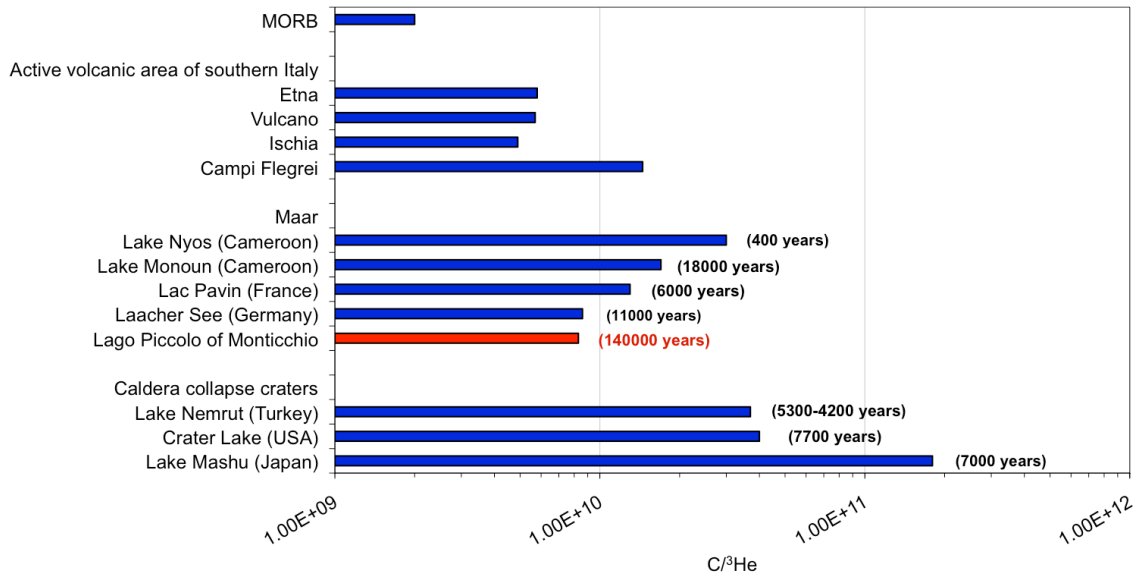

Figure 5.24 - Comparison of C/^{3}He ratio of many volcanic lakes and active volcanic areas of Southern Italy. The years in brackets are referred to the last volcanic activity. Datum of Lago Piccolo of Monticchio from this work. Data of volcanic lakes from Kipfer et al. (2002) and reference therein, Nagao et al. (2010). Data of active volcanic areas of Southern Italy from Marty et al. (1994).

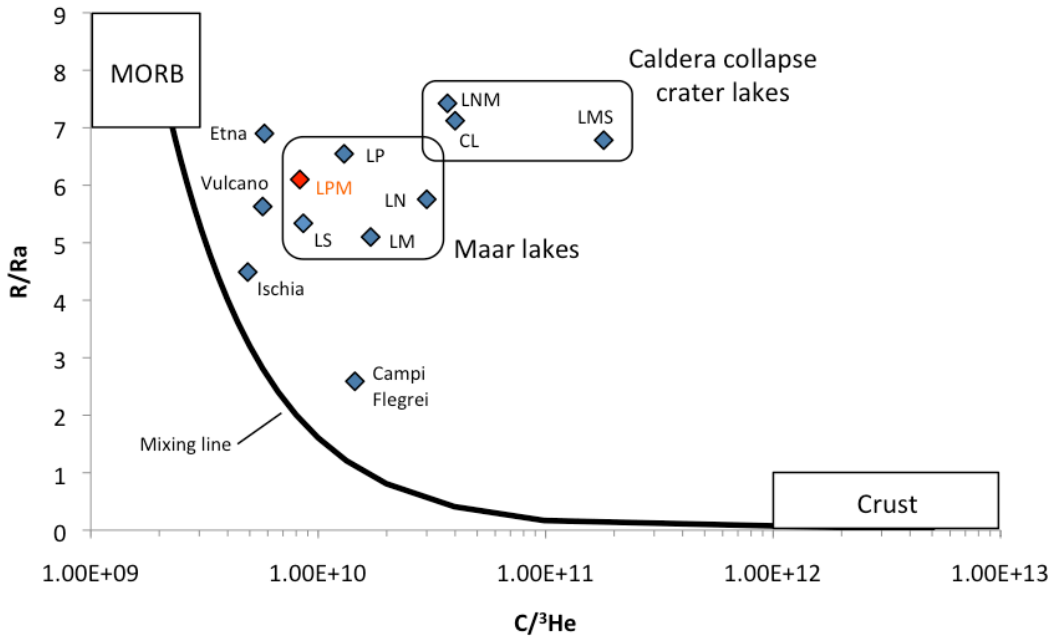

Figure 5.25 – R/Ra versus C/^{3}He in fluids from maar lakes, caldera collapse crater lakes and active volcanic areas of Southern Italy. Datum of Lago Piccolo of Monticchio from this work. Data of volcanic lakes from Kipfer et al. (2002) and reference therein, Nagao et al. (2010). Data of active volcanic areas of Southern Italy (Etna, Vulcao, Ischia, Campi Flegrei) from Marty et al. (1994). LPM = Lago Piccolo of Monticchio; LN = Lake Nyos; LM = Lake Monoun; LS = Laacher See; LP = Lac Pavin; LNM = Lake Nemrut; LMS = Lake Mashu; CL = Crater Lake.

In LPM both ^{3}He/heat and C/^{3}He ratios fall within the range of values typical of maar lakes in quiescent areas. The C/^{3}He and R/Ra ratio are within values reported for active volcanic area of Southern Italy (e.g., Etna, Vulcano, Ischia, Campi Flegrei; fig. 5.25), moreover magmatic volatiles are continuously released both in Monticchio lakes and in the entire Vulture area (e.g., Chiodini et al., 2000; Cioni et al., 2006; Gambardella, 2006; Caracausi et al., 2009; Paternoster et al., 2009). Mt. Vulture volcano had extreme long gaps of volcanic activity (up to ~350000 years; Stoppa and Principe, 1998; Buetner et al., 2006). Therefore, although the last volcanic activity of Mt. Vulture happened 140000 years b.p., taking into account the evolution of volcanism, the acquired data suggest the possibility that Mt. Vulture is a quiescent volcano rather than inactive (as often considered, e.g., Iliceto & Santarato, 1997; Pontevivo & Panza, 2006; Cantore et al., 2010).

6.0 Concluding remarks

- Some water samples of Monticchio Lakes (of deep waters) show charge unbalance (cationic excess) on analysis of major elements (to over 50%). Analogous unbalances are often solved considering the difference in the concentrations between cations and anions (excluding HCO_3^-) as the bicarbonate concentration (Nojiri et al., 1993; Kusakabe et al. 2000). In Monticchio lakes the HCO_3^- contents, computed by TDIC and pH values, are not able to balance the high charge difference in lake waters, so we believe that the presence of organic matter (e.g., fulvic and humic acids) can highly affect the chemistry of Monticchio lake waters.
- We have defined the mixing and stratification processes of LGM: only one turnover yearly (occurring in the coldest months) and the process of stratification starts in May/June. Despite literature classifies LGM as a dimictic lake (Schettler & Albéric, 2008) we consider that LGM is a monomictic lake.
- This study confirms the meromictic nature of LPM (Cioni et al., 2006), furthermore the genesis of monimolimnion is both of crenogenic and endogenic type.
- The thermal stratification is variable in time and involves mixolimnion in both lakes, with a typical distinction of epilimnion, thermocline and hypolimnion. On the basis of both major elements and isotopes of lake waters we reckon that Monticchio lakes are fed by groundwater with an average recharge altitude of about 920 m a.s.l.
- Moreover the concentration of dissolved helium and the temperature profiles highlighted a water inflow at about 28m of depth in the LPM.
- Our results show that the evaporation rate is similar at the two lakes (the mean annual evaporation rates are 3.1 and 2.9 mm/day for LGM and LPM, respectively), even if isotopic data and δD -Chloride systematics indicate that LGM is always more evaporated than LPM. This is related to the smaller thickness of evaporating water volume (epilimnion) at LGM. Moreover, different to what assumed until now (Mongelli et al., 1975; Chiodini et al., 2000; Celico & Summa, 2004; Paternoster et al., 2008), we established that LGM waters cannot derive from evaporation process of LPM waters.
- The abundance and isotopic value of dissolved Ar and Ne showed the atmospheric origin of Monticchio lakes waters. Moreover, these noble gases highlight a degassing process in groundwater, which also involves He and CO_2.
- The CH_4 is produced by bacterial methyl-type fermentation and carbonate reduction, as suggested by carbon and hydrogen isotopic data.

- Monitoring of dissolved gases of deep-inorganic, organic and atmospheric origins allows us to highlight the alternation of stratification and mixing of lake waters. Therefore, monitoring of dissolved gas is a precise and reliable geochemical tool for the study of circulation processes in the lakes.
- We evaluated the stability of water lakes taking into account the water density and the gas saturation pressure. The LGM is always in strong undersaturation due to the periodic turnovers that gradually release the accumulated gases in deep water volumes. In the LPM the gases pressure of near bottom waters is not distant from the saturation and certainly a forced motion (e.g., landslides, earthquakes, a sudden carbon dioxide inflow) can trigger a turnover and a paroxistic gas release (Schmid et al. 2004b). The historical documents (Tata, 1778; Palmieri and Scacchi, 1852; Ciarallo and Capaldo, 1995) report some events of massive gas released from LPM.
- Despite LPM and LGM have the same genesis and the distance between the two lakes is about 100 meters, the two lakes are substantially different in water and gas chemistry. Then, it can be inferred that the morpho-bathymetry is a fundamental parameter for the circulation dynamics, which have a leading role, e.g., in accumulation of dissolved gases.
- The estimated heat flow from LPM bottom is about 75 mW m^{-2} s^{-1}. This value indicates a heat flow excess of 20 mW m^{-2} if compared to that reported for Mt Vulture area (heat contribution by decay of U and Th in volcanic rocks was considered).
- Our results show that isotope signature of helium entering into the lakes has the same isotope signature of that entrapped in fluid inclusions of mantle xenoliths (olivines), indicating that He isotope signature of under Mt. Vulture mantle is 6.1 Ra.
- The restored pristine isotope composition $\delta^{13}C$ of CO_2 entering into lakes ranges between -4.0 and -4.8 ‰ (vs PDB), surprisingly close to that of carbonatitic matrix (-4.8 ‰) of LPM maar ejecta.
- ^3He/heat, C/^3He, R/Ra ratios and magmatic volatiles fluxes suggest that Mt. Vulture can be considered a quiescent volcano (not inactive as often reported; e.g., Iliceto & Santarato, 1997; Pontevivo & Panza, 2006; Cantore et al., 2010).

Acknowledgments

The whole work is the product of team in which the research mixes with friendship.
First of all I wish to thank my tutor, Prof. P.M. Nuccio: with his fresh passion for the research, he taught me scientific method and intellectual humility.
Many thanks to my co-tutor Dr. A. Caracausi: his example has been the greatest teaching.
I'm very gratefull to the Director Dr. Sergio Gurrieri and all the staff of the Istituto Nazionale di Geofisica e Vulcanologia (Sez. Palermo) for the availability of human and material resources.
I wish to thank Dr. M. Paternoster for his logistic and technical support during samplings and for making available precious data.
I am indebted to my prestigious reviewers (Dr. B. Boehrer, UFZ, Magdeburg, Germany; Dr. W.C. Evans, USGS, Menlo Park, California, USA; Prof. M. Kusakabe, University of Toyama, Japan; Prof. Y. Sano, University of Tokyo, Japan) for the very precious comments and suggestions, which have sensibly improved the final version.
Affectionate thanks to A. Rosciglione, V. Armato and to the important people in my life.

References

Abd Ellah R.G. (2009) - Evaporation Rate at Wadi El-Rayan Lake, Egypt, World Applied Sciences Journal 6 (4): 524-528.

Aeschbach-Herting W., Kipfer R., Hofer M., Imboden D.M., Wieler R., Signer P. (1996) - Quantification of gas fluxes from the subcontinental mantle: The example of Laacher See, a maar lake in Germany, Geochim. Cosmochim. Acta 60:31-41.

Aeschbach-Hertig, W., F. Peeters, U. Beyerle, and R. Kipfer (1999a) - Interpretation of dissolved atmospheric noble gases in natural waters. Water Resour. Res. 35(9):2779-2792.

Aeschbach-Hertig, W., Hofer, M., Kipfer, R., Imboden, D. M., Wieler, R. (1999b) - Accumulation of mantle gases in a permanently stratified volcanic Lake (Lac Pavin, France). Geochimica Cosmochimica Acta, 63 (19/20), 3357-3372.

Aeschbach-Hertig, W., Hofer, M., Schmid, M., Kipfer, R., Imboden, D. (2002) - The physical structure and dynamics of a deep, meromictic crater lake (Lac Pavin, France). Hydrobiologia, 487, 111-136.

Aka F.T., Kusakabe M., Nagao K., Tanyileke, G. (2001) - Noble gas isotopic compositions and water/gas chemistry of soda springs from the islands of Bioko, Sao Tome and Annobon, along with Cameroon volcanic line, West Africa: Applied Geochemistry, v. 16, no. 3, p. 323-338.

Allen J. R. M., Brandt U., Brauer A.,. Hubbertens A.-W, Huntley B., Keller J., Kraml M., Mackensen A., Mingram J., Negendank J. F. W, Nowaczyk N. R., Oberhänsli H., Watts W. A., Wulf S., Zolitschka B. (1999) - Rapid environmental changes in southern Europe during the last glacial period. Nature 400, pp. 740–743.

Ambrosetti W., Barbanti L. (2002) - Physical limnology of Italian lakes. 2. Relationship between morphometric parameters, stability and Birgean work. J. Limnol., 61 (2): 159-167.

Armienta M.A., Vilaclara G., De la Cruz-Reyna S., Ramos S., Ceniceros N., Cruz O., Aguayo A., rcega-Cabrera F. (2008) – Water chemistry of lakes related to active andinactive Mexican volcanoes. Journal of Volcanology and Geothermal Research, 178, 249-258.

Baker E T, Lupton J E. (1990) - Changes in submarine hydrothermal 3He/heat ratios as an indicator of magmatic/tectonic activity. Nature, 346: 556－558.

Ballentine C. J., Burgess R., and Marty B. (2002) - Tracing fluid origin, transport and interaction in the crust. Rev. Min. Geochem. 47, 539-614.

Barbieri M., Morotti M. (2003) - Hydrogeochemistry and strontium isotopes of spring and mineral waters from Monte Vulture volcano, Italy. Applied Geochemistry 18, pp.117–125.

Beccaluva L., Brotzu P., Macciotta G., Morbidelli L., Serri G., Traversa G. (1989) - "Ceinozoic tectonomagmatic evolution and inferred mantle sources in the Sardo-Tyrrenian area." Acc. Naz. Lincei, The Lithosphere in Italy, 229-248.

Beccaluva L., Coltorti M., Di Girolamo P., Melluso L., Milani L., Morra V., Siena F. (2002) - Petrogenesis and evolution of Mt. Vulture alkaline volcanism (southern Italy). Mineralogy and petrology, 74, 277-297.

Benoit, G. and Hemond H.F. (1996) - Vertical eddy diffusion calculated by the gradient flux method: Significance of sediment-water heat exchange. Limnol. Oceanogr. 41(1): 157–168.

Bernard, A., Escobar C. D., Mazot A., Gutiérrez R. E. (2004) - The acid volcanic lake of Santa Ana volcano, El Salvador. GSA Special Paper, 375, 121-134.

Bishop P.K. (1990) - Precipitation of dissolved carbonate species from natural waters for δ13C analysis – a critical appraisal. Chem. Geol. (Isot. Geosci. Sec.), 80, 251–259.

Boehrer B., Schultze M. (2008) - Stratification of lakes, Rev. Geophys., 46, RG2005, doi:10.1029/2006RG000210.

Borrelli, J., (2008) - Evaporation from Lakes and Large Bodies of Water. in Encyclopedia of Water Science, Second Edition, Ed.: Trimble S. W., Stewart B. A., Howell T. A.

Botz R., Pokojski H.D., Schmitt M., Thomm M. (1996) – Carbon isotope fractionation during bacterial methanogenesis by CO_2 reduction. Org. Geochem., 25 (3/4), 255-262.

Bowie G., Mills W., Porcella D., Campbell C., Pagenkopf J., Rupp G., Johnson K., Chan P., Gherini S. (1985) - Rates, constants and kinetics formulations in surface water quality modelling. EPA/600/3-85/040, Athens, USA.

Brakke, D. E, Henriksen A., Norton S. A. (1987) - The relative importance of acidity sources for humic lakes in Norway. Nature 329, 432-434.

Buettner, A., Principe, C., Villa, A.I. and Brocchini, D. (2006) - A $^{39}Ar/^{40}Ar$ geochronology of Monte Vulture. In: The geology of Mount Vulture (Italian), edited (C. Principe, ed.), pp. 73–84. Consiglio Nazionale delle Ricerche, Regione Basilicata.

Calace N., Capolei M., Lucchese M., Petronio B.M. (1999) - The structural composition of humic compounds as indicator of organic carbon sources, Talanta, 49, 277-284.

Caliro S., Chiodini G., Izzo G., Minopoli C., Signorini A., Avino R. and Granieri D. (2008) - Geochemical and biochemical evidence of lake overturn and fish kill at Lake Averno, Italy. J. Volcanol. Geotherm. Res. doi:10.1016/j.jvolgeores.2008.06.023.

Camarda M., Gurrieri S., Valenza M. (2009) - Effects of soil gas permeability and recirculation flux on soil CO2 flux measurements performed using a closed dynamic accumulation chamber. Chem. Geol. 265, 387-393.

Cantore L., Convertito V., Zollo A. (2010) - Development of a site-conditions map for the Campania-Lucania region (southern Apennines, Italy). Annals of Geophysics, 53, 4, doi: 10.4401/ag-4648.

Capasso G., Inguaggiato S. (1998) - A simple method for the determination of dissolved gases in natural waters. An application to thermal waters from Vulcano Island. Appl. Geochem.. vol 13/5, pp 631-642.

Caracausi A., Nuccio P. M., Favara R., Nicolosi M., Paternoster M. (2009) - Gas hazard assessment at the Monticcio crater Lakes of Mt. Vulture, a volcano in Southern Italy. Terra Nova 21, 83-87.

Cardellini C., Chiodini G., Frondini F., Granieri D., Lewicki J., Peruzzi L. (2003) - Accumulation chamber measurements of methane fluxes from natural environments and landfills, Applied Geochemistry, 18, 45-54.

Celico P., Summa G. (2004) - Idrogeologia dell'area del Vulture (Basilicata). Boll. Soc. Geol. It., 123, 343-356.

Cello G. and Mazzoli S. (1999) – Apennine tectonics in Southern Italy: a review. Journal of Geodynamics, 27, 191-211.

Chiodini, G., Frondini, F., Raco, B. (1996) - Diffuse emission of CO2 from the Fossa crater, Vulcano Island (Italy). Bull. Volcanol. 58, 41-50.

Chiodini G., Cioni R., Guidi M., Marini L., Principe C., Raco B. (1997) - Water and gas chemistry of the Lake Piccolo of Monticchio (Mt. Vulture, Italy). Current Research on Volcanics Lakes, Editor S.J. Freth.

Chiodini, G., Cioni, R., Guidi, M., Marini, L., Raco, B. (1998) - Soil CO2 flux measurements in volcanic and geothermal areas. Appl. Geochem. 13, 543-552.

Chiodini G., Cioni R., Guidi M., Magro G., Marini L., Raco B. (2000a) - Gas chemistry of Lake Piccolo of Monticchio, Mt. Vulture, in December 1996. Acta Vulcalologica, 12 (1-2), 139-143.

Chiodini G., Frondini F., Cardellini C., Parello F. & Peruzzi L. (2000b) - Rate of diffuse carbon dioxide earth degassing estimated from carbon balance of regional aquifers: the case of central Apennine, Italy. J.Geophys.Res. 105 (B4), 8423-8434.

Ciarallo, A. and Capaldo, L. (1995) - Journey to Vulture; comments on Tenore and Giussone's Travel Diary (1838). (Osanna Venosa eds) Venosa (Pz) (Italian).

Ciaranfi N., Guida M., Iaccarino G., Pescatore T., Pieri P., Rapisardi L., Ricchetti G., Sgrosso I., Torre M., Tortorici M., Turco E., Scarpa R., Cuscito M., Guerra I., Iannaccone G., Panza G.F., Scandone P. (1983) - Elementi sismotettonici dell'Appennino meridionale. Boll. Soc. Geol. It., 102, 201-222.

Cicerone, R.J., Setter, J.D. (1981) - Sources of atmospheric methane: measurements in rice paddies and discussion. J. Geophys. Res. 86, 7203–7209.

Cioni R., Marini L. Raco B. (2006) - Il lago Piccolo di Monticchio: geochimica dei fluidi e valutazione del rischio di eruzione limnica. In La Geologia del Monte Vulture. Regione Basilicata. pp. 171-177.

Console R., Di Giovanbattista R., Favalli P., Presgrave B.W., Smriglio G. (1993) - Seismicity of the Adriatic microplate. Tectonophysics, 218, 343-354.

Cosenza P., Riccobono G., Caracausi A., Nicolosi M. (2008) - Campionatori di profondità, Rapporti Tecnici INGV, n.66, 1-8.

Costa M. (2010) - Degassamento profondo nell'area del Monte Vulture (Basilicata): rilevanza, processi che lo governano e sua origine. Thesis. Università degli studi di Palermo.

Craig H., Lupton J.E. (1978) - A mantle helium component in Circum –Pacific volcanic gases. Hakone, the Marianas and Mt. Lassen. In Terrestrial Rare Gas (ed. E.C. Alexander and M. Ozima), 3-16. Japan Sci. Soc. Press.

Craig H. Lupton J.E., Horibe Y. (1978) - A mantle helium component in Circum-Pacific volcanic gases: Hakone, the Marianas and Mt. Lassen. In Terrestrial Rare Gases (Alexander E.C. and Ozima M. eds.) (Center for Academic Publishing Japan, Tokyo) pp. 3–16.

Craig H., Gordon L.I. (1965) - Deuterium and oxygen-18 variations in the ocean and the marine atmosphere. In E. Tongiorgi, ed, Proceedings of a Conference on Stable Isotopes in Oceanographic Studies and Paleotemperatures. Spoleto, Italy, pp 9-130.

D'Alessandro, W., Giammanco, S., Parello, F., Valenza, M. (1997) - CO2 output and d13C (CO2) from Mount Etna as indicators of degassing of shallow asthenosphere. Bull. Volcanol. 58, 455-458.

De Astis G., Kempton P.D., and Peccerillo A. (2006) - Trace element and isotopic variations from Mt. Vulture to Campanian volcanoes: Constraints for slab detachment and mantle inflow beneath southern Italy. Contrib. Mineral. Petrol., 151, 331 – 351, doi:10.1007/s00410-006-0062-y.

De Fino M:, La Volpe L., Piccareta G. (1982) - Magma evolution al Mt. Vulture (Southern Italy). Bull. Volcan., 45 (2), 115-126.

De Fino M., La Volpe L., Peccerillo A., Piccareta G., Poli G. (1986) - Petrogenesis of Monte Vulture volcano (Italy): inferences from mineral chemistry, major and trace element date. Contrib. Mineral. Petrol., 92, 135-145.

Deines P., Langmuir D., Harmon R.S. (1974) – Stable carbon isotope ratios and the existence of a gas phase in the evolution of carbonate ground waters. Grochem. Cosmochem. Acta, 38, 1147-1164.

Delmelle, P. and Bernard, A. (2000) - Volcanic lakes. In: Encyclopedia of volcanoes (H. Sigurdsson, ed.), pp. 877-895.

Doglioni C., Mongelli F., Pieri P. (1994) - The Puglia uplift (SE Italy): An anomaly in the foreland of the Apenninic subduction due to buclink of a thick continental lithosphere. Tectonics, 13, 1309-1321.

Doglioni C., Gueguen E., Harabaglia P., Mongelli F., (1999) - "On the origin of west-directed subduction zones and applications to the western Mediterranean". In Durand B., Jolivet L., Horvath F., Seranne M., (eds) The Mediterranean Basin: Tertiary Extension within the Alpine Orogen. Geological Society, London, Special Publications, 156, 541-561.

Doglioni C., Innocenti F., Mariotti G. (2001) - "Why Mt Etna?". Terra Nova, 13, 25-31.

Dongarrà G., Varrica D. (2004) - Geochimica e ambiente. Ed. Edises.

D'Orazio M., Innocenti F., Tonarini S., Doglioni C. (2007) - Carbonatites in a subduction system: The Pleistocene alvikites from Mt. Vulture (southern Italy). Lithos 98, 313–334.

Downes H., Kostoula T., Jones, A. P., Beard A.D., Thirlwall M.F., Bodinier J.L. (2002) - Geochemistry and Sr-Nd isotopic compositions of mantle xenoliths from the Monte Vulture carnonatite-melilite volcano, central southern Italy. Contrb. Mineral. Petrol., 144, 78-92.

Drexler J.Z., Snyder R.L., Spano, D., Paw U.K.T. (2004) - A review of models and micrometeorological methods used to estimate wetland evapotranspiration. Hydrological Processes 18, 2071- 2101.

Duchemin E., Lucotte M., Canuel R., Chamberland A. (1995) - Production of the greenhouse gases CH4 and CO2 by hydroelectric reservoirs of the boreal region. Global Biogeochemical Cycles, 9, 529–540.

Emrich, K., Ehhalt D. H., Vogel J. C. (1970) - Carbon isotope fractionation during the precipitation of calcium carbonate, Earth Planet. Sci., 8, 363-371.

Engle D. and Melack J.M. (2000) - Methane emissions from an Amazon floodplain lake: Enhanced release during episodic mixing and during falling water. Biogeochemistry 51, 71-90.

Epstein S., Mayeda T. (1953) - Variation of $d^{18}O$ content of water from natural sources. Geoch. Cosmoc. Acta, 4, 213-224.

Eshleman, K.N., and Hemond H.F. (1985) - The role of organic acids in the acid-base status of surface waters at Bickford Watershed, Massachusetts. Wat Resour. Res. 21. 1503-1510.

Evans W.C., Kling G.W., Tuttle M.L., Tanyileke G., White L.D. (1993) - Gas buildup in Lake Nyos, Cameroon: the recharge process and its consequences. Applied Geochemistry, 8, 207-221.

Evans W.C., White L.D., Tuttle M. L., Kling G.W., Tanyileke G., Michel R.L. (1994) - Six years of change at Lake Nyos, Cameroon, yield clues to the past and cautions for the future. Geochemical Journal 28,139-162.

Evans W.C., Sorey M.L., Kennedy B.M., Stonestrom D.A., Rogie J.D., Shuster D.L. (2001) - High CO2 emissions through porous media: transport mechanisms and implications for flux measurement and fractionation. Chem. Geol. 177, 15–29.

Fantucci R. (2007) - Dendrogeomorphological analysis of shore erosion along Bolsena lake (Central Italy). Dendrochronologia 24, 69-78.

Finetti I., Bricchi A., Del Ben A., Pipan M., Xuan Z. (1987) - Geophysical study of the Adria plate. Mem. Soc. Geol. Ital., 40, 335-344.

Follieri M., Giardini M., Magri D., Sadori L. (1998) - Palynostratigraphy of the last glacial period in the volcanic region of central Italy. Quaternary International, 47-48: 3-20.

Fornai, T. (1992) - Flussi di CO2 dai laghi craterici e dai suoli. PhD Thesis, University of Pisa.

Fuganti A. Sigillito V. (2008) - Caratteristiche, origine ed età di acque da sorgenti e da pozzi presenti sul Monte Vulture (regione Basilicata, Italia). Italian Journal of Engineering Geology and Environment. 2, 47-70.

Fukui, Y., Doskey, P.V. (1996) - An enclosure technique for measuring non-methane organic compound emissions from grassland. J. Environ. Qual. 25, 601–610.

Funicello R., Montone P., Parlotto F., Salvini F., Tozzi M. (1991) - Geodynamical evolution of an intra-orogenic forelnd: The Abulia case history. (Italy). Boll. Soc. Geol. Ital., 110, 419-425.

Gambardella B. (2006) - Flussi diCO2 profonda disciolta nelle acque sotterranee del Monte Vulture. In: La Geologia del Monte Vulture, Regione Basilicata, pp 155-169.

Gambardella B., Giosa P., Marini L. (2006) - Il ruolo della interazione acqua-roccia nella genesi delle acque minerali del Monte Vulture. In: La geologia del Monte Vulture, 133-148.

Gianniou S., Antonopoulos V. (2007) - Evaporation and energy budget in Lake Vegoritis, Greece. Journal of Hydrology, Vol. 345, pp. 212-223.

Gibson, J.J., Prowse, T.D., and Edwards, T.W.D., (1996) - Evaporation from a small lake in the continental arctic using multiple methods, Nordic Hydrology, 27, 1-24.

Gonfiantini (1986) - Environmental isotopes in lake studies. In: Fritz, P., Fontes, J.C. (Eds.), Handbook of Environmental Isotopes Geochemistry, vol. 3. Elsevier, New York, pp. 113-168.

Gräfe, H., B. Boehrer, N. Hoppe, S. C. Müller, Hauptmann P. (2002) - Ultrasonic measurements of density, adiabatic compressibility and stability frequency, Limnol. Oceanogr., 47(4), 1255–1260.

Griesshaber E., O'Nions R.K., Oxburgh E.R. (1992) – Helium and carbon isotope systematics in crustal fluids from the Eifel, the Rhine Graben and Black Forest, F.R.G. Chem. Geol. 99, 213-235.

Gunkel, G., Beulker, C., Grupe, B. and Viteri, F. (2008) - Hazards of volcanic lakes: analysis of Lakes Quilotoa and Cuicocha, Ecuador. Adv. Geosci., 14, 29–33.

Gunkel G., Beulker C., Grupe B., Vteri F. (2009) - Survey and assessment of post volcanic activities of a young caldera lake, lake Cuicocha, Ecuador. Nat. Hazards Earth Syst. Sci., 9, 699-712.

Gutsalo, L.K., (2008) - Isotope fractionation in the system CH4-H2O and CH4-CO2 during microbial methane genesis in the Earth's crust. Russian Geology and Geophysics 49, 397-407.

Hansen, R.B. (1993) - Sonar investigations in the Laghi di Monticchio (mt Vulture, Italy). Lect. Notes Earth Sci., 49, 119–128.

Henderson-Sellers, B. (1984) - Engineering Limnology. Pitman Publishing, Great Britain.

Henderson-Sellers B. (1986) - Calculating the surface energy balance for lake and reservoir modeling: a review. Reviews of Geophysics, 24 (3), 625–649.

Hernandez, P.A., Notsu, K., Okada, H., Mori, T., Sato, M., Barahona, F., Perez, N.M. (2006) - Diffuse emission of CO2 from Showa-Shinzan, Hokkaido, Japan: a sign of volcanic dome degassing. Pure Appl. Geophys. 163, 869–881.

Hoefs J. (1987) – Stable isotope geochemistry. Third edition. Springer-Verlag, berlin.

Hoffmann G., Masson V. and Jouzel J. (2000) - Stable waters isotopes in atmospheric general circulation models. Hydrological Processes, 14, 1385-1406.

Idso S. B. (1973) - On the concept of lake stability. Limnol. Oceanogr. 18, pp 681-683.

Idso S.B., Gilbert R.G. (1974) - On the universality of the Poole and Atkins Secchi disk-light extinction equation, Journal of Applied Ecology, 11, 399-401.

Iliceto V., Santarato G. (1997) - A MT 2D modelling of the Apenninic margin and Bradanic trough after identification of an artificial e.m. wide-band source on the natural MT data. Annals of Geophysics, 40 (5).

Imboden D.M., Lemmin U., Joller T., Schurter M. (1983) - Mixing processes in lakes: Mechanisms and ecological relevance. Schweiz. Z. Hydrol. 45, 1l-44.

Jassby A., Powell T.M. (1975) - Vertical patterns of eddy diffusion during stratification in Castle Lake, California. Limnol. Oceanogr. 20, 530- 543.

Jean-Baptiste, P., Fourré, E., Charlou, J. L., German, C. and Radford-Knoery, J. (2004) - Helium isotopes at the Rainbow hydrothermal site (MAR, 36°14N). Earth Planet. Sci. Lett. 221, 325-335.

Jimenez-Lopez C., Romanek C.S. (2004) – Precipitation kinetics and carbon isotope partitioning of inorganic siderite at 25°C and 1 atm. Geochimica and cosmochimica acta, 68 (3), 557-571.

Jones A.P., Kostoula T., Stoppa F. and Woolley A.R. (2000) - Petrography and mineral chemistry of mantle xenoliths in a carbonate-rich melilitic tuff from Mt. Vulture volcano, Southern Italy. Min. Mag., 64, 341-361.

Jenden P.D., Kaplan I.R., (1986) - Comparison of microbial gases from thr Middle American Trench and Scripps Submarine Canyon: Implications for the origin of natural gases. Appl. Geochem. 1, 631-646.

Kanemasu, E.T., Powers, W.L., Sij, J.W. (1974) - Field chamber measurement of CO2 flux from soil surface. Soil Sci. 118 (4), 233–237.

Kapitanov, V.A.,. Tyryshkin I.S, Krivolutskii N.P., Ponomarev Y.N., , De Batist M. and Gnatovsky R.Y. (2007) - Spatia distribution of methane over Lake Baikal surface. Spectrochim. Acta A 66: 788–795, doi:10.1016/j.saa.2006.10.036.

Katsev S., Crowe S.A., Mucci A., Sundby B., Nomosatryo S., Haffner G. D., Fowlef D. A. (2010) - Mixing and its effects on biogeochemistry in the persistently stratified, deep, tropical Lake Matano, Indonesia, Limnol. Oceanogr., 55(2), 763–776.

Kendall C., Coplen T. B. (1985) - Multisample conversion of water to hydrogen by zinc for stable isotope determination. Anal. Chem., 57, 1437-1440.

Kerr, R.A. (1986) - Nyos, the Killer Lake, May Be Coming Back. Science, 233, 1257–1258.

Kipfer, R., Aeschbach-Hertig, W., Peeters, F., and Stute, M. (2002) - Noble gases in lakes and ground waters. In: Porcelli, D., Ballentine, C. J., and Wieler, R. Eds., Noble gases in geochemistry and cosmochemistry. Mineralogical Society of America, Geochemical Society.

Kling G.W. (1987) - Seasonal Mixing and catastrophic Degassing in Tropical Lakes, Cameroon, West Africa. Nature, 237, 1022-1024.

Kling G. W. (1988) - Comparative transparency, depth of mixing, and stability of stratification in lakes of Cameroon, West Africa. Limnol. Oceanogr. 33, 27-40.

Kling, G.W., Tuttle, M.L. and Evans, W.C. (1989) - The evolution of thermal structure and water chemistry in Lake Nyos. J. Volcanol. Geotherm. Res. 39, 151-165.

Kling G. W., Kipphut G. W. and Miller M. C. (1991) - Artic Lakes and Streams as Gas Conduits to the Atmosphere: Implications for Tundra Carbon Budgets. Science, 251, 298-301.

Kling G.W., Evans W. C., Tuttle M. L., Tanyileke G., (1994) - Degassing of Lake Nyos, Nature, 368, 405–406.

Kling G. W., Evans W. C., Tanyileke G., Kusakabe M., Ohba T., Yoshida Y., Hell J. V. (2005) - Degassing Lakes Nyos and Monoun: defusing certain disaster. Proc. National Academy of Sciences 102, 14185-14190.

Kusakabe M., Nojiri Y., Narita M. (1990) - A simple plastic syringe sampler for in situ fixing of the total CO2, dissolved in lake water. lnt. Working Group Crater Lakes Newslett. 2, p. 11-14.

Kusakabe M. (1994) - Special Issue: Geochemistry of Crater Lakes (Preface). Geochem. J., Vol. 28, pp 137-138.

Kusakabe M., Tanyileke G.Z., McCord S.A., Schladow S.G. (2000) - Recent pH and CO2 profiles at Lakes Nyos and Monoun, Cameroon: implications for the degassing strategy and its numerical simulation, Journal Of Volcanology And Geothermal Research (97)1-4 (2000), pp. 241-260.

Lenters J.D., Kratz T.K., Bowser C.J. (2005) - Effects of climate variability on lake evaporation: results from a long-term energy budget study of Sparkling Lake, northern Wisconsin (USA). Journal of Hydrology 308, 168-195.

Lewis W.M. Jr. (1983) - Water budget of Lake Valencia, Venezuela. Acta Cientifica 34, 248-251.

Li Y. H. (1973) - Vertical eddy diffusion in Lake Zurich, Schweiz Z. Hydrol 35(1), 1-7.

Longinelli A., Deganello S. (1999) - Introduzione alla geochimica. Ed. UTET.

Lupton J. E. (1983) - Terrestrial inert gases: isotopie tracer studies and clues to primordial components in the mantle. Ann. Rev. Earth Plane. Sciences, 11, 371-414.

Marty B., Trull T., Lussiez P., Basile I., Tanguy J.C. (1994) - He, Ar, O, Sr and Nd isotope constraints on the origin and evolution of Mount Etna magmatism: Earth & Planetary Science Letters, 126 (1-3), 23-39.

Mazot, A., (2005) - CO2 degassing and fluid geochemistry at Papandayan and Kelud volcanoes, Java Island, Indonesia. Ph. D. Thesis, Université Libre de Bruxelles, Brussels, 294 pp.

Mazot A. and Taran Y. (2009) - CO2 flux from the volcanic lake of El Chichón (Mexico). Geofísica Internacional 48 (1), 73-83.

McConnaughey T.A., Burdett J., Whelan J.E, Paull C.K. (1997) - Carbon isotopes in biological carbonates: respiration and photosynthesis. Geochim. Cosmochim., 61, 611-622.

Mamyrin B. A., Tolstikhin J. N. (1984) "Helium isotopes in nature". Elsevier, Amsterdam, 273 pp.

Mancino G., Nolè A., Urbano V., Amato M., Ferrara A. (2009) - Assessing water quality by remote sensing in small lakes: the case study of Monticchio lakes in southern Italy. iForest, 2, pp. 154-161.

Mantovani E., Albarello D., Babbucci D., Tamburelli C. (1993) - Post-Tortonian deformation pattern in the central Mediterranean: a result of extrusion tectonics driven by the Africa-Eurasia convergence, in Recent evolution and seismicity of the Mediterranean region. pp 65-104, eds Boschi E., Mantovani E., Morelli A., Kluwer, Dordrecht.

Marini L. (2006) - Le caratteristiche isotopiche delle acque sotterranee del Monte Vulture e delle acque dei Laghi di Monticchio. In: La Geologia del Monte Vulture, Regione Basilicata, pp 149-154.

Marty, B., and Le Cloarec, M.-F. (1992) - Helium-3 and CO_2 fluxes from subaerial volcanoes estimated from polonium-210 emissions. Journal of Volcanology and Geothermal Research, 53, 67–72.

Marty B., Trull T., Lussiez P., Basile I., Tanguy J.C. (1994) - He, Ar, O, Sr and Nd isotope constraints on the origin and evolution of Mount Etna magmatism. Earth Planetary Science Letters 126, 23-39.

Melluso L., Morra V., Di Girolamo P. (1996) - The Mt. Vulture volcanic complex (Italy): evidence for distinct parental magmas and for residual melts with melilite. Mineralogy and petrology, 56, 225-250.

Meyer W.S. (1999) - Standard reference evaporation calculation for inland, south eastern Australia. Technical Report 35/98, CSIRO Land & Water, Adelaide, SA.

Mongelli F., Loddo M., Calcagnile G., (1975) - Some observations on the Apennines gravity field. Earth Planet. Sci. Lett., 24, 385-393.

Mongelli F., Panichi C., Tongiorgi E. (1975) - Studio termico ed isotopico dei crateri-laghi di Monticchio (Lucania). Arch. Oceanogr. Limnol., 18, 167-188.

Mongelli F., Harabaglia P., Martinelli G., Squarci P., Zito G. (1996) - Nuove misure di flusso geotermico in Italia meridionale: possibili implicazioni sismo-tettoniche. in atti del XIV Convegno Annuale del GNGTS, Roma 929-939.

Myrbo A., Shapley M.D., (2006) - Seasonal water-column dynamics of dissolved inorganic carbon stable isotopic compositions (δ13CDIC) in small hardwater lakes in Minnesota and Montana: Geochimica et Cosmochimica Acta, 70, 2699-2714.

Nagao K., Kusakabe M., Yoshida Y., Tanyileke G. (2010) - Noble gases in the crater lakes Nyos and Monoun, Cameroon. Geochem. J., 44, 519-543.

Navarre-Sitchler A.K., Brantley S.L. (2007) - Basalt weathering across scales, Earth and Planetary Science Letters, 261, 321-334.

Nicolosi M. (2007). Laghi craterici di Monticchio (M. Vulture – Basilicata): processi di degassamento profondo. Thesis, Università degli studi di Palermo.

Nojiri, Y., Kusakabe M., Tietze K., Hirabayashi J.-I., Sato H., Sano Y., Shinohara H., Njine T., Tanyileke G. (1993) - An estimate of CO2 flux in Lake Nyos, Cameroon. Limnology and Oceanography 38(4), 739-752.

Oliver, B.G., Thurman, E.M., Malcolm, R.L. (1983) - The contribution of humic substances to the acidity of colored natural waters. Geochim. Cosmochim. Acta 47, 2031-2035.

O'Sullivan P.E., Reynolds C.S. (2003) - The lakes handbook. Volume 1. Limnology and limnetic ecology. Blackwell Publishing, Oxford, 699 pp.

Oxburgh E.R., O'Nions R.K., Hill R.I. (1986) - Helium isotopes in sedimentary basins. Nature 324, 632-635.

Palmieri, L. and Scacchi, A. (1852) - The volcanic region of Mount Vulture and the earthquake that took place there on August 14th 1851. (Printing Office Gaetano Nobile, Naples) (Italian), pp. 160.

Parisi S. (2009) - Hydrogeochemical tracing of the groundwater flow pathways in the Mount Vulture volcanic aquifer system (basilicata, southern italy). PhD Thesis, University of Basilicata.

Patacca E., Sartori R., Scandone P. (1993) - Tyrrhenian basin and Apennines. Kinematic evolution and related dynamic constraints, in Recent evolution and seismicity of the Mediterranean region, pp 161-171, eds Boschi E., Mantovani E., Morelli A., Kluwer, Dordrecht.

Paternoster M. (2005) - Mt. Vulture volcano (Italy): a geochemical contribution to the origin of fluids and to a better definition of its geodynamic setting. PhD Thesis, University of Palermo.

Paternoster M., Liotta M., Favara R. (2008) - Stable isotope ratios in meteoric recharge and groundwater at Mt. Vulture volcano, southern Italy. Journal of Hydrology, 348, 87-97.

Paternoster M., Parisi S., Caracausi A., Favara R., Mongelli G. (2009) - Groundwaters of Mt. Vulture volcano, southern Italy: Chemistry and sulfur isotope composition of dissolved sulfate. Geochem. J., 44 (2), 125-135.

Paw U.K.T., Gao W. (1988) - Applications of solutions to non-linear energy budget equations, Agric. For. Meteorol. 43, 121-145.

Pearson F.J., Friedman I. (1970) – Sources of dissolved carbonate in an aquifer free of carbonate minerals. Water Resour. Res., 6, 1775-1781.

Pecoraino, G., Busca, L., D'alessandro, W., Giammanco, S., Iinguaggiato, S., Longo, M. (2005) - Total CO2 output from Ischia Island volcano (Italy). Geochem. J. 39, 451–458.

Pontevivo A. and Panza G.F. (2006) - The lithosphere-asthenosphere system in the Calabrian Arc and surrounding seas – Southern Italy. Pure appl. Geophys., 163, 1617-1659.

Poole H.H., Atkins W.R.G. (1929) - Photo-electric measurements of submarine illumination throughout the year, J. Mar. Biol. Assoc., 16, pp 297-324.

Powell T.M. and Jassby A.J. (1974) - The estimation of vertical eddy diffusivities below the thermocline in lakes, Water Resour. Res. 10, pp. 191-198.

Priestley C. and Taylor R. (1972) - On the assessment of surface heat flux and evaporation using large-scale parameters Monthly Weather Review, 100 (2), 81-92.

Principe C., Stoppa F. (1994) - Caratteristiche litologiche delle piroclastiti associate alla genesi dei Maar di monticchio: prima segnalazione di depositi carbonatitico-melilitici al Mt. Vulture (Basilicata). Plinius, 12, 86-90.

Robarts R.D., Ward P.R.B. (1978) – Verical diffusion and nutrient tran sport in a tropical lake (Lake McIlwaine, Rhodesia). Hydrobiologia, 59, 3, 213-221.

Romanek C. S., Zhang C. L., Li Y., Vali H., Horita J., and Cole D. R. (2003) - Carbon and hydrogen isotope fractionations asscoaited with dissimilatory iron-reducing bacteria. Chem. Geol.(Isot. Geosci. Sect.) 195, 5-16.

Rosatelli G., Stoppa F., Jones A.P. (2000) - Intrusive calcite-carbonatite occurence from Mt. Vulture volcano, southern Italy. Mineralogical Magazine, vol 64 (4), 615-624.

Rose T.P., Davisson M.L. (1996) – Radiocarbon in hydrologic systems containing dissolved magmatic carbon dioxide. Science, 237, 1367-170.

Rosenberry D.O., Stannard D.I., Winter T.C., Martinez M.L. (2004) - Comparison of 13 equations for determining evapotranspiration from a prairie wetland, Cottonwood Lake area, North Dakota, USA. Wetlands 24 (3), 483–497.

Rosenberry, D.O., Winter, T.C., Buso, D.C., Likens, G.E., (2007) - Comparison of 15 evaporation methods applied to a small mountain lake in the northeastern USA. J. Hydrol. 340 (3–4), 149–166.

Sabroux, J.C., Dubois, E., Doyotte, C. (1987) - The limnic eruption: a new geological hazard? Int. Scientific Congr. on Lake Nyos Disaster, Younde, Cameroon, 16–20 March 1987.

Sano Y., Tominaga T., Nakamura Y., Wakita, H. (1982) - 3He/‘He ratios of methane-rich natural gases in Japan. Geochem. J., 16: 237-245.

Sano Y., Wakita H., Ohsumi T., Kusakabe M. (1987) - Helium isotope evidence for magmatic gases in Lake Nyos, Cameroon, Geophys. Res. Lett. 14, pp. 1039–1041.

Sano Y., Kusakabe M., Hirabayashi J., Nojiri Y., Shinohara H., Njine T. and Tanyileke G. (1990) - Helium and carbon fluxes in lake Nyos, Cameroon: constrain on next gas burst, Earth Planet. Sci. Lett., 99, 303–314.

Sano Y, Marty B. (1995) – Origin of carbon in fumarolic gas fromisland arcs. Chemical Geology, 119, 265-274.

Sano Y., Nishio Y., Sasaki S., Gamo T. and Nagao K. (1998) - Helium and carbon isotope systematics at Ontake volcano, Japan. J. Geophys. Res. 103, 23863–23873.

Schellhase HU, MacIsaac EA, Smith H. (1997) - Carbon budget estimates for reservoirs on the Columbia River in British Columbia. The Environmental Professional 19: 48–57.

Schettler, G.; Albéric, P. (2008). Laghi di Monticchio (Southern Italy, Region Basilicata): genesis of sediments - a geochemical study, Journal of Paleolimnology, 40, 1, 529-556.

Schiattarella M., Beneduce P., Giano S.I., Giannandrea P. & Principe C. (2005) - Assetto strutturale ed evoluzione morfotettonica quaternaria del vulcano del Monte Vulture (Appennino Lucano). Bollettino della Società Geologica Italiana 124, 543-562.

Schiattarella M., Beneduce P. (2006) - Caratteri geomorfologici, assetto strutturale ed evoluzione morfotettonica del Monte Vulture e delle aree contigue. In: La Geologia del Monte Vulture, Regione Basilicata, pp 17-24.

Schmid, M., Lorke, A., Dinkel, C., Tanyileke, G., and Wüest, A. (2004) - Double-diffusive convection in Lake Nyos, Cameroon, Deep-Sea Research I, 51, 1097–1111.

Schoell M. (1980) - The Hydrogen and carbon isotopic composition of methane from natural gases of various origin, Geochim. Cosmoch. Acta, 44, 649-661.

Sigurdsson, H., Devine, J. D., Tchoua, F. M., Presser, T. S., Pringle, M. K. W., and Evans, W. C., (1987) - Origin of the lethal gas burst from Lake Monoun, Cameroon. J. Volcanology Geothermal Research, 31, 1-16.

Stoppa, F., Principe, C. (1998) - Eruption stile and petrology of a new carbonatitic suite from the Mt. Vulture (Southern Italy): the Monticchio Lakes Formation. Journal of Volcanology and Geothermal Research 80, 137–153.

Stumm, W. and Morgan, J.J. (1996) - Aquatic Chemistry, Chemical Equilibria and Rates in Natural Waters, 3rd ed. John Wiley & Sons, Inc., New York, 1022p.

Sturrock A.M., Winter T.C., Rosenberry D.O. (1992) - Energy budget evaporation from Williams Lake: a closed lake in north central Minnesota. Water Resources Research 28 (6), 1605– 1617.

Sugisaki R. and Taki K. (1987) - Simplified analyses of He, Ne, and Ar dissolved in natural waters. Chemical J. 21, 21-23.

Tassi F., Vaselli O., Tedesco D., Montegrossi G., Darrah T., Cuoco E., Mapendano M.Y., Poreda R., Delgado Huertas A. (2009) - Water and gas chemistry at Lake Kivu (DRC): Geochemical evidence of vertical and horizontal heterogeneities in a multibasin structure. Geochem. Geophys. Geosyst, 10, Q02005, doi:10.1029/2008GC002191.

Tata, D. (1778) - Letter about Mount Vulture addressed to his Excellency D. Guglielmo Hamilton, Knight of the Royal Order of ‘‘Bagno’’, His Britannic Majesty’s Envoy and Minister Plenipoteniary at the Court of Naples. (Simoniaca Printing Office, Naples) (Italian) pp. 62.

Tipping E., Woof C., Hurley M.A. (1991) - Humic substances in acid surface waters; modelling aluminium binding, contribution to ionic charge-balance, and control of pH. Wat. Res. Vol. 25, No. 4, pp 425-435.

Tipping E. (2002) - Cation Binding by Humic Substances (United Kingdom: Campridge University Press).

Tonani, F., Miele, G. (1991) - Methods for measuring flow of carbon dioxide through soils in the volcanic setting. International Conference Active Volcanoes and Risk Mitigation, IAVCEI, Naples, Italy, 27 Aug. to 1 Sept.

Torgersen, T., Top Z., Clarke W.B., Jenkins W. J., Broecker W. S. (1977) - A new method for physical limnology – tritium-helium- 3 ages – results for Lakes Erie, Huron and Ontario. Limnol. Oceanogr. 22, 181-193.

Trua T., Serri G., Marani M.P. (2003) - Lateral flow of African mantle below the nearby Tyrrhenian plate: Geochemical evidence. Terra Nova, 15, 433 – 440, doi:10.1046/j.1365-3121.2003.00509.x.

Van Loon G.W., Duffy, J. (2005) - Environmental Chemistry: A Global Perspective. Oxford University Press. 257-258.

van Soest M.C., Hilton D.R., Kreulen R. (1998) – Tracing crustal and slab contributions to arc magmatism in the Lesser Antilles island arc using helium and carbon relationships in geothermal fluids, Geochim. Cosmochim. Acta 62, 3323-3335.

Vardavas I., M., Fountoulakis, A. (1996) - Estimation of lake evaporation from standard meteorological measurements: application to four Australian lakes in different climatic regions. Ecological Modelling 84 (1996) 139-150.

Varekamp J.C. (2008) - The volcanic acidification of glacial Lake Caviahue, Province of Neuquen, Argentina. Journal of Volcanology and Geothermal Research 178, 184–196.

Vollmer, M. K., Weiss R. F., Schlosser P. and Williams R. T. (2002) - Deep-water renewal in Lake Issyk-Kul, Geophys. Res. Lett., 29, No. 8, doi:10.1029/2002GL014763.

Wetzel, R.G. (2001) - Limnology: Lake and River Ecosystems, 3rd ed. Academic Press, pp. 1006

Walkusz E., Jańczak J. (2007) - Comparative study of evaporation rate from surface water of Lake Raduńskie Górne and that from an evaporimeter pan placed on land. Limnological Review 7, 4: 241-246.

Whiticar M.J., Faber E., Schoell M. (1986) - Biogenic methane formation in marine and freshwater environments: CO2 reduction vs. acetate fermentation-Isotope evidence. Geochim. Cosmochim. Acta 50, 693-709.

Whiticar M.J. (1999) - Carbon and hydrogen isotope systematics of bacterial formation and oxidation of methane. Chem. Geol., 161, 291-314.

Winter T.C. (1981) - Uncertainties in estimating the water balance of lakes. Water Resources Bulletin 17 (1), 82-115.

Winter, T.C., Rosenberry, D.O., Sturrock, A.M. (1995) - Evaluation of 11 equations for determining evaporation for a small lake in the north central United States. Water Resources Research 31 (4), 983–993.

Wissmar R.C., McKnight D.M., DAHM C.N. (1990) - Contribution of organic acids to alkalinity in lakes within the Mount St. Helens blast zone. Limnol. Oceanogr., 35(2), 535-542.

Woltemate, I., Whiticar, M.J., Schoell, M. (1984) - Carbon isotopic composition of bacterial methane in a shallow lake. Limnolo. Oceanograph. 29, 985-992.

Wüest, A., Piepke G., Halfman J. D. (1996) - Combined effects of dissolved solids and temperature on the density stratification of Lake Malawi, p. 183–202. In T. C. Johnson and E. O. Odada, [eds.], The limnology, climatology and paleoclimatology of the East African Lakes. Gordon and Breach.

Wüest A., Piepke G. and Van Senden D.C. (2000) - Turbulent kinetic energy balance as a tool for estimating vertical diffusivity in wind-forced stratified waters. Limnol. Oceanogr., 45(6), 1388-1400.

Xing, Y. P., Xie P., Yang H., Ni Y., Wang Y. S., and Rong K. W. (2005) - Methane and carbon dioxide fluxes from a shallow hypereutrophic subtropical lake in China. Atmospheric Environment 39:5532–40.

Zhang S.R., Lu X.X., Sun H.G., Han J.T., Higgitt D.L. (2009) - Major ion chemistry and dissolved inorganic carbon cycling in a human-disturbed mountainous river (the Luodingjiang River) of the Zhujiang (Pearl River), China. Sci Total Environ 407, 2796–2807.

Appendix I

Alkalinity, charge balance and tables

Commonly, in lake systems the deep water samples for water chemistry analyses are collected with Niskin bottle (or similar) or pumping systems (e.g., Kling et al., 1989; Nojiri et al., 1993; Aeschbach-Hertig et al., 2002; Vollmer et al, 2002; Varekamp, 2008; Gunkel et al, 2009; Tassi et al, 2009).

A most used method for the estimation of total alkalinity $\left([Alk]=\left[HCO_3^-\right]+2\left[CO_3^{2-}\right]+\left[OH^-\right]-\left[H^+\right]\right)$ in lake waters is the titration of the waters that are sampled with these techniques (e.g., Kling et al., 1989; Aeschbach-Hertig et al., 2002; Armienta et al., 2008; Tassi et al, 2009). In lake waters with high amounts of dissolved CO_2 the sampling of deep waters is subject to gas exsolution due to the depressurization of sample, when it is carried towards surface and in subaerial conditions. A removal of CO_2 will have no effect on total alkalinity (fig. A I.1). However this will increase both the pH and the content of total carbon (TDIC), also modifying the speciation of carbonate species. Therefore, in CO_2 rich waters the alkalinity titrations can give errors in calculations of HCO_3^- and CO_3^{2-} concentrations (it depends on pH of water).

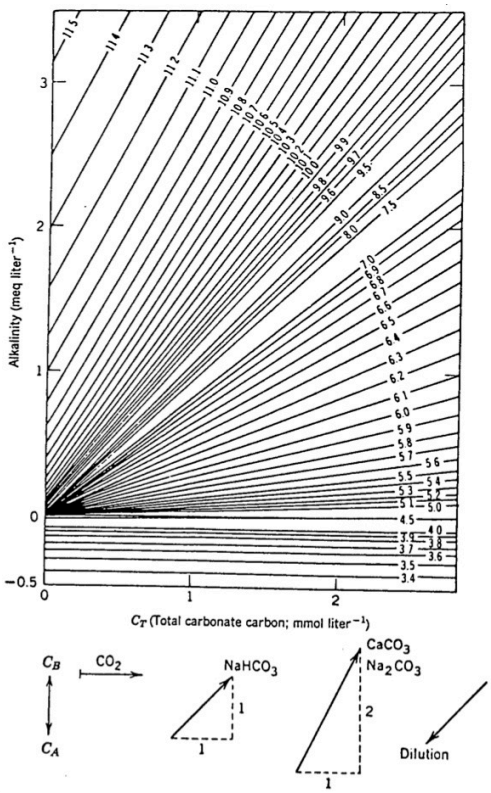

Figure A I.1 - Deffeyes diagram relatıng the pH, alkalınıty, and total carbon of carbonate (C_T=TDIC). The solution composition moves as a vector in the diagram as a result of the

addition (or removal) of CO_2, HCO_3^- (e.g., $NaHCO_3$), CO_3^{2-} (e.g., $CaHCO_3$, Na_2CO_3), alkalinity (C_B) and acidity (C_A). From Stumm & Morgan (1996).

A more important problem affects total alkalinity titrations in iron-rich waters (like deep waters of LPM). The precipitation of iron hydroxides from the anoxic sample can occur during titration, as follow:

$$Fe^{2+} + 3H_2O \rightarrow Fe(OH)_{3(S)} + 3H^+ + e$$

The release of H^+ can drastically reduce the total alkalinity (Stumm & Morgan, 1996). Also for Mn a similar oxidation take place.

Another process able to produce H^+ and reduce the total alkalinity is the nitrification, especially in waters rich in NH_4^+ (like deep waters of LPM and LGM):

$$NH_4^+ + 2O_2 \rightarrow NO_3^- + H_2O + 2H^+$$

By the same standards of literature, for the months of September and October 2008 and February and March 2009 we evaluated the total alkakinity ([Alk]$\approx[HCO_3^-]$ for the pH in water of Monticchio lakes) by in field acid titrations (0.1 N HCl) using a mixed indicator of methyl red and bromocresol green. The values obtained did not permit to close the charge balance of major elements, an excess of positive (cationic) charge occur. Due to discussed limits of alkalinity titration for waters of Monticchio lakes, from May 2009 to now, we estimate the HCO_3^- concentration by means of pH (in situ measured by multiparametric probe) and the total dissolved inorganic carbon (TDIC) measurements (see section 3.0), evaluating the distribution of carbonate species (appendix III). With the TDIC sampling method (see section 3.1) if the gas exsolution occurs, it happens within the sampling syringe, therefore no gas amount is lost. Moreover with the same sample of TDIC we estimated the isotopic signature ($\delta^{13}C_{TDIC}$), also evaluating the isotopic contribute of each carbonate species. In spite of improvement of bicarbonate sampling method, the charge balance of major elements is still unbalanced, with an excess of positive (cationic) charge. As suggested in literature (Oliver et al., 1983; Eshleman and Hemond, 1985; Brakke et al., 1987; Tipping et al., 1991; Tipping, 2002; Van Loon and Duffy, 2005) the humic matter, in some cases, may be a major source of anionic charge in the dissolved phase and it must be taken into account for the ionic charge balance in water, particularly in slightly acidic lakes with high dissolved organic matter (DOC) concentrations. In fact, the free form of humic matter are acids (e.g.,

fulvic and humic acids), which are associated with the carboxylate and phenolic groups, that remain substantially deprotonated when dissolved in water (Van Loon and Duffy, 2005). In natural waters (frequently in lake waters) the organic acids can give a relevant contribution on the total alkalinity (e.g., Wissmar et al., 1990). This is a potential source of error if total alkalinity is carried out by titration.

The ionic charge balance in water sample of Monticchio lakes is in excess of positive charge, in our opinion it is caused by the humic matter. The difficult evaluation of humic matter contribute was not carried out mainly because it goes beyond both the aims of this work and our expertise.

Table A1: Chemical and isotopic composition of lake waters.

Sample	Date	Depth (m)	T (°C)	EC (mS cm^{-1})	pH	$\delta^{18}O$	δD	Na	K	Mg	Ca	NH_4	F	Cl	SO4	HCO_3^-
LPM	Sep-08	3	21.75	0.38	8.1	-	-	1.39	0.54	0.53	1.14	0.0012	0.05	0.56	0.17	-
LPM	Sep-08	12	7.47	0.41	6.95	-5.18	-39	1.35	0.53	0.52	1.12	0.0000	0.05	0.53	0.16	-
LPM	Sep-08	18	7.27	0.94	6.34	-6.10	-44	1.48	0.58	0.70	1.50	0.5254	0.03	0.66	0.1	-
LPM	Sep-08	25	7.79	1.00	6.33	-8.02	-51	1.64	0.64	0.91	1.86	0.7756	0.03	0.56	0.03	-
LPM	Sep-08	28	7.91	1.04	6.33	-7.90	-52	1.62	0.65	0.94	1.92	0.8499	0.03	0.57	0.03	-
LPM	Sep-08	32	8.32	1.15	6.34	-8.10	-52	1.68	0.66	0.99	2.00	0.7758	0.03	0.58	0.04	-
LPM	Sep-08	36.5	8.93	1.54	6.38	-8.29	-53	1.68	0.67	1.03	2.07	1.1878	0.03	0.58	0.05	-
LGM	Sep-08	3	19.60	0.46	7.91	-0.68	-17	1.52	0.54	0.84	1.28	0.0000	0.04	0.77	0.29	-
LGM	Sep-08	10	6.60	0.54	6.75	-	-	1.41	0.51	0.80	1.55	0.1176	0.04	0.73	0.23	-
LGM	Sep-08	15	5.70	0.55	6.3	-2.64	-25	1.36	0.49	0.80	1.73	0.1750	0.04	0.70	0.2	-
LGM	Sep-08	20	5.75	0.64	5.94	-3.14	-28	1.36	0.50	0.82	1.78	0.1804	0.04	0.68	0.19	-
LGM	Sep-08	25	5.89	0.64	5.83	-3.22	-28	1.36	0.50	0.90	2.00	0.7438	0.03	0.68	0.17	-
LGM	Sep-08	30	5.92	0.69	5.83	-3.02	-30	1.35	0.51	0.93	2.09	1.0193	0.04	0.68	0.18	-
LGM	Sep-08	35	5.95	0.83	5.99	-3.27	-29	1.36	0.52	0.94	2.12	1.0814	0.04	0.67	0.14	-
LPM	Oct-08	3	16.78	0.37	7.8	-4.14	-35	1.37	0.54	0.52	1.12	0.0000	0.05	0.57	0.179	-
LPM	Oct-08	12	7.85	0.42	6.71	-4.76	-39	1.33	0.53	0.52	1.12	0.0000	0.05	0.55	0.164	-
LPM	Oct-08	18	7.33	0.94	6.14	-7.23	-49	1.49	0.58	0.81	1.62	0.4077	0.04	0.49	0.056	-
LPM	Oct-08	25	7.80	0.97	6.16	-8.13	-53	1.54	0.61	0.91	1.79	0.6981	0.03	0.50	0.026	-
LPM	Oct-08	28	7.94	0.98	6.17	-8.27	-53	1.55	0.61	0.92	1.80	0.7328	0.03	0.50	0.026	-
LPM	Oct-08	32	8.39	1.16	6.18	-8.22	-54	1.60	0.63	0.95	1.88	0.8716	0.03	0.51	0.026	-
LPM	Oct-08	36.5	8.95	1.58	6.21	-8.37	-53	1.57	0.62	1.00	1.94	0.9413	0.03	0.46	0.04	-
LGM	Oct-08	3	16.01	0.44	8.25	-0.68	-18	1.50	0.54	0.85	1.36	0.0000	0.05	0.78	0.285	-
LGM	Oct-08	10	6.86	0.53	6.59	-2.34	-25	1.34	0.49	0.76	1.65	0.0423	0.04	0.72	0.205	-
LGM	Oct-08	15	5.72	0.52	6.16	-2.60	-27	1.32	0.49	0.79	1.73	0.1910	0.04	0.71	0.209	-
LGM	Oct-08	20	5.78	0.64	5.84	-2.99	-27	1.32	0.50	0.83	1.85	0.4818	0.04	0.71	0.21	-
LGM	Oct-08	25	5.89	0.66	5.75	-3.27	-30	1.31	0.50	0.88	2.00	0.8052	0.04	0.69	0.173	-
LGM	Oct-08	30	5.93	0.70	5.75	-3.43	-30	1.31	0.51	0.90	2.06	0.9226	0.04	0.70	0.191	-
LGM	Oct-08	35	5.95	0.72	5.85	-3.41	-30	1.31	0.51	0.91	2.10	0.9792	0.04	0.70	0.13	-

Legend: LPM and LGM are the abbreviation of Lago Piccolo and Lago Grande of Monticchio, respectively; PM is the abbreviation of Pozzo Maria; (EC) is the electric conductivity (25°C); ionic contents are in meq/l; δD and $\delta^{18}O$ values are in ‰ vs. V-SMOW.

Table A1: Continuation.

Sample	Date	Depth (m)	T (°C)	EC (mS cm^{-1})	pH	$\delta^{18}O$	δD	Na	K	Mg	Ca	NH_4	F	Cl	SO4	HCO_3^-
LPM	Feb-09	3	6.58	0.40	7.42	-4.93	-38	1.30	0.53	0.52	1.15	0.0000	0.04	0.55	0.168	-
LPM	Feb-09	12	6.54	0.42	7.43	-4.87	-40	1.29	0.53	0.51	1.11	0.0000	0.04	0.56	0.168	-
LPM	Feb-09	18	7.41	0.93	6.5	-6.84	-46	1.41	0.59	0.71	1.50	0.0889	0.04	0.54	0.066	-
LPM	Feb-09	25	7.84	0.98	6.52	-8.14	-52	1.54	0.64	0.88	1.82	0.5202	0.03	0.58	0.017	-
LPM	Feb-09	28	7.98	1.04	6.52	-8.41	-53	1.57	0.63	0.92	1.92	0.6684	0.03	0.58	0.009	-
LPM	Feb-09	32	8.44	1.18	6.53	-8.41	-53	1.57	0.65	0.94	1.94	0.8057	0.03	0.53	0.009	-
LPM	Feb-09	36.5	8.92	1.52	6.58	-8.38	-54	1.59	0.66	0.98	2.15	1.3050	0.03	0.55	0.009	-
LGM	Feb-09	0.5	6.55	0.54	6.76	-2.33	-26	1.33	0.50	0.83	1.77	0.0000	0.04	0.73	0.355	-
LGM	Feb-09	4	5.72	0.49	6.65	-2.31	-26	1.33	0.51	0.84	1.74	0.0000	0.04	0.72	0.35	-
LGM	Feb-09	11	5.67	0.52	6.54	-2.50	-26	1.33	0.51	0.84	1.77	0.0000	0.04	0.72	0.348	-
LGM	Feb-09	16	5.67	0.49	6.5	-2.47	-26	1.33	0.50	0.84	1.78	0.0000	0.04	0.72	0.349	-
LGM	Feb-09	21	5.70	0.55	6.35	-2.44	-26	1.33	0.50	0.85	1.75	0.0285	0.04	0.74	0.345	-
LGM	Feb-09	26	5.74	0.55	6.09	-2.61	-25	1.35	0.50	0.87	1.89	0.0771	0.04	0.74	0.34	-
LGM	Feb-09	31	5.93	0.69	5.69	-3.16	-28	1.31	0.51	0.87	1.97	0.5301	0.04	0.73	0.245	-
LGM	Feb-09	35	6.00	0.95	5.91	-3.27	-30	1.26	0.50	0.87	2.03	0.7568	0.04	0.68	0.175	-
PM	Feb-09	-	12	0.37	6.45	-9.22	-59	0.57	0.19	0.65	2.17	-	0.03	0.51	0.114	
LPM	Mar-09	0.5	6.83	0.37	7.15	-5.20	-36	1.32	0.52	0.49	1.07	-	0.05	0.54	0.162	-
LPM	Mar-09	3	5.93	0.41	7.16	-5.29	-38	1.32	0.52	0.50	1.08	0.0147	0.05	0.54	0.161	-
LPM	Mar-09	12	5.53	0.41	7.02	-5.26	-36	1.32	0.52	0.50	1.08	0.0194	0.05	0.54	0.16	-
LPM	Mar-09	18	7.26	0.89	6.07	-6.99	-45	1.48	0.60	0.72	1.53	0.4548	0.04	0.57	0.069	-
LPM	Mar-09	25	7.84	0.98	6.09	-8.35	-51	1.62	0.65	0.89	1.85	0.8851	0.03	0.57	0.016	-
LPM	Mar-09	28	7.98	1.00	6.11	-8.20	-51	1.62	0.64	0.90	1.88	0.7675	0.03	0.58	0.018	-
LPM	Mar-09	32	8.35	1.18	6.13	-8.40	-51	1.62	0.65	0.96	1.96	0.9111	0.03	0.56	0.026	-
LPM	Mar-09	36.5	8.84	1.47	6.17	-8.47	-52	1.62	0.66	1.02	2.09	1.1931	0.03	0.59	0.025	-
LGM	Mar-09	0.5	6.46	0.48	7.12	-2.97	-27	1.34	0.49	0.82	1.81	-	0.04	0.71	0.378	-
LGM	Mar-09	4	6.46	0.49	7.13	-2.89	-28	1.32	0.49	0.82	1.85	0.0385	0.03	0.72	0.375	-
LGM	Mar-09	11	5.27	0.51	6.79	-2.78	-27	1.34	0.48	0.84	1.83	0.0516	0.03	0.71	0.369	-
LGM	Mar-09	16	5.09	0.53	6.63	-2.92	-28	1.36	0.50	0.85	1.85	0.0668	0.03	0.72	0.364	-
LGM	Mar-09	21	4.96	0.53	6.59	-2.62	-25	1.36	0.49	0.86	1.88	0.0935	0.04	0.73	0.357	-
LGM	Mar-09	26	4.95	0.53	6.56	-2.63	-26	1.35	0.50	0.85	1.83	0.0932	0.04	0.72	0.355	-
LGM	Mar-09	31	4.96	0.56	6.54	-2.50	-25	1.36	0.49	0.86	1.86	0.1279	0.04	0.76	0.353	-
LGM	Mar-09	35	5.02	0.62	6.23	-2.73	-25	1.33	0.51	0.88	2.02	0.5463	0.04	0.73	0.3	-

Table A1: Continuation.

Sample	Date	Depth (m)	T (°C)	EC (mS cm^{-1})	pH	$\delta^{18}O$	δD	Na	K	Mg	Ca	NH_4	F	Cl	SO4	HCO_3^-
LPM	May-09	3	14.38	0.37	8.22	-5.10	-54	1.27	0.50	0.49	1.09	0.0045	0.04	0.52	0.158	2.24
LPM	May-09	12	5.82	0.42	6.66	-5.00	-38	1.32	0.51	0.50	1.08	0.0147	0.05	0.54	0.161	2.20
LPM	May-09	18	7.20	0.92	5.91	-6.69	-39	1.54	0.60	0.71	1.53	0.4186	0.03	0.54	0.06	2.33
LPM	May-09	25	7.84	0.98	5.93	-8.10	-46	1.67	0.65	0.89	1.88	0.7874	0.03	0.56	0.021	3.99
LPM	May-09	28	7.98	0.98	5.95	-8.22	-51	1.70	0.66	0.93	1.93	0.8804	0.03	0.56	0.017	4.55
LPM	May-09	32	8.39	1.22	5.98	-8.18	-51	1.77	0.68	0.99	2.02	0.8550	0.03	0.55	0.023	4.72
LPM	May-09	36.5	8.93	1.60	6.08	-8.65	-50	1.82	0.72	0.98	2.28	1.2832	0.03	0.55	0.021	7.30
LGM	May-09	3	13.93	0.48	7.3	-2.85	-38	1.34	0.48	0.82	1.90	0.0052	0.04	0.66	0.408	2.04
LGM	May-09	10	5.74	0.49	6.59	-2.39	-28	1.37	0.48	0.85	1.93	0.0935	0.04	0.68	0.353	2.15
LGM	May-09	15	5.39	0.51	6.47	-2.39	-25	1.40	0.50	0.86	1.93	0.1092	0.04	0.68	0.349	2.76
LGM	May-09	20	5.18	0.56	6.34	-2.48	-26	1.41	0.51	0.86	1.93	0.1235	0.04	0.68	0.341	2.39
LGM	May-09	25	5.12	0.53	6.29	-2.16	-25	1.42	0.51	0.87	1.93	0.1483	0.04	0.68	0.329	1.80
LGM	May-09	30	5.10	0.51	6.26	-2.53	-27	1.43	0.51	0.88	1.95	0.1785	0.04	0.68	0.327	1.86
LGM	May-09	35	5.10	0.58	6.25	-2.75	-27	1.43	0.51	0.87	1.93	0.1941	0.04	0.69	0.324	1.44
LPM	Jun-09	3	23.77	0.42	8.32	-4.68	-34	1.37	0.53	0.47	1.13	0.0031	0.05	0.54	0.165	2.87
LPM	Jun-09	12	6.14	0.40	6.76	-5.29	-39	1.39	0.54	0.52	1.19	0.0093	0.05	0.54	0.162	1.81
LPM	Jun-09	18	7.11	0.96	6.02	-6.94	-46	1.35	0.53	0.60	1.41	0.4213	0.04	0.53	0.064	3.23
LPM	Jun-09	25	7.80	1.02	6.04	-8.52	-53	1.50	0.58	0.82	1.77	0.8184	0.03	0.54	0.009	3.71
LPM	Jun-09	28	7.95	1.00	6.05	-8.65	-53	1.54	0.60	0.88	1.85	0.8668	0.03	0.54	0.01	-
LPM	Jun-09	32	8.38	1.18	6.07	-8.71	-54	1.53	0.60	0.91	2.01	1.1795	0.03	0.53	0.019	6.14
LPM	Jun-09	36	8.88	1.57	6.13	-8.74	-52	1.58	0.62	0.98	2.23	1.5428	0.03	0.55	0.029	10.12
LGM	Jun-09	3	17.34	0.49	7.33	-2.50	-23	1.34	0.47	0.74	1.41	0.0125	0.04	0.67	0.389	-
LGM	Jun-09	10	5.78	0.50	6.62	-3.11	-24	1.30	0.48	0.71	1.88	0.1086	0.04	0.68	0.33	2.42
LGM	Jun-09	15	5.52	0.49	6.54	-2.95	-25	1.31	0.48	0.74	1.87	0.1283	0.03	0.69	0.338	2.24
LGM	Jun-09	20	5.24	0.53	6.32	-2.94	-25	1.32	0.48	0.77	1.88	0.1438	0.04	0.69	0.332	1.94
LGM	Jun-09	25	5.20	0.56	6.24	-2.83	-24	1.33	0.49	0.79	1.89	0.1839	0.03	0.69	0.314	2.01
LGM	Jun-09	30	5.20	0.56	6.23	-2.86	-25	1.34	0.49	0.81	1.84	0.2025	0.04	0.69	0.308	1.82
LGM	Jun-09	35	5.31	1.13	5.9	-2.88	-24	1.32	0.48	0.81	1.84	0.2467	0.03	0.66	0.285	1.51
PM	Jun-09	-	13	0.90	6.05	-9.52	-55	0.74	0.26	1.55	4.32	-	0.02	0.52	0.278	

Table A1: Continuation.

Sample	Date	Depth (m)	T (°C)	EC (mS cm^{-1})	pH	$\delta^{18}O$	δD	Na	K	Mg	Ca	NH_4	F	Cl	SO4	HCO_3^-
LPM	Sep-09	1	21.84	0.37	7.91	-4.29	-34	-	-	-	-	-	0.05	0.55	0.18	-
LPM	Sep-09	3	21.81	0.38	7.91	-4.19	-34	1.47	0.57	0.54	1.15	0.0012	0.05	0.55	0.171	2.46
LPM	Sep-09	12	7.22	0.39	6.48	-5.43	-39	1.43	0.55	0.55	1.18	0.0008	0.04	0.54	0.156	1.38
LPM	Sep-09	18	7.23	0.89	5.91	-8.24	-51	1.74	0.67	0.88	1.91	0.7610	0.03	0.58	0.007	1.75
LPM	Sep-09	25	7.80	0.99	5.91	-8.48	-53	1.77	0.68	0.93	2.01	0.8285	0.03	0.60	0.007	4.71
LPM	Sep-09	28	7.95	1.00	5.92	-8.53	-53	1.78	0.68	0.94	2.05	0.8985	0.03	0.59	0.008	4.79
LPM	Sep-09	32	8.46	1.17	5.93	-8.52	-54	1.78	0.70	0.98	2.19	1.2360	0.03	0.55	0.006	4.94
LPM	Sep-09	37	9.02	1.56	5.96	-8.79	-54	1.84	0.76	1.06	2.58	2.0665	0.03	0.67	0.009	7.24
LGM	Sep-09	1	20.25	0.44	7.31	-0.88	-19	-	-	-	-	-	-	-	-	-
LGM	Sep-09	3	20.19	0.47	7.31	-0.65	-18	1.59	0.57	0.92	1.60	0.0097	0.04	0.76	0.388	3.43
LGM	Sep-09	10	6.25	0.54	6.41	-2.85	-27	1.47	0.52	0.88	2.05	0.1646	0.04	0.70	0.333	2.06
LGM	Sep-09	15	5.66	0.52	6.26	-2.74	-27	1.46	0.51	0.87	2.01	0.1669	0.04	0.71	0.33	1.69
LGM	Sep-09	20	5.41	0.52	6.02	-2.79	-27	1.47	0.52	0.89	2.00	0.2266	0.04	0.72	0.312	1.28
LGM	Sep-09	25	5.38	0.52	5.96	-2.43	-26	1.45	0.52	0.89	1.99	0.2659	0.04	0.72	0.303	1.52
LGM	Sep-09	30	5.38	0.57	5.97	-2.61	-26	1.46	0.52	0.89	1.99	0.2833	0.04	0.72	0.308	1.56
LGM	Sep-09	35	5.48	1.11	5.79	-2.73	-26	1.46	0.52	0.89	2.03	0.2810	0.04	0.67	0.292	1.36
PM	Sep-09	-	-	-	6.29	-8.99	-58	0.61	0.19	0.68	1.67	-	0.04	0.53	0.058	-
LPM	Jun-10	3	18.57	0.40	8.21	-	-	1.31	0.49	0.53	1.21	0.0046	0.05	0.54	0.1681	3.22
LPM	Jun-10	8	8.02	0.41	7.11	-	-	1.30	0.48	0.53	1.24	0.0073	0.05	0.54	0.1705	-
LPM	Jun-10	12	6.62	0.41	6.75	-	-	1.33	0.50	0.54	1.33	0.0175	0.05	0.54	0.1686	1.94
LPM	Jun-10	18	7.34	0.95	6.04	-	-	1.54	0.56	0.83	2.06	0.7873	0.03	0.60	0.0148	1.54
LPM	Jun-10	25	7.84	1.02	6.04	-	-	1.41	0.60	0.86	2.19	0.9067	0.04	0.58	0.007	3.48
LPM	Jun-10	28	8.00	1.05	6.05	-	-	1.56	0.59	0.87	2.17	0.9887	0.04	0.58	0.0141	4.01
LPM	Jun-10	32	8.44	1.22	6.06	-	-	1.22	0.45	0.70	1.74	1.2493	0.03	0.59	0.0077	4.95
LPM	Jun-10	37	8.98	1.73	6.11	-	-	1.60	0.64	0.92	2.41	2.0825	0.03	0.60	0.013	7.03
LGM	Jun-10	3	17.33	0.49	8.33	-	-	1.35	0.47	0.85	1.73	-	0.04	0.71	0.3607	2.87
LGM	Jun-10	10	6.78	0.55	6.85	-	-	1.35	0.48	0.84	2.16	0.1048	0.04	0.71	0.3707	2.68
LGM	Jun-10	15	6.56	0.55	6.79	-	-	1.38	0.47	0.87	2.16	0.1047	0.04	0.71	0.3717	2.56
LGM	Jun-10	20	6.40	0.56	6.56	-	-	1.35	0.48	0.87	2.12	0.1332	0.04	0.71	0.3595	2.53
LGM	Jun-10	25	6.40	0.56	6.53	-	-	1.36	0.49	0.87	2.13	0.1520	0.04	0.70	0.4374	2.44
LGM	Jun-10	30	6.39	0.56	6.49	-	-	1.35	0.48	0.87	2.08	0.1707	0.04	0.71	0.3496	2.54
LGM	Jun-10	35	6.39	0.57	6.46	-	-	1.35	0.48	0.85	2.09	0.1832	0.04	0.71	0.3556	3.00

Table A2: Chemical composition of dissolved trace elements in Monticchio lakes waters.

Sample	Date	Depth	Li	B	Al	Ti	V	Cr	Mn	Fe^{2+}	Co	Ni	Zn	As	Se	Rb	Sr	Mo	Cs	Ba	Pb	U	Si
LPM	Sep-09	3	5.7	52.16	2.1	0.16	4.08	0.00	0.45	10.4	0.00	0.20	0.6	1.21	0.00	30.89	278	1.69	0.19	67.7	0.020	0.268	7488.1
LPM	Sep-09	12	5.8	52.86	0.5	0.18	0.19	0.00	300.6	3.1	0.14	0.17	1.0	0.44	0.00	29.65	280	1.26	0.18	78.2	0.027	0.198	10860.0
LPM	Sep-09	18	6.4	69.47	1.9	1.23	6.85	0.27	1839	106348	2.07	0.24	1.1	4.89	0.20	36.34	478	0.22	0.41	327	0.00	0.129	39774.6
LPM	Sep-09	25	6.5	73.33	5.4	1.38	10.39	0.36	1887	117932	2.04	0.37	6.4	5.32	0.21	38.16	521	0.18	0.45	358	0.312	0.110	42443.7
LPM	Sep-09	28	6.5	74.46	5.6	1.53	11.70	0.36	1916	123225	2.01	0.47	0.8	5.50	0.17	38.89	535	0.16	0.47	370	0.00	0.112	43552.9
LPM	Sep-09	32	5.7	72.66	6.1	2.10	18.43	0.46	2006	150613	1.96	0.29	1.0	5.74	0.21	40.95	581	0.16	0.52	412	0.00	0.121	45343.8
LPM	Sep-09	37	4.2	74.21	9.3	4.67	33.31	0.76	2538	243930	2.14	0.51	2.4	5.97	0.29	53.35	810	0.23	0.82	521	0.00	0.174	48126.4
LGM	Sep-09	3	2.8	56.05	2.9	0.16	1.24	0.06	16.22	1669	0.09	0.25	0.5	1.42	0.00	36.32	455	0.63	0.18	92.3	0.014	0.178	2912.5
LGM	Sep-09	10	2.4	48.01	1.2	0.32	0.99	0.00	1332	492.9	0.12	0.23	0.3	0.97	0.25	32.59	458	0.18	0.16	139	0.00	0.106	3228.3
LGM	Sep-09	15	2.4	47.65	1.4	0.31	0.94	0.09	1199	454.7	0.12	0.24	0.7	0.96	0.14	32.07	456	0.19	0.16	132	0.00	0.109	3292.8
LGM	Sep-09	20	2.4	47.11	2.1	0.39	1.00	0.07	1288	976.1	0.13	0.21	0.6	0.95	0.13	32.53	476	0.15	0.17	143	0.00	0.108	3737.1
LGM	Sep-09	25	2.4	48.79	2.5	0.54	1.04	0.07	1361	1253	0.14	0.21	0.3	0.99	0.09	32.95	470	0.14	0.17	154	0.00	0.106	3926.6
LGM	Sep-09	30	2.4	48.23	3.3	0.45	1.04	0.08	1363	1324	0.14	0.32	2.2	1.00	0.13	32.92	469	0.13	0.18	153	0.098	0.100	3948.0
LGM	Sep-09	35	2.4	48.09	3.6	0.55	1.02	0.10	1377	1312	0.15	0.26	1.7	0.99	0.09	33.21	471	0.12	0.18	155	0.057	0.096	3947.6
LPM	Jun-10	3	5.47	50.58	2.90	0.23	1.89	0.15	4.1	5.51	0.06	0.30	1.9	0.69	0.030	28.93	286.9	1.5	0.16	61.1	0.10	0.253	7079.0
LPM	Jun-10	8	5.68	52.39	2.12	0.30	1.39	0.17	1.3	7.34	0.07	0.38	2.7	0.61	0.047	29.24	289.5	1.5	0.16	64.1	0.19	0.234	9512.7
LPM	Jun-10	12	7.18	66.23	3.73	0.20	0.41	0.18	6.2	11.31	0.09	0.25	1.2	0.39	0.043	37.18	374.0	1.8	0.20	84.3	0.20	0.256	8930.2
LPM	Jun-10	18	6.72	74.26	3.16	0.92	6.14	0.46	1853.0	106783.7	2.11	0.33	1.2	4.27	0.084	38.55	546.8	0.2	0.39	329.3	0.10	0.158	38864.7
LPM	Jun-10	25	6.48	73.31	4.05	1.39	11.22	0.64	1845.0	124508.8	2.08	0.40	1.1	5.85	0.096	38.08	562.2	0.1	0.41	345.8	0.04	0.127	43381.6
LPM	Jun-10	28	6.68	75.38	4.61	1.29	12.10	0.61	1848.0	122156.8	2.02	0.39	0.8	5.57	0.097	39.80	583.0	0.2	0.42	355.6	0.03	0.128	42661.4
LPM	Jun-10	32	4.70	56.73	4.30	1.29	12.63	0.46	1475.0	112057.3	1.57	0.26	0.6	4.15	0.095	31.04	469.2	0.1	0.35	304.7	0.02	0.099	32937.8
LPM	Jun-10	37	4.94	78.59	10.70	4.88	46.09	1.06	2495.0	258923.2	2.34	0.57	2.1	8.31	0.295	54.17	895.1	0.3	0.74	575.3	0.05	0.215	49406.8
LGM	Jun-10	3	2.89	57.30	2.82	0.11	1.33	0.14	2.5	3.3	0.13	0.30	0.4	1.19	0.047	32.18	449.0	0.9	0.14	85.8	0.05	0.305	2102.5
LGM	Jun-10	15	2.90	56.30	1.27	0.17	0.71	0.20	442.3	2.9	0.13	0.35	0.3	1.22	0.020	32.15	488.7	0.6	0.15	106.4	0.05	0.254	2345.8
LGM	Jun-10	20	2.99	57.21	1.36	0.19	0.73	0.21	1666.0	35.6	0.14	0.97	0.3	1.01	0.044	33.40	505.2	0.6	0.16	128.5	0.06	0.247	2554.9
LGM	Jun-10	25	2.92	55.98	2.28	0.27	0.85	0.39	2254.0	77.3	0.15	0.42	0.4	1.11	0.041	32.92	496.8	0.6	0.16	143.3	0.05	0.235	2656.2
LGM	Jun-10	30	3.00	57.14	1.73	0.24	0.89	0.30	2413.0	95.5	0.15	0.37	0.3	1.14	0.031	33.90	509.1	0.6	0.16	145.6	0.03	0.218	2654.0
LGM	Jun-10	35	2.96	56.26	1.70	0.25	0.86	0.30	2398.0	102.7	0.15	0.38	0.4	1.07	0.034	33.27	503.4	0.6	0.16	147.2	0.03	0.241	2683.7
Error			3.3	0.6	12.4		7.2	0.8	3.8		1.3	1.0	17.9	7.7	11.9	5.7	4.2	1.8	4.1	0.9	1.4	12.2	0.4

Legend: LPM and LGM are the abbreviation of Lago Piccolo and Lago Grande of Monticchio, respectively; the concentrations are in ppb; the error of each specie is in percentage (%).

Table A3: The carbonate system

Sample	Date	Depth (m)	TDIC	$CO3^{2-}$	HCO_3^-	$CO_{2(aq)}$	$\delta\ ^{13}C_{TDIC}$
LPM	May-09	3	2.29E-03	1.38E-05	2.24E-03	3.56E-05	-3.21
LPM	May-09	12	3.74E-03	2.89E-07	2.20E-03	1.54E-03	-5.16
LPM	May-09	18	1.12E-02	5.71E-08	2.33E-03	8.85E-03	-2.85
LPM	May-09	25	1.82E-02	1.04E-07	3.99E-03	1.42E-02	-1.87
LPM	May-09	28	2.00E-02	1.25E-07	4.55E-03	1.54E-02	-1.37
LPM	May-09	32	1.95E-02	1.41E-07	4.72E-03	1.48E-02	-1.03
LPM	May-09	37	2.52E-02	2.79E-07	7.30E-03	1.79E-02	-0.21
LGM	May-09	3	2.31E-03	1.49E-06	2.04E-03	2.72E-04	-2.04
LGM	May-09	10	3.93E-03	2.40E-07	2.15E-03	1.77E-03	-3.66
LGM	May-09	15	5.79E-03	2.31E-07	2.76E-03	3.03E-03	-3.71
LGM	May-09	20	5.95E-03	1.47E-07	2.39E-03	3.56E-03	-3.25
LGM	May-09	25	4.81E-03	9.86E-08	1.80E-03	3.01E-03	-3.00
LGM	May-09	30	5.20E-03	9.50E-08	1.86E-03	3.34E-03	-3.53
LGM	May-09	35	6.25E-03	3.96E-08	1.44E-03	4.81E-03	-3.64
LPM	Jun-09	3	2.92E-03	2.73E-05	2.87E-03	3.13E-05	-3.35
LPM	Jun-09	6	2.86E-03	4.36E-06	2.70E-03	1.60E-04	-1.41
LPM	Jun-09	12	2.81E-03	3.03E-07	1.81E-03	9.98E-04	-3.75
LPM	Jun-09	18	1.28E-02	1.02E-07	3.23E-03	9.55E-03	-2.82
LPM	Jun-09	25	1.40E-02	1.25E-07	3.71E-03	1.03E-02	-2.25
LPM	Jun-09	32	2.18E-02	2.25E-07	6.14E-03	1.57E-02	-1.86
LPM	Jun-09	36	3.18E-02	4.45E-07	1.01E-02	2.17E-02	-0.40
LGM	Jun-09	10	4.28E-03	2.90E-07	2.42E-03	1.86E-03	-2.54
LGM	Jun-09	15	4.32E-03	2.21E-07	2.24E-03	2.08E-03	-2.39
LGM	Jun-09	20	4.96E-03	1.14E-07	1.94E-03	3.02E-03	-2.36
LGM	Jun-09	25	5.77E-03	9.84E-08	2.01E-03	3.76E-03	-2.72
LGM	Jun-09	30	5.31E-03	8.72E-08	1.82E-03	3.49E-03	-2.40
LGM	Jun-09	35	7.68E-03	3.39E-08	1.51E-03	6.17E-03	-2.09
LPM	Sep-09	3	2.54E-03	8.79E-06	2.46E-03	7.09E-05	-3.01
LPM	Sep-09	12	2.79E-03	1.25E-07	1.38E-03	1.41E-03	-2.84
LPM	Sep-09	18	8.38E-03	4.29E-08	1.75E-03	6.63E-03	-4.13
LPM	Sep-09	25	2.23E-02	1.18E-07	4.71E-03	1.76E-02	-1.86
LPM	Sep-09	28	2.22E-02	1.23E-07	4.79E-03	1.74E-02	-2.08
LPM	Sep-09	32	2.23E-02	1.32E-07	4.94E-03	1.74E-02	-1.46
LPM	Sep-09	37	3.07E-02	2.11E-07	7.24E-03	2.34E-02	0.13
LGM	Sep-09	3	3.83E-03	2.97E-06	3.43E-03	4.02E-04	-3.43
LGM	Sep-09	10	4.59E-03	1.55E-07	2.06E-03	2.53E-03	-3.40
LGM	Sep-09	15	4.67E-03	8.79E-08	1.69E-03	2.98E-03	-3.87
LGM	Sep-09	20	5.25E-03	3.81E-08	1.28E-03	3.97E-03	-4.21
LGM	Sep-09	25	6.91E-03	3.92E-08	1.52E-03	5.39E-03	-2.94
LGM	Sep-09	30	6.97E-03	4.13E-08	1.56E-03	5.41E-03	-2.76
LGM	Sep-09	35	8.47E-03	2.38E-08	1.36E-03	7.11E-03	-2.43

Legend: LPM and LGM are the abbreviation of Lago Piccolo and Lago Grande of Monticchio, respectively; total dissolved inorganic Carbon (TDIC) and carbonate species are in mol/litre; $\delta^{13}C_{TDIC}$ values are in ‰ vs. V-PDB.

Table A3: Continuation.

Sample	Date	Depth (m)	TDIC	$CO3^{2-}$	HCO_3^-	$CO_{2(aq)}$	$\delta\ ^{13}C_{TDIC}$
LPM	**Jun-10**	**3**	**3.29E-03**	**2.13E-05**	**3.22E-03**	**4.87E-05**	**1.90**
LPM	**Jun-10**	**12**	**3.02E-03**	**3.22E-07**	**1.94E-03**	**1.08E-03**	**-2.80**
LPM	**Jun-10**	**18**	**5.85E-03**	**5.10E-08**	**1.54E-03**	**4.31E-03**	**-2.80**
LPM	**Jun-10**	**25**	**1.31E-02**	**1.17E-07**	**3.48E-03**	**9.62E-03**	**-2.00**
LPM	**Jun-10**	**28**	**1.48E-02**	**1.39E-07**	**4.01E-03**	**1.08E-02**	**-1.90**
LPM	**Jun-10**	**32**	**1.79E-02**	**1.78E-07**	**4.95E-03**	**1.29E-02**	**-1.80**
LPM	**Jun-10**	**37**	**2.31E-02**	**2.89E-07**	**7.03E-03**	**1.61E-02**	**-0.50**
LGM	**Jun-10**	**3**	**2.94E-03**	**5.13E-05**	**2.87E-03**	**1.63E-05**	**2.70**
LGM	**Jun-10**	**10**	**3.88E-03**	**5.53E-07**	**2.68E-03**	**1.20E-03**	**0.00**
LGM	**Jun-10**	**15**	**4.06E-03**	**4.05E-07**	**2.56E-03**	**1.50E-03**	**-1.30**
LGM	**Jun-10**	**20**	**4.63E-03**	**2.82E-07**	**2.53E-03**	**2.10E-03**	**-1.80**
LGM	**Jun-10**	**25**	**4.85E-03**	**2.29E-07**	**2.44E-03**	**2.41E-03**	**-2.00**
LGM	**Jun-10**	**30**	**5.23E-03**	**2.22E-07**	**2.54E-03**	**2.69E-03**	**-1.90**
LGM	**Jun-10**	**33**	**5.51E-03**	**2.23E-07**	**2.63E-03**	**2.88E-03**	**-1.60**
LGM	**Jun-10**	**35**	**6.27E-03**	**2.54E-07**	**3.00E-03**	**3.27E-03**	**-2.80**

Table A4: Chemical and isotopic composition of dissolved gases.

Sample	date	Depth (m)	CH_4	Ar	O_2	CO	He	R/Ra	He/Ne	$(R/Ra)_c$	ERROR
LPM	sett.08	12	5.57E-02	-	2.90E-01	1.06E-04	2.10E-04	2.90	1.17	3.51	0.06
LPM	sett.08	18	5.09E+01	2.36E-01	1.84E-01	3.81E-04	1.44E-03	5.50	9.16	5.65	0.05
LPM	sett.08	25	6.95E+01	2.44E-01	2.90E-01	2.77E-04	1.97E-03	5.24	14.60	5.32	0.06
LPM	sett.08	28	7.68E+01	2.50E-01	1.74E-01	4.36E-04	2.00E-03	5.19	14.99	5.27	0.05
LPM	sett.08	32	8.19E+01	2.47E-01	1.07E-01	3.20E-04	1.88E-03	5.32	12.70	5.42	0.04
LPM	sett.08	36.5	1.29E+02	2.13E-01	8.79E-02	5.71E-04	1.67E-03	4.99	13.22	5.08	0.05
LGM	sett.08	3	3.09E-02	-	1.82E+00	2.01E-05	7.93E-04	0.39	3.55	0.33	0.01
LGM	sett.08	10	3.65E+00	-	2.30E-01	5.83E-05	5.53E-04	2.85	3.42	3.01	0.04
LGM	sett.08	15	6.84E+00	2.78E-01	2.43E-01	1.90E-04	7.10E-04	4.61	4.42	4.86	0.05
LGM	sett.08	20	2.34E+01	2.76E-01	2.01E-01	1.92E-04	1.75E-03	5.25	9.36	5.38	0.04
LGM	sett.08	25	3.26E+01	2.67E-01	2.87E-01	2.75E-04	1.90E-03	5.26	22.25	5.31	0.06
LGM	sett.08	30	4.88E+01	3.30E-01	2.99E-01	2.08E-04	3.58E-03	5.30	17.51	5.37	0.05
LGM	sett.08	35	4.59E+01	2.87E-01	2.61E-01	1.98E-04	3.00E-03	5.28	18.07	5.35	0.05
LPM	Oct-08	3	-	-	-	-	1.70E-03	0.92	1.40	0.97	0.02
LPM	Oct-08	12	4.67E-01	-	1.69E-01	1.46E-05	1.56E-04	4.36	0.90	6.01	0.08
LPM	Oct-08	18	3.72E+01	-	1.16E-01	1.59E-04	8.09E-04	5.71	5.56	5.97	0.05
LPM	Oct-08	25	6.80E+01	-	2.44E-01	2.58E-04	1.51E-03	5.90	10.87	6.03	0.06
LPM	Oct-08	28	7.36E+01	-	2.02E-01	2.68E-04	1.57E-03	5.81	11.27	5.94	0.06
LPM	Oct-08	32	8.10E+01	-	1.18E+00	1.94E-04	1.57E-03	5.86	11.43	5.99	0.06
LPM	Oct-08	36.5	1.06E+02	-	2.16E-01	1.61E-04	1.47E-03	5.67	13.67	5.77	0.05
LGM	Oct-08	3	1.06E-02	-	1.87E+00	1.76E-05	1.25E-04	0.65	0.55	0.57	0.01
LGM	Oct-08	10	2.95E+00	-	1.17E-01	9.75E-05	-	-	-	-	-
LGM	Oct-08	15	6.87E+00	-	1.69E-01	1.22E-04	1.45E-04	4.65	4.37	4.92	0.04
LGM	Oct-08	20	1.73E+01	-	2.22E-01	2.27E-04	6.44E-04	5.20	9.03	5.34	0.03
LGM	Oct-08	25	3.30E+01	-	1.10E-01	1.37E-04	1.11E-03	5.41	13.87	5.51	0.03
LGM	Oct-08	30	4.30E+01	-	5.04E-02	1.97E-04	1.85E-03	5.60	18.95	5.67	0.03
LGM	Oct-08	35	4.32E+01	-	1.23E-01	1.83E-04	2.03E-03	5.57	14.19	5.67	0.03

Legend: LPM and LGM are the abbreviation of Lago Piccolo and Lago Grande of Monticchio, respectively; concentrations of dissolved gases are expressed as cc/litre at standard temperature and pressure conditions of 25°C and 1 atm (STP). $^3He/^4He$ ratios are reported to the atmospheric value ($Ra=1{,}38 \times 10^{-6}$) as R/Ra. Error is referred to $(R/Ra)_c$.

Table A4: Continuation.

Sample	date	Depth (m)	CH_4	Ar	O_2	CO	He	R/Ra	He/Ne	R/Ra c	ERROR
LPM	Feb-09	3	3.40E-02	3.28E-01	4.03E+00	6.05E-05	8.01E-05	2.44	0.43	5.63	0.10
LPM	Feb-09	12	2.92E-01	3.21E-01	4.16E+00	5.89E-05	8.13E-05	2.70	0.50	5.20	0.09
LPM	Feb-09	16	-	-	-	-	1.52E-03	5.54	11.83	5.65	0.06
LPM	Feb-09	18	4.61E+01	2.86E-01	1.12E-01	5.68E-04	9.55E-04	5.37	6.30	5.59	0.05
LPM	Feb-09	25	7.86E+01	2.58E-01	1.08E-01	1.78E-04	-	-	-	-	-
LPM	Feb-09	28	8.15E+01	2.54E-01	1.67E-01	1.80E-04	1.44E-03	5.57	12.06	5.68	0.06
LPM	Feb-09	32	9.78E+01	2.56E-01	1.21E-01	3.47E-04	1.42E-03	5.55	12.11	5.66	0.05
LGM	Feb-09	4	6.70E-03	3.28E-01	1.34E+00	3.81E-05	1.22E-04	3.23	0.61	5.39	0.08
LGM	Feb-09	11	4.57E-03	3.34E-01	1.09E-01	2.47E-05	1.65E-04	3.74	0.88	5.14	0.06
LGM	Feb-09	16	7.47E-03	3.28E-01	1.88E-01	4.31E-05	1.91E-04	4.03	1.09	5.17	0.05
LGM	Feb-09	21	1.04E+00	3.29E-01	2.36E-02	6.57E-05	4.09E-04	4.88	2.44	5.42	0.05
LGM	Feb-09	26	5.05E+00	3.18E-01	2.45E-01	9.52E-05	4.38E-04	4.97	2.46	5.52	0.05
LGM	Feb-09	31	3.03E+01	2.85E-01	1.39E-01	1.55E-04	1.27E-03	5.45	9.79	5.59	0.05
LGM	Feb-09	35	6.24E+01	2.95E-01	2.06E-01	3.90E-05	1.88E-03	5.66	15.02	5.75	0.06
LPM	Mar-09	3	1.01E-01	2.77E-01	2.05E+00	8.25E-05	6.27E-05	1.88	0.36	5.97	0.11
LPM	Mar-09	18	4.14E+01	2.59E-01	1.10E-01	2.33E-04	8.97E-04	5.79	5.84	6.05	0.05
LPM	Mar-09	25	7.26E+01	2.41E-01	9.69E-02	1.79E-04	1.43E-03	5.90	9.52	6.05	0.05
LPM	Mar-09	28	7.87E+01	2.32E-01	1.12E-02	1.70E-04	1.39E-03	5.95	12.06	6.07	0.05
LPM	Mar-09	32	8.94E+01	2.31E-01	8.29E-02	1.13E-04	1.37E-03	5.98	12.80	6.09	0.05
LPM	Mar-09	36.5	1.42E+02	-	1.64E-01	1.24E-04	6.36E-04	5.91	9.40	6.07	0.06
LGM	Mar-09	4	2.81E-03	-	1.78E+00	1.41E-05	5.42E-05	1.84	0.38	4.99	0.14
LGM	Mar-09	11	2.81E-03	2.45E-01	1.08E+00	3.24E-05	7.57E-05	3.00	0.49	6.06	0.12
LGM	Mar-09	16	6.88E-03	2.60E-01	1.22E-01	1.24E-05	1.10E-04	3.84	0.68	6.03	0.08
LGM	Mar-09	21	5.29E-03	3.06E-01	6.30E-02	3.65E-05	1.32E-04	4.04	0.75	6.01	0.07
LGM	Mar-09	26	1.38E-02	3.23E-01	6.56E-02	1.04E-04	1.54E-04	4.06	0.74	6.08	0.07
LGM	Mar-09	31	1.95E-01	3.35E-01	5.88E-02	2.02E-04	1.77E-04	4.46	0.94	6.04	0.07
LGM	Mar-09	35	2.70E+00	3.24E-01	1.35E-01	1.53E-04	2.33E-04	4.76	1.18	6.01	0.06

Table A4: Continuation.

Sample	date	Depth (m)	CH_4	Ar	O_2	CO	He	R/Ra	He/Ne	R/Ra c	ERROR
LPM	May-09	3	1.04E-02	-	4.47E+00	2.24E-05	4.87E-05	1.33	0.36	3.56	0.04
LPM	May-09	12	1.79E-02	-	2.94E+00	3.05E-05	9.11E-05	2.48	0.48	5.00	0.14
LPM	May-09	18	4.10E+01	2.37E-01	8.33E-02	1.11E-04	8.16E-04	5.82	7.06	6.04	0.11
LPM	May-09	25	7.20E+01	2.38E-01	8.74E-02	1.13E-04	1.34E-03	5.83	12.11	5.95	0.06
LPM	May-09	28	7.92E+01	2.48E-01	1.29E-01	9.38E-05	1.39E-03	5.92	12.23	6.04	0.05
LPM	May-09	32	9.08E+01	2.36E-01	1.64E-01	1.68E-04	1.25E-03	5.92	11.61	6.05	0.05
LPM	May-09	36.5	1.22E+02	1.96E-01	4.83E-01	1.11E-04	6.41E-04	5.82	8.03	6.01	0.06
LGM	May-09	3	2.08E-02	2.75E-01	2.79E+00	1.94E-05	6.76E-05	1.02	0.34	2.38	0.02
LGM	May-09	10	7.38E-03	2.88E-01	9.76E-02	1.29E-05	1.06E-04	2.64	0.50	5.12	0.04
LGM	May-09	15	2.16E-01	3.00E-01	1.20E-01	1.36E-04	1.24E-04	3.70	0.66	5.90	0.18
LGM	May-09	20	4.43E-01	2.97E-01	2.93E-01	1.29E-05	1.75E-04	4.24	0.82	6.05	0.13
LGM	May-09	25	1.08E+00	2.93E-01	1.20E-01	3.88E-05	2.30E-04	4.63	1.24	5.77	0.07
LGM	May-09	30	1.55E+00	3.00E-01	8.26E-02	5.82E-05	2.53E-04	4.85	1.25	6.04	0.08
LGM	May-09	35	1.78E+00	3.05E-01	1.65E-01	6.60E-05	-	-	-	-	-
LPM	Jun-09	3	5.03E-03	2.20E-01	5.38E+00	3.11E-05	5.77E-05	1.05	0.42	1.69	0.01
LPM	Jun-09	12	2.35E-02	3.02E-01	3.40E+00	3.81E-05	1.14E-04	2.58	0.65	3.98	0.03
LPM	Jun-09	18	3.74E+01	2.96E-01	1.08E-01	1.94E-04	8.60E-04	5.50	4.43	5.82	0.14
LPM	Jun-09	25	8.06E+01	2.66E-01	9.04E-02	1.15E-04	1.63E-03	5.72	9.45	5.87	0.07
LPM	Jun-09	28	8.53E+01	2.56E-01	8.29E-02	4.01E-04	1.61E-03	5.76	11.70	5.89	0.06
LPM	Jun-09	32	1.02E+02	2.56E-01	1.02E-01	1.13E-04	1.51E-03	5.74	9.77	5.89	0.04
LPM	Jun-09	36.0	1.62E+02	1.66E-01	9.17E-02	-	6.47E-04	5.63	6.98	5.84	0.04
LGM	Jun-09	3	1.09E-03	2.14E-01	1.50E-01	3.26E-05	7.03E-05	1.22	0.42	2.20	0.06
LGM	Jun-09	10	1.05E+00	2.81E-01	1.49E-01	6.87E-05	1.46E-04	2.91	0.66	4.52	0.18
LGM	Jun-09	15	9.82E-01	2.99E-01	1.24E-01	7.17E-05	1.75E-04	4.15	1.03	5.44	0.15
LGM	Jun-09	20	-	-	-	-	2.69E-04	4.39	1.32	5.37	0.07
LGM	Jun-09	25	2.75E+00	3.16E-01	1.11E-01	1.56E-04	3.26E-04	4.80	1.51	5.73	0.06
LGM	Jun-09	30	3.52E+00	2.98E-01	1.12E-01	1.69E-04	3.60E-04	5.30	2.22	5.97	0.07
LGM	Jun-09	35	8.65E+00	3.16E-01	1.42E-01	8.97E-05	4.01E-04	5.06	1.79	5.86	0.06

Table A4: Continuation.

Sample	date	Depth (m)	CH_4	Ar	O_2	CO	He	R/Ra	He/Ne	R/Ra c	ERROR
LPM	Sep-09	3	8.61E-03	2.66E-01	9.15E+00	1.28E-04	7.11E-05	1.33	0.36	3.55	0.03
LPM	Sep-09	12	2.42E-02	3.55E-01	1.05E+01	2.92E-04	1.30E-04	2.96	0.68	4.55	0.05
LPM	Sep-09	18	5.34E+01	3.01E-01	1.02E-01	9.19E-05	9.73E-04	4.73	4.08	5.03	0.12
LPM	Sep-09	25	8.53E+01	2.74E-01	1.87E-01	8.38E-05	1.65E-03	4.75	10.66	4.86	0.06
LPM	Sep-09	28	9.13E+01	2.64E-01	1.39E-01	0.00E+00	1.69E-03	5.38	11.25	5.50	0.06
LPM	Sep-09	32	1.05E+02	2.52E-01	7.42E-02	3.54E-04	1.58E-03	4.59	11.82	4.68	0.04
LPM	Sep-09	37	1.67E+02	1.82E-01	1.38E-01	9.66E-05	8.63E-04	5.43	8.94	5.58	0.05
LGM	Sep-09	3	4.96E-03	2.20E-01	1.24E-01	2.51E-04	6.13E-05	0.88	0.32	1.95	0.02
LGM	Sep-09	10	2.92E+00	-	9.10E-01	4.53E-05	2.14E-04	1.64	0.86	2.08	0.02
LGM	Sep-09	15	2.71E+00	3.03E-01	1.58E-01	1.36E-04	2.92E-04	2.04	1.39	2.38	0.07
LGM	Sep-09	20	6.29E+00	2.99E-01	1.39E-01	5.81E-05	5.24E-04	4.01	2.62	4.40	0.09
LGM	Sep-09	25	6.75E+00	3.14E-01	1.15E-01	5.92E-05	5.49E-04	3.97	2.41	4.39	0.09
LGM	Sep-09	30	6.97E+00	3.03E-01	9.94E-02	7.61E-05	6.03E-04	4.11	3.27	4.43	0.05
LGM	Sep-09	35	6.30E+01	3.00E-01	9.92E-02	0.00E+00	6.13E-04	3.96	2.32	4.40	0.05
LPM	Jun-10	3	5.57E-02	2.62E-01	9.03E+00	0.00E+00	7.40E-05	0.97	0.47	0.92	0.02
LPM	Jun-10	12	1.64E-03	3.31E-01	9.13E+00	1.60E-05	1.27E-04	1.91	0.65	2.63	0.07
LPM	Jun-10	18	4.70E+01	2.91E-01	2.28E-01	1.25E-04	1.10E-03	5.68	6.54	5.89	0.06
LPM	Jun-10	25	7.22E+01	-	1.16E+00	9.24E-05	1.54E-03	5.76	9.33	5.91	0.05
LPM	Jun-10	28	8.39E+01	-	7.24E-01	8.38E-05	1.73E-03	5.75	9.83	5.89	0.05
LPM	Jun-10	32	1.04E+02	-	1.28E+00	1.12E-04	1.78E-03	5.75	10.30	5.88	0.05
LPM	Jun-10	37	1.65E+02	1.58E-01	4.51E-01	0.00E+00	1.15E-03	5.72	8.24	5.89	0.06
LGM	Jun-10	3	4.12E-03	-	3.80E+00	2.78E-05	5.44E-05	0.88	0.44	0.65	0.01
LGM	Jun-10	10	6.72E-01	-	2.69E-01	0.00E+00	1.37E-04	2.63	0.68	3.80	0.05
LGM	Jun-10	15	2.99E-01	-	1.12E-01	7.55E-05	1.63E-04	3.83	1.05	4.89	0.15
LGM	Jun-10	20	9.47E-01	-	3.61E-01	4.53E-05	2.31E-04	4.22	1.52	4.96	0.05
LGM	Jun-10	25	1.48E+00	-	3.92E+00	0.00E+00	2.67E-04	4.31	2.02	4.85	0.05
LGM	Jun-10	30	5.42E-01	-	1.34E+01	0.00E+00	2.52E-04	5.23	1.85	6.00	0.06
LGM	Jun-10	35	2.57E+00	-	3.78E-01	0.00E+00	2.90E-04	5.17	1.70	6.02	0.06

Appendix II

Water isotopes and local meteoric water line

The hydrogen and oxygen water isotopes are important tracers of source and/or process within the water cycle (e.g., Hoffmann et al., 2000). For example, the stable isotopes of water are a powerful tool in hydrological studies on regional and global scale because give the possibility to localize the recharge areas of studied water and identify some processes that may have modified it (e.g., evaporation and water-rock interactions). In lake studies water isotopes are largely used, not only to verify the evaporation process, proper of open waters, but also to recognize the relations with aquifer. Moreover, with a good dataset is possible to make refined isotopic mass balances to estimate input and output water amounts (Gonfiantini, 1986).

The δD vs $\delta^{18}O$ plot is a powerful graph, much used to identify and evaluate the processes that have modified the isotopic value of water. To follow the evolution of water is important to know the starting water, which is generally the meteoric water. For this reason it is important to identify a meteoric water line as firstly published by Craig in 1961. It is a linear relation in the form of:

$$\delta D = 8\delta^{18}O + 10 \quad \text{(A1)}$$

where the y-intercept 10 is the deuterium excess (d-excess) for global meteoric waters. However, the d-excess may vary locally and regionally, because it depends on evaporation conditions that can be locally different. For example, in the aast Mediterranean the MWL is better defined as (Gat, 1980; Gat & Carmi, 1987):

$$\delta D = 8\delta^{18}O + 22 \quad \text{(A2)}$$

Because of local processes, even the slope value can change. That being so, detailed hydrogeochemical studies need a local meteoric water line (LMWL).

In Vulture area many isotopic studies of waters have been carried out, each one analysing more or less different portions of the volcano and examining particular geochemical aspects (e.g.: Mongelli et al. 1975; Marini, 2006; Fuganti & Sigillito, 2008; Paternoster et al., 2008). An important aim of some literature works has been the identification of LMWL, which was affected by significant evolutions:

$$\delta D = 8.0\delta^{18}O + 17.4 \quad \text{Mongelli et al. (1975)} \quad \text{(A3)}$$

$$\delta D = 8.33\delta^{18}O + 20.39 \quad \text{Marini (2006)} \quad \text{(A4)}$$

$$\delta D = 6.56\delta^{18}O + 4.12 \quad \text{Paternoster et al. (2008)} \quad \text{(A5)}$$

In this work the linear regression of Paternoster et al. (2008) is used, because supported by a rich and updated database.

Appendix III

Carbonate speciation

When $CO_{2(gas)}$ dissolves into water, some of it reacts chemically with the water to produce carbonic acid:

$$CO_{2(aq)} + H_2O \leftrightarrow H_2CO_3 \tag{A6}$$

Commonly these two carbonate species are combined in a single term: $[H_2CO_3^*] = [CO_{2(aq)}] + [H_2CO_3]$. Since the $CO_{2(aq)}$ dominates over the form H_2CO_3 with the ratio about 650:1, in good approximation $[H_2CO_3^*] \approx [CO_{2(aq)}]$. The distribution of carbonate species in the water solution is controlled by following equations:

$$H_2CO_3^* \leftrightarrow H^+ + HCO_3^- \qquad K_1(25°C) = \frac{\left[HCO_3^-\right]\left[H^+\right]}{\left[H_2CO_3^*\right]} = 10^{-6.35} \tag{A7}$$

$$HCO_3^- \leftrightarrow H^+ + CO_3^{2-} \qquad K_2(25°C) = \frac{\left[CO_3^{2-}\right]\left[H^+\right]}{\left[HCO_3^-\right]} = 10^{-10.33} \tag{A8}$$

the concentration of total carbonates species in solution is the TDIC (total dissolved inorganic carbon) as follows:

$$TDIC = [H_2CO_3^*] + [HCO_3^-] + [CO_3^{2-}] \tag{A9}$$

Equations A7, A8 and A9 represent a system of three equations with three unknowns ($H_2CO_3^*$, HCO_3^-, and CO_3^{2-}) for a given TDIC concentration. Solving equations we obtain:

$$\frac{\left[H_2CO_3^*\right]}{TDIC} = \frac{1}{\frac{K_1}{\left[H^+\right]} + \frac{K_1K_2}{\left[H^+\right]^2} + 1} \tag{A10}$$

$$\frac{\left[HCO_3^-\right]}{TDIC} = \frac{1}{\frac{\left[H^+\right]}{K_1} + \frac{K_2}{\left[H^+\right]} + 1} \tag{A11}$$

$$\frac{\left[CO_3^{2-}\right]}{TDIC} = \frac{1}{\frac{\left[H^+\right]^2}{K_1K_2} + \frac{\left[H^+\right]}{K_2} + 1} \qquad \text{(A12)}$$

Equations A10, A11 and A12 are only functions of the proton concentration, H^+ (pH = $-\log_{10}[H^+]$). Therefore it is possible to obtain values for the three carbonate species using pH values (fig. A II.1).

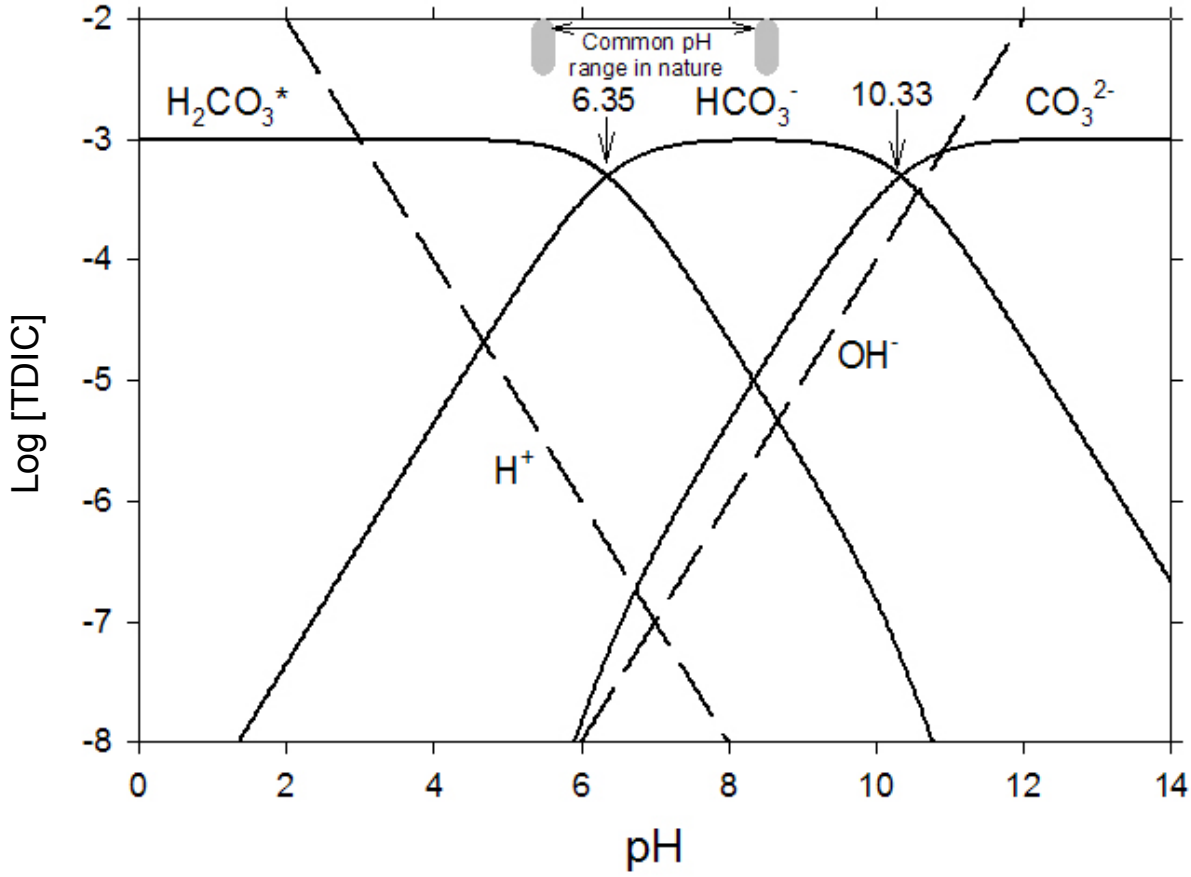

Figure A II.1 - Speciation diagram of the three carbonate species in the pH range of 0 to 14 for a value of TDIC of 10^{-3} mol/litre. In the figure are plotted the described equations (A10, A11 and A12). The values are calculated for T = 25 °C and P = 1 atm.

Appendix IV

Methane isotopes

In the approach proposed by Gutsalo (2008) the theoretical hydrogen isotope composition of methane both produced through CO_2-reduction ($\delta D(_{CH_4})_R$) as well as through acetate fermentation ($\delta D(_{CH_4})_F$) were computed as follows:

$$\delta D\left(CH_4\right)_R = \alpha_D^e \delta D\left(H_2O\right) + b^e \tag{A13}$$

$$10^3 \ln \alpha_D^e CH_4 - H_2O = -10.37\left(\frac{10^6}{T^2}\right) - 76.22 \tag{A14}$$

$$b^e = 10^3\left(\alpha_D^e - 1\right) \tag{A15}$$

and

$$\delta D\left(CH_4\right)_F = \alpha_D^b \delta D\left(H_2O\right) + b^b \tag{A16}$$

$$10^3 \ln \alpha_D^b = -477.357\left(\frac{10^6}{T^2}\right) + 3458.55 \tag{A17}$$

$$b^b = 27.35\left(\frac{10^6}{T^2}\right) + m \tag{A18}$$

where α_D^e and α_D^b are the biologic isotope fractionation factors under equilibrium and kinetic conditions respectively, T is the temperature in °K, δD_{H_2O} is the isotope composition of coexisting water and *m* is a specific parameter depending on biocenosis of bacteria.

Appendix V

Helium equations

Assuming that dissolved helium in the water samples is composed of mantle helium, crustal helium and atmospheric helium, we can build the mixing lines in the plot R/Ra and $^4He/^{20}Ne$ (fig. 4.22, 5.8) using the three-components mixing model (Sano et al., 1982), as follow:

$$\left(\frac{^3He}{^4He}\right)_s = \left(\frac{^3He}{^4He}\right)_m \times M + \left(\frac{^3He}{^4He}\right)_c \times C + \left(\frac{^3He}{^4He}\right)_a \times A \qquad \text{(A19)}$$

$$\frac{1}{\left(\frac{^4He}{^{20}Ne}\right)_s} = \frac{M}{\left(\frac{^4He}{^{20}Ne}\right)_m} + \frac{C}{\left(\frac{^4He}{^{20}Ne}\right)_c} + \frac{A}{\left(\frac{^4He}{^{20}Ne}\right)_a} \qquad \text{(A20)}$$

$$M + C + A = 1 \qquad \text{(A21)}$$

In our application M, C and A represent contributions of under Vulture mantle, crust and atmospheric helium, respectively, and subscripts m, c and a denote under Vulture mantle, crust and atmospheric. In this calculation, we have used the values of following table:

Table A5

	$^3He/^4He$	R/R_a	$^4He/^{20}Ne$
Atmosphere (ASW)	1.39×10^{-6}	1	0.267 (20°C)
Crust	0.015×10^{-6}	0.01	≥1000
Under Vulture Mantle	8.54×10^{-6}	6.1	≥1000

Since the $^4He/^{20}Ne$ ratio of mantle and radiogenic helium is significantly larger than that of ASW, it is possible to correct the atmospheric helium contamination as follows (Craig et al., 1978; Sano et al., 1987; Sano et al., 1990):

$$\left(\frac{^3He}{^4He}\right)_{cor} = \frac{\left[\left(\frac{^3He}{^4He}\right)_s - r\right]}{(1-r)} \qquad \text{(A22)}$$

$$r = \frac{\left(\frac{^4He}{^{20}Ne}\right)_a}{\left(\frac{^4He}{^{20}Ne}\right)_s} \tag{A23}$$

where $(^3He/^4He)_{cor}$ and $(^3He/^4He)_s$ are the helium isotopic ratio corrected and not corrected for the atmospheric contamination, respectively.

Appendix VI

Evaporation

Factors affecting the rate of evaporation can be generically divided into two groups, meteorological factors and surface factors. The first ones include energy and aerodynamic variables (i.e., solar radiation and heat flux or wind speed and vapour pressure, respectively). The second ones concern the characteristics of the evaporating surface (i.e.: free water surfaces or land surfaces).

Estimating methods of evaporation are generally indirect, direct measurements from extended natural water or land surfaces are not practicable at present (Vardavas I., M. & Fountoulakis, A., 1996 and references therein).

The four types of methods are:

- indirect measurements with evaporimeters
- estimation with meteorological methods
- estimation with water budget
- estimation with empirical and semiempirical methods (e.g., Priestley-Taylor, DeBruin-Keijman)

Evaporimeters

The only one instrument that can measure, indirectly, the evaporation is the evaporimeter, that exist in two formats: the atmometer and the evaporation pan. The difference consist in a different evaporating surface, a porous flat surface for atmometer and a free water surface for the pan. Obviously, the second method can better represent the evaporation on any water body as a lake.

The rate of evaporation from a pan evaporimeter is easily measured by the change in level of its free water surface. This measurement is advantageous because: i) is the actual result of the impact of total meteorological variables, ii) the data are immediately available. The only disadvantage is the heat-storage properties of pan are different from those of a natural system; therefore the evaluation of building material of evaporimeter and his positioning are difficult and delicate. About lakes is recommend the installation of pan on floating system on lake, in fact the monthly evaporation from floating evaporimeter on lake can be several millimetres higher than the monthly evaporation from the land evaporimeter (Walkusz & Janczak 2007).

Meteorological methods

These methods solve the evaporation parameter using meteorological data (e.g.: air temperature, relative humidity, solar radiation) and introducing its in theoretical equations. These are the most accurate estimating evaporation methods, frequently used as standard of comparison as regards of other ones. The most common used are: Bowen-ratio energy budget (BREB), eddy covariance, surface renewal and LIDAR (Drexler et al., 2004; Rosenberry et al., 2007).

The BREB method is based on energy balance equation (eq. A1) introducing the Bowen ratio expression (eq. A5) and only the temperatures and humidity are needed to measure directly. Eddy covariance method needs to air temperature, air humidity and measurement of eddy flux motions with a sonic anemometer, all data have to be with sufficient frequency response (of the order of 5-10 Hz). Surface renewal method use an accurate estimation (with sonic anemometer calibrations) of energy conducted to or from the evaporating body (H) obtaining the evaporation as the residual of energy budget equation (eq. 1). The Lidar method use a laser with radiations in the infrared, visible or ultraviolet range and measured data (i.e.: roughness length, humidity, temperature, specific heat and friction velocity) are elaborate with Monin-Obukhov similarity theory (Drexler et al., 2004).

All these methods, with the exception of BREB, require more expensive instruments and/or too frequent measurement of data, not ever available in the studied area. Considering, in our case, the sparse and remotely collected data, only a long-term evaporation monitoring is possible, so the BREB result the most appropriate method as previously reported (e.g., Lenters et al. 2005; Gianniou et al., 2007; Rosenberry et al., 2007).

The evaporation obtained with BREB method is assumed to have accuracy within 10% when averaged over a season and within 15% when over a month (Winter, 1981). Evaporation rates were determined for monthly to seasonal periods.

Water budget

The estimating of evaporation with water budget method requires measurement of changes in lake level, precipitation, inflow and outflow. The evaporation is the residual component of the equation (1), but, as previously discussed, the difficulty on estimation of I and O, does not permit an easy use of water budget to evaluate the evaporation.

Empirical and semiempirical methods

The estimation methods until now considered require measurement of a grate number of variable and a wide range of data. When the installation of a monitoring station for all the interesting parameters is too difficult or pricey, then it can be useful the employ of empirical and semiempirical methods. Many of these methods were developed to calculate potential evapotranspiration, but in a lake system they can be assumed to represent evaporation. These estimation methods have the main advantage to use a restrict number of variable. Unfortunately, their general principles have been defined in specific locations, so the robustness of empirical methods can depend on the ambient climate of application.

There are many detailed studies investigating the suitability of empirical evaporation methods on various physical and climatic lake settings (e.g., Winter et al., 1995; Rosenberry et al., 2004; Rosenberry et al., 2007). In all these studies many types of methods are evaluated (more then 15), but only three empirical methods compare very well with BREB values (BREB is used as standard method) in many lake environments: Priestley-Taylor, DeBruin-Keijman and Penmen. These are combination methods that include available-energy and aerodynamics terms and are the most commonly used for empirical estimation.

Used methods

In this work the evaporation rate on LPM and LGM are determined with different methods: BREB, Priestley-Taylor, DeBruin-Keijman and floating evaporimeter. A review of these methods is presented, in the form and to the extent used here.

Bowen-ratio energy budget (BREB)

The BREB method is based on the conservation of energy law and account for incoming, outgoing and stored energy in the lake system. The energy budget can be expressed as (Sturrock et al., 1992; Gianniou et al., 2007):

$$S = Rs - Rsr + Ra - Rar - Rb - H - LE + G + Av \qquad (A24)$$

S = change of the thermal content of the water body

Rs = short-wave (solar) radiation incident at the lake water surface

Rsr = reflected short-wave radiation from the water surface

Ra = long-wave (atmospheric diffuse radiation) radiation incident at the lake water surface

Rar = reflected long-wave radiation from the water surface
Rb = back (long-wave) radiation emitted from the lake water
H = energy conducted to or from the body of water
LE = energy utilized for evaporation
G = heat transfer between the lake bottom and the lake water
Av = energy advected into the lake

Conceptually, the net addition of heat into the lake that does not increase the lake heat storage can be considered as energy utilized for evaporation.
Av represent the energy coming from precipitations, surface water and groundwater. This component and G often are very small, especially in large and deep lakes, then are commonly ignored. The chemical and isotopic characteristics of Monticchio lakes waters are enough different respect to groundwater or precipitations, mainly in the epilimnion, then considerable inflow of both water sources can be rejected. It allow us to neglect the energy advected into the lake (Av).
An heat flux from the lakes bottom was highlight, in particular for LPM. It was estimated a maximum heat flux of 0.8 W/m^2 , evidently negligible if compare with other components of BREB. Then in good approximation Av and G are neglected, so the equation A24 takes the following form:

$$S = Rs - Rsr + Ra - Rar - Rb - H - LE \quad (A25)$$

This equation is used to calculate lake evaporation as residual component. LE is directly linked to evaporation rate E ($m\ s^{-1}$) through

$$LE = \rho_w L_v E \quad (A26)$$

where ρ_w is the water density (=1000 $Kg\ m^{-3}$), L_v is the latent heat of vaporization of water that, in good approximation, depends on water temperature, according to (Gianniou et al., 2007)

$$L_v = 2.5 - 0.0024T \quad (A27)$$

in which T is water temperature (°C) and L_v is expressed in MJ Kg^{-1}.

If the heat flux to or from the body of water (H) cannot be evaluated we have to use another variable, more easy to evaluate that is the Bowen ratio (β) (Henderson-Sellers, 1984)

$$\beta = \frac{H}{LE} = \gamma \frac{Ts - Ta}{e_{sw} - e_d} \tag{A28}$$

Ts = surface water temperature (°C)

Ta = air temperature above the lake

e_{sw} = saturation vapour pressure at the surface water temperature (mbar)

e_d = air vapour pressure above the lake (mbar)

γ = psycrometric constant (mbar °C^{-1})

e_{sw} and e_d are calculated in the same manner

$$e_i = 0.6108 \exp\left(\frac{17.27 T_i}{T_i + 237.3}\right) \tag{A29}$$

substituting Ts and Td, respectively. Td is dew point temperature that is the temperature to which the water vapour condenses into water.

$$Td = \frac{b\alpha_{(T,rh)}}{a - \alpha_{(T,rh)}} \qquad \alpha_{(T,rh)} = \frac{aT}{b+T} + \ln\left(\frac{rh}{100}\right) \tag{A30a, b}$$

where T (=°C), a=17.271 and b=237.7 °C. This expression is based on August-Roche-Magnus approximation and is considered valid for the following ranges: 0°C < T < 60°C; 1% < rh < 100%; 0°C < Td < 60°C.

The psychrometric constant is estimated using the equation (Mayer 1999; Gianniou et al., 2007)

$$\gamma = \frac{c_p P}{\varepsilon Lv} \tag{A31}$$

c_p is the specific heat of air at constant pressure, ε (=0.622) is the ratio of molecular weight of water vapour to that of dry air and P is the atmospheric pressure (mbar).

Combining equations (A25), (A26) and (A28), the evaporation can be estimated with the formulation of BREB, simplify of Av and G components

$$E = \frac{R_s - R_{sr} + R_a - R_{ar} - R_b - S}{\rho_w L_v (1+\beta)} \tag{A32}$$

The main subject of this energy budget is the incoming and outgoing radiation. The most of this radiation, that arrive on the earth surface, is of short-wave type (Rs) otherwise knows as daily global solar radiation. Rs data are commonly measured directly or estimate from equations based on dataset of national or international energy agencies (in this study are used data of ENEA, for the period 1995-1999). The reflected short-wave radiation (Rsr) is given by

$$R_{sr} = \alpha_s R_s \tag{A33}$$

in which $\alpha_s = 0.07$ and is the short-wave albedo on water.

A conspicuous amount of energy exchanges between heart surface and atmosphere fall in the range of long-wave electromagnetic spectrum. The energetic exchanges of long-wave type mainly depend on the heart surface and atmospheric temperature according to the equation

$$R_a = \varepsilon_a \sigma (T_a + 273)^4 \tag{A34}$$

where σ (=5.67x10^{-8} W m^{-2} K^{-4}) is the Stefan-Boltzmann constant and ε_a is the atmospheric emissivity. ε_a was estimated using formulation developed by Henderson-Seller (1986)

$$\varepsilon_a = 0.87 - \frac{n}{N}(0.175 - 29.92 \times 10^{-4} e_d) + 2.693 \times 10^{-3} e_d \qquad \text{for } \frac{n}{N} \le 0.4 \tag{A35a}$$

$$\varepsilon_a = 0.84 - \frac{n}{N}(0.100 - 9.973 \times 10^{-4} e_d) + 3.491 \times 10^{-3} e_d \qquad \text{for } \frac{n}{N} \ge 0.4 \tag{A35b}$$

where *n* is hours of sunshine per day, that depend on cloudy condition and on surrounding environment (e.g., topography, vegetation) and N is the maximum number of sunshine hours per day (n/N is the fractional number of hours of sunshine).

The reflected short-wave radiation (Rsr) is given by:

$$R_{ar} = \alpha_l R_a \tag{A36}$$

in which $\alpha_l = 0.03$ and is the long-wave albedo on water.

The back long-wave radiation emitted from the lake water (Rb) have the same formulation of Ra, but uses surface water temperature (Ts) and $\varepsilon_b = 0.97$ (Bowie et al., 1985).
The heat storage in the lake (S) in the *dt* time can be evaluated in according to Gianniou et al. (2007)

$$S = \frac{\rho_w c_{pw}}{A_s} \frac{d\int_0^z A_z T_z dz}{dt} \tag{A37}$$

where c_{pw} is the specific heat of water (J Kg^{-1} $°C^{-1}$), A_s is the surface area of the lake (m^2), A_z is the area of the lake at z depth (m^2), Tz is the temperature at z depth.

Priestley-Taylor method

The Priestley-Taylor equation is an empirical formulation, a modification of Penman formula, presented by Priestley and Taylor in 1972, hear in follow form:

$$E = \alpha \frac{s}{s+\gamma} \frac{R_N - S}{\rho_w L_v} \tag{A38}$$

$\alpha = 1.26$, Priestley-Taylor empirically derived constant
s = slope of saturation vapour pressure, temperature curve (Pa $°C^{-1}$)
R_N = net radiation ($R_s - R_{sr} + R_a - R_{ar} - R_b$)
$\gamma = 66$ Pa $°C^{-1}$, psychrometric constant

DeBruin-Keijman method

The DeBruin-Keijman method is similar to previous one, but uses different constants, as follow (Rosenberry et al. 2007):

$$E = \frac{s}{0.85s + 0.63\gamma} \frac{R_N - S}{\rho_w L_v} \tag{A39}$$

Floating evaporimeter

About evaporation pan, because of problems linked to building material and positioning (see above), the evaporimeter installed on Monticchio lakes was constituted by a transparent plastic for the pan and a floating structure of thin aluminium (fig. A VI.3). During installation

the evaporation pan was located in the water, with the internal water at the same level of the lake one. A low interference with solar radiation and a heat exchange between evaporimeter water and lake water allow a better simulation of the lake water evaporation.

Application of methods

The absence of mean monthly meteorological data (i.e., air temperature and relative humidity) in the lake site, constrain us to use data of the Melfi meteorological station, located at 10 Km from lakes at an altitude of 580 m a.s.l. (altitude of Monticchio Lakes is 660 m a.s.l); therefore only monthly evaporation estimating are take out, but enough period for hydrogeochemical studies.

The lakes temperature data was took in various sampling campaigns, distributed in the period between September 2008 and September 2009. The vertical sampling profiles was took in the same point of the lake for all campaigns and the horizontal homogeneity of water temperature at various depths was verify. The changes in thermal content of the water body (S), that represents the heat storage in the lake, was calculated with equation (A37) for irregular sampling intervals defined by sampling campaigns.

Because of the lack of monthly mean surface water temperature (Ts) and air temperature above the lake (Ta), the monthly Bowen ratio (β) was estimated using the following empirical formulation (Spence et al. 2003)

$$\beta = -0.2063\ln(VPD) + 0.0814 \qquad \text{(A40)}$$

where VPD is the vapour pressure deficit (e_s–e_a); e_a=e_s(rh_m/100) in which rh_m is monthly relative humidity and e_s was calculated using equation (A29) substituting in T_i the mean monthly air temperature (T_m).

The equation (A40) is an empirical relationship specific to Skeeter Lake (a small lake in the Northwest Territories of Canada), applicable to other lakes where the turbulent fluxes are controlled by temperature and vapour pressure gradients between lake and atmosphere (Spence et al. 2003), therefore with moderate presence of wind. This equation was tested on El-Rayan lake (a warm subtropical lake in an arid zone of Egypt), using data of Abd Ellah (2009). The result is show in Fig. A VI.1.

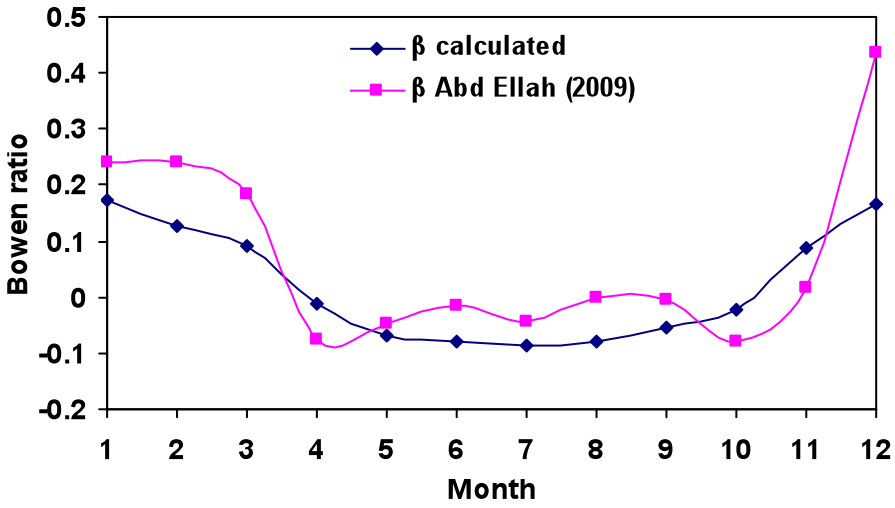

Figure AVI.1 - Bowe ratio (β) at El-Rayan lake. Comparison between calculated values by means of equation A40 and calculated values with measured data by Abd Ellah (2009).

Considering the big difference between the two lake environments, is interesting to note the good agreement in the trend with a little flatting of β calculated curve regarding the relative variations in confront of β of Abd Ellah. That being so, the equation (A40) was used for monthly Bowen ratio estimating in the Monticchio lakes, since the values of relative humidity rh_m and of mean monthly air temperature (T_m) of Melfi meteorological station.

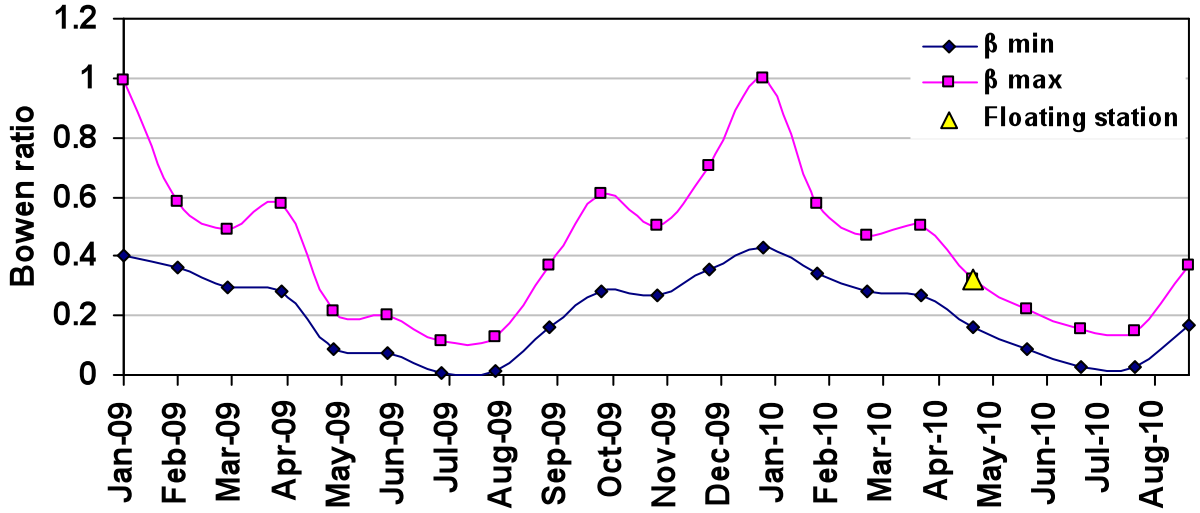

Figure AVI.2

In the period from 31/05/10 to 04/06/10, a floating station that acquired meteorological data and water temperature at the centre of LGM (fig. A VI.3), permitted to estimate β with equation (A28). The calculated value (0.31) fall near the bowen ratio at higher humidity

estimated with equation (A40) (fig. A VI.2). The value estimated with floating station data confirms the applicability of equation (A40).

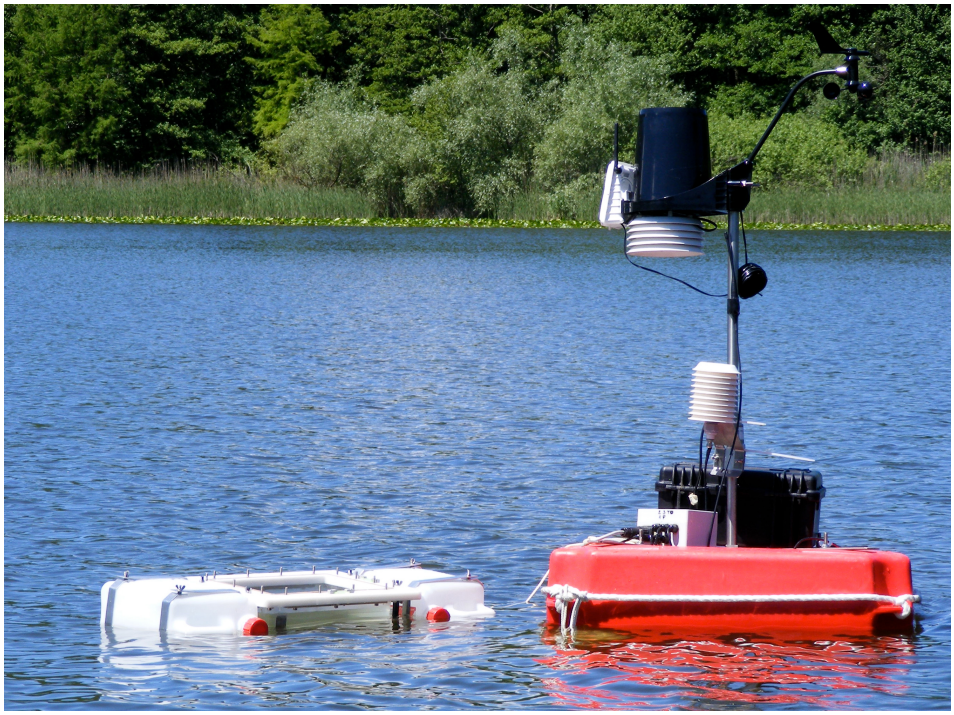

Figure A VI.3 - Floating self-made evaporimeter and meteorological station during measurements.

The Priestley-Taylor constant (α) is an empirically derived term by Priestley & Taylor (1972) and same as 1.26. In literature this value was bring into question by Paw and Gao (1988) that note little variation of α for different environment. Then is better to estimate this value as follow (Drexler et al., 2004):

$$\alpha = \frac{\Delta + \gamma}{\Delta(1+\beta)} \tag{A41}$$

where Δ is the slope of the saturation vapour pressure curve at air temperature in KPa °C^{-1}, expressed as

$$\Delta = \frac{2504 \exp\left[\frac{17.27Ta}{(237.3+Ta)}\right]}{(237.3+Ta)^2} \tag{A42}$$

The monthly solar radiation incident on the lake water surface was taken from on-line dataset of ENEA and is the mean value of 1995/1999 period. The hours of light on Lake per day (n) was considered N-2 (N is the maximum number of sunshine hours per day), because at least for one hour after sunrise and one hour before sunset the lakes are in the shade of the mountain and trees. The cloudy covering was not considered in the calculation of hours of sunshine per day, then the evaporation estimating toward to more high values then the actual ones, particularly for cool and rainy periods.

The minimum value of relative humidity was fixed with the mean monthly one of the Melfi meteorological station and the maximum value as the previous one increased of a fixed 20% (this value was established because in winter periods premises to assume a maximum relative humidity near 100%, the higher value admitted). Since the temperature on Monticchio lakes are lower than Melfi ones and considering the lakes as a source of humidity, because an unending availability of water, most likely the actual value of relative humidity fall in the fixed maximum-minimum monthly range. Obviously the evaporation rate was estimated considering the relative humidity range and so evaluating the potential variability of this datum.

Table A6. Annual evaporation from Lakes (Borrelli, 2008).

Lake	Annual evaporation (cm)	Longitude	Latitude	Area (ha)	Average depth (m)
Pyramid Lake2	128	119°40'	40°00'	46,640	61
Salton Sea2	179	116°10'	33°05'	88,100	8
Lake Ontario2	73	77°00'	44°00'	1,940,000	86
Hyco Lake2	94	79°05'	36°15'	1,760	6
Hungary Horse Reservoir2	51	113°55'	46°00'	9,700	15
Lake Kerr2	118	81°50'	29°20'	1,040	5
Lake Mead2	223	114°30'	36°05'	51,400	54
Lake Okeechobee9	147	80°55'	27°00'	182,130	3
Amistad Reservoir2	203	101°20'	29°20'	27,900	16
Great Salt Lake2	101	112°30'	41°00'	388,900	10

Appendix VII

Water density

In limnology, the most practical methods to evaluate the water density take into account not only the temperature but also the salinity (Chen & Millero, 1977; Chen & Millero, 1986) or directly the electrical conductivity (Bührer & Ambühl, 1975; Bäuerle et al., 1998; Karakas et al., 2003; Schmid et al. 2004a). An alternative method, able to consider the contribute of all dissolved substances was described by Wüest et al. (1996). This method was used to calculate the density (ρ) of Monticchio lakes waters, by means of formulation of Schmid et al. (2004b):

$$\rho = \rho_{TP}\left(1 + \beta_{TDS}TDS + \beta_{CO_2}\left[CO_{2(aq)}\right] + \beta_{CH_4}\left[CH_{4(aq)}\right]\right) \tag{A43}$$

$$\beta_x = 1 - \frac{\rho_{TP}\sum_i v_i c_i}{\sum_i M_i c_i} \tag{A44}$$

where ρ_{TP} (g/cm^3) is the density of water at in situ temperature and pressure, β (dimensionless) is the coefficient of haline contraction of considered chemical components, the χ represents the contributes of TDS, dissolved CO_2 and dissolved CH_4; M_i, c_i and v_i are the molar mass (g/mol), the molar concentration (mol/cm^3) and the partial molal volume (cm^3/mol) of *i* species , respectively (table 1).

The ρ_{TP} equation is in the form of Chen & Millero (1977):

$$\rho_{TP} = \frac{\rho_T}{1 - \frac{P}{K}} \tag{A45}$$

$$\begin{aligned}\rho_T = {} & 0.9998395 + 6.7914\times10^{-5}t - 9.0894\times10^{-6}t^2 + 1.0171\times10^{-7}t^3 \\ & -1.2846\times10^{-9}t^4 + 1.1592\times10^{-11}t^5 - 5.0125\times10^{-14}t^6 \\ & +\left(8.221\times10^{-4} - 3.87\times10^{-6}t + 4.99\times10^{-8}t^2\right)S\end{aligned} \tag{A46}$$

$$\begin{aligned}K = {} & 19652.17 + 148.37t - 2.329t^2 + 1.3963\times10^{-2}t^3 - 5.9\times10^{-5}t^4 \\ & +\left(3.2918 - 1.719\times10^{-3}t + 1.684\times10^{-4}t^2\right)P \\ & +\left(-0.8985 + 2.428\times10^{-2}t + 1.114\times10^{-2}P\right)S\end{aligned} \tag{A47}$$

in which ρ_T (g/cm^3) is the density of water at in situ temperature, P is the pressure in bar, t is the temperature in °C and S is the salinity (‰); considering only the temperature and pressure contributes was imposed S=0, the salinity was considered by means of coefficient of haline contraction (see above).

The equations proposed by Chen & Millero (1977) are showed in figure A VII.1 at different temperature and pressure and S=0.

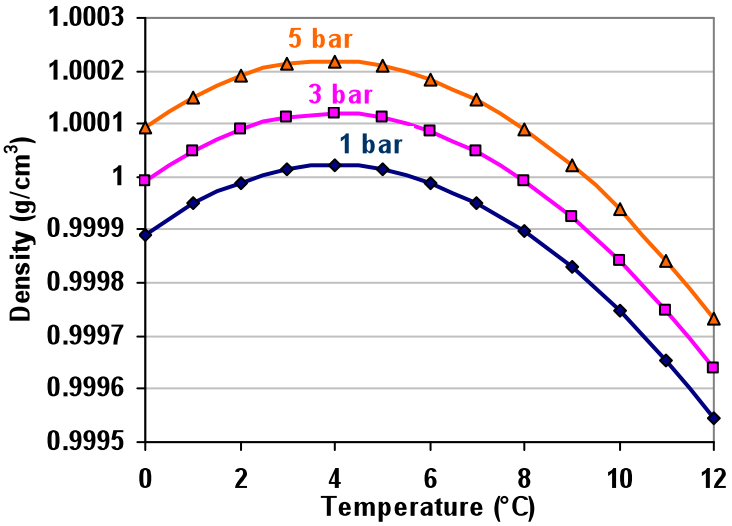

Figure A VII.1 - Density of pure water (g/cm^3) at various temperature and pressure.

The conventional partial molal volume ($v_{i(conv)}$) was corrected by means of formulations presented by Millero (1972):

$$v_i = v_{i(conv)} + Zv_{H^+} \qquad \text{for cations} \qquad \text{(A48a)}$$

$$v_i = v_{i(conv)} - Zv_{H^+} \qquad \text{for anions} \qquad \text{(A48b)}$$

where Z is the absolute charge and v_{H^+} is the absolute partial molal volume of the proton; as suggested by Kling et at. (1989) $v_{H^+} = -5cm^3/mol$. The v_i values of major ions are reported in table A7.

Table A7

Substance	M_i (g/mol)	v_i (cm^3/mol)
Ca	40.00	-27.85
Mg	24.30	-31.17
K	39.00	4.02
Na	23.00	-6.21
NH_4	18.00	12.86
Fe	55.85	-58.7
Cl	34.45	22.83
HCO_3	61.00	28.4
SO_4	96.10	23.98
CO_2	44.00	31
CH_4	16.00	36.2

Appendix VIII

Heat from radioactive decay

The heat contribution (H, in calories per gram of rock per year) from radioactive decay is given by the following equation:

$$H = 0.72\ U + 0.20\ Th + 0.27\ K \qquad (A49)$$

where U and Th are the uranium and thorium content of rock (ppm), respectively, and K is potassium content of rock in percentage (%).

Appendix IX

About eddy diffusion

In this appendix we evaluate the weight of radiant heat by sunlight and thermal exchange with sediments in the estimation of eddy diffusion coefficient (equation 5.3-3) in the Monticchio lakes context.

First of all, we take into account the absorption in both lakes waters, defined as diminution of light energy with depth by transformation to heat (Wetzel, 2001 and reference therein).

All waters have a high absorption of infrared and red wavelength generating a significant heating in the first meters of water. A rapid decrease of absorption is in the lower wavelengths to a minimum value in the blue. With high turbidity and dissolved organic compounds there is an increasing of absorption at lower wavelengths of visible spectrum, particularly in UV range.

The figure A IX.1 clearly shows that over 90% of IR radiation (>700 nm) is absorbed in the first meter of water for all selected lakes, instead the visible radiation (400-700 nm) is less absorbed, but becomes extinct at the most in the first 4 or 5 meters.

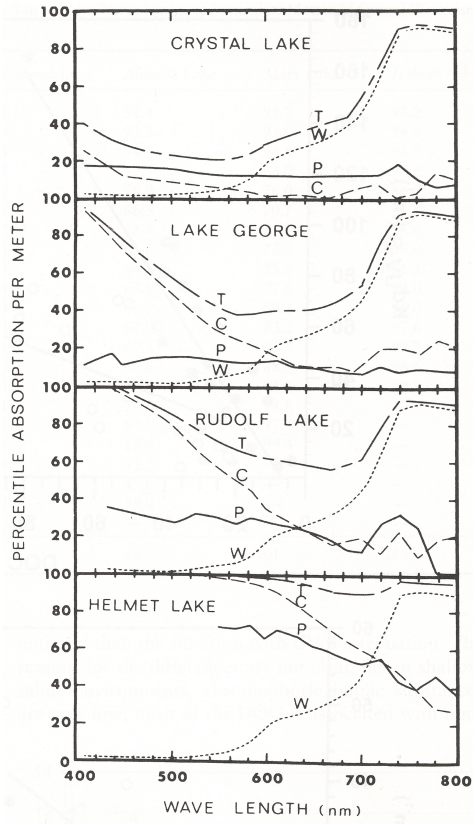

Figure AIX.1 - Percentile absorption of light versus wavelength , through 1m of lake water (T) compared to the absorption of: distilled water of 1 meter depth (W), suspended particulate matter (P), lake waters 1mm filtered (colour absorption)(C). (Wetzel, 2001)

Practically the absorption of each wavelengths is evaluated means of extinction coefficient (η in m^{-1}), constant for a given wavelengths:

$$I_z = I_0 e^{-\eta z} \tag{A50}$$

where, z is the depth in meters, I_z is the irradiance at z depth, I_0 is the irradiance at the surface. Obviously a natural total extinction coefficient (η_t) exists, which represents the average value of all wavelength and also the contribute of absorption for: the only water (η_w), suspended particles (η_p) and coloured compound (η_c):

$$\eta_t = \eta_w + \eta_p + \eta_c \tag{A51}$$

A very simple method to estimate η_t, uses an empirical relation presented by Poole & Atkins (1929) and confirmed by successive studies (e.g., Idso and Gilbert, 1974), that is:

$$\eta = \frac{1.7}{z_{sd}} \tag{A52}$$

where z_{sd} is the Secchi disk depth, a simple and common method for evaluating the water transparency. In Monticchio lakes this parameter was measured, for the LPM the value is 5.5 meters and for LGM is 0.3 meters (as confirmed by literature, Schettler and Albéric, 2008; Mancino et al. 2009); consequently η are 0.31 and 5.7 m^{-1} respectively. These values regard only the visible spectrum (400-700 nm), but are certainly lower values than the η_t that include even the IR and UV spectra because, as shown above, these wavelengths are more absorbed at a lower depth than the visible spectrum (fig. A IX.1).

To verify the reliability of the estimated extinction coefficient we compare our data with other lakes ones. Lawrence Lake is an unproductive hardwater lake with high concentrations of colloidal $CaCO_3$ and has a mean η_t of 0.39 m^{-1}.Wintergreen Lake, extremely productive, has a mean η_t of 1.00 m^{-1} (Wetzel, 2001). In the first lake, very similar to the LPM, between 8 and 12 m of depth all solar light is absorbed. In the second lake, that has a minor extinction coefficient than LGM, already in 5 m of depth the solar light is absorbed (Fig. A IX.2). That so being, the radiant heating by sunlight ($R_{(z)}$) can be neglected for the computing of K_z in the deep portions of lakes.

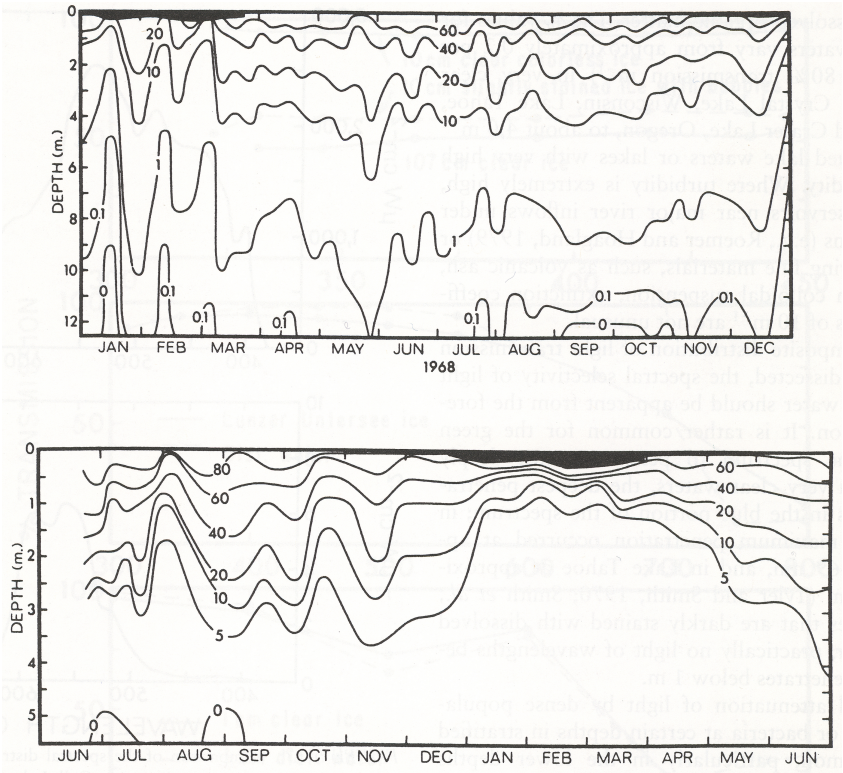

Figure A IX.2 - Isopleths of the percentage transmission of sunlight with depth and time in Lawrence Lake (upper) and Wintergreen Lake (lower). (Wetzel, 2001)

Another important term of equation (5.3-3) is the thermal exchange with sediments ($H_{(z)}$). Effectively, the thermal gradient from bottom of LPM suggests a thermal exchange with sediments (heat flux from bottom). Practically, as in details studied by Benoit and Hemond (1996), the influence of this process on heat budget, and so on calculating of K*z*, is function of the change of temperature in the water and, in this case, also in the bottom. As shown in multiparametric probe chapter, below 15 m of depth the temperature gradient is always the same over time, the temperature variations are below 0.1 °C from month to month and in the near bottom water are even below 0.05°C. This thermal steady state condition permits to neglect the thermal exchange with sediments.

Anyway, Benoit and Hemond (1996) also assert that heat loss to sediments can be a significant term in the heat budget of shallow (< 25m) lakes, the Monticchio lakes are both deeper than 35 m. Nevertheless, not having the possibility of estimating its contribution this term was neglected also in LGM.